# Novel Insights into Schwann Cell Dynamics in Peripheral Nervous System Myelination

A Dissertation Presented

By

Cheryl Lynn Gatto

Submitted to the Faculty of the

University of Massachusetts Graduate School of Biomedical Sciences, Worcester

In partial fulfillment of the requirements for the degree of

DOCTOR OF PHILOSOPHY

April Seventh, Two-thousand and Four

Department of Cell Biology

Novel Insights into Schwann Cell Dynamics in Peripheral Nervous System Myelination

A Dissertation Presented
By
Cheryl Lynn Gatto

Approved as to style and content by:

_____
Stephen N. Jones, Ph.D., Chairman of Committee

_____
Elizabeth J. Luna, Ph.D., Member of Committee

_____
Ann R. Rittenhouse, Ph.D., Member of Committee

_____
Greenfield Sluder, Ph.D., Member of Committee

_____
Timothy Vartanian M.D., Ph.D., Member of Committee

_____
Stephen Lambert, Ph.D., Thesis Advisor

_____
Anthony Carruthers, Ph.D.,
Dean of the Graduate School of Biomedical Sciences

Department of Cell Biology

April Seventh, Two-thousand and Four

**Acknowledgments**

I would like to thank Dr. Stephen Lambert for his guidance and encouragement throughout my course of study. Without his involvement, the evolution of this work and my development as a scientist would not have been possible. I was fortunate to find both an outstanding mentor and a wonderful friend. Thank you, in addition, to Barbara Walker for sharing her technical expertise and being a source of constant support in all of my pursuits, in and out of the lab. Many thanks to Corrie Painter for critically reading portions of this thesis and providing insightful discussion. I would also like to thank the members of my research advisory and thesis committees, Drs. Stephen Jones, Elizabeth Luna, Greenfield Sluder, and Ann Rittenhouse, for their input and direction as these projects have unfolded. I would like to extend a special thanks to Dr. Timothy Vartanian, for joining us from Beth Israel Deaconess Medical Center, Boston, MA, for my dissertation defense.

I would like to acknowledge that these studies were supported by the NIH Grant RO1NS36637, DOD Award DAMD 17-02-1-0649, the Pilot Project Award from the Worcester Foundation for Biomedical Research (to S.L.), and the Neuroscience Training Grant 5T32NS07366 (to C.G.). In addition, the NCRR Shared Equipment Grant (1S10RR15775) was used to purchase the microscopy system used in the live cell imaging studies presented.

Last, but certainly not least, I would like to graciously thank my family and friends for their endless love, support, and understanding. Mom, John, Chris – I couldn't have done this without you!!

## Abstract

This body of work details the exploitation of an incredibly powerful neural culture system, which enables the *in vitro* study of events involved in peripheral nervous system (PNS) development. Using a myelinating dorsal root ganglion (DRG) explant culture system, node of Ranvier formation and maintenance and the associated generation and maturation of myelin segments was examined. In addition, Schwann cell (SC) development, dynamics, and migration were extensively studied.

First, in characterizing these cultures, the discrete axonal localization of specific ankyrin isoforms was revealed. Ankyrins are peripheral membrane proteins that immobilize classes of integral membrane proteins to the spectrin based-membrane skeleton. Ankyrins interact with proteins such as the voltage-dependent/gated sodium channel (vgsc) and members of the L1 family of cell adhesion molecules. These interactions are physiologically relevant to the formation of membrane specializations involved in axon guidance and the initiation and propagation of action potentials.

We examined ankyrin$_B$ and ankyrin$_G$ expression in cultured DRG explants, which allowed visualization of individual axons. Ankyrin$_B$ and ankyrin$_G$ exhibited differential localizations to specific axonal populations. This was evident as early as one day *in vitro* and persisted over time. In mature pre-myelinated cultures, axons having an apparent diameter of less than 1 μm predominantly expressed ankyrin$_B$, whereas axons having a diameter greater than or equal to 1 μm predominantly expressed ankyrin$_G$ (based on immunocytochemical reactivity). When myelination was induced, ankyrin$_G$ was appropriately localized to sites of nodal development flanked by myelinating glial processes in the large caliber axons. These observations suggest that axons destined for

myelination may express a distinct complement of peripheral, and perhaps integral, membrane proteins as compared to those observed in non-myelinated axons. These distinguishing features may play a role in the selection of axons for myelination.

This work was followed with defining the role axo-glial interactions play in organizing domains along the axon being myelinated. Nodes of Ranvier are specialized, highly polarized axonal domains crucial to the propagation of saltatory action potentials. In the PNS, axon-glial cell contacts have been implicated in SC differentiation and the formation of nodes of Ranvier. SC microvilli establish axonal contact at mature nodes, and their components have been observed to localize early to sites of developing nodes. However, a role for these contacts in node formation remains controversial.

Using the myelinating explant culture system, we observed that SCs reorganize and polarize microvillar components, such as the ezrin-binding phosphoprotein 50kDa (EBP50)/regulatory co-factor of the sodium-hydrogen exchanger isoform 3 (NHERF-1), actin, and the activated ezrin, radixin, and moesin (ERM) family of proteins, concomitant with myelination in response to inductive signals. These components were targeted to the SC distal tips where live cell imaging revealed novel, dynamic growth cone-like behavior. Further, localized activation of the Rho signaling pathway at SC tips gave rise to these microvillar component-enriched “caps” and influenced the efficiency of node formation.

Extending these findings, a more profound examination of SC dynamics was undertaken. This was a particularly important experimental transition, as SC motility is crucial in the development and regeneration of the PNS. The seemingly equivalent bipolarity of mature SCs represents a conundrum in terms of directed motility.

Fluorescence time-lapse microscopy of transfected SCs within the myelinating DRG explants revealed a novel cycling of these cells between static, bipolar and motile, unipolar morphologies via asymmetric process retraction and extension. Concentrations of PIP2 (phosphatidylinositol (4,5)-bisphosphate), activated ERMs, and EBP50 delineated the transitory asymmetry associated with the generation and neuron-like migration of the unipolar cell. EBP50 over-expression enhanced unipolar SC migration, suggesting a new role for this adaptor protein in cell motility. Further, the ERMs themselves were found to be essential to both motility and process dynamics with ERM disruption yielding a dysfunctional, multipolar SC phenotype. We propose this novel form of motility may be associated with the correct alignment and spacing of SCs along axons prior to elaboration of the myelin sheath.

These compiled studies present significant advances in understanding and examining axo-glial interactions in the PNS. This work establishes the foundation for further, novel exploration of normal PNS development and the regeneration and repair mechanisms involved in PNS injury and disease states.

## Table of Contents

## List of Figures

## Copyright Notice

Portions of this thesis have appeared in the following publications:

Gatto C.L., B.J. Walker, and S. Lambert. 2003. "Local ERM activation and dynamic growth cones at Schwann cell tips implicated in efficient node of Ranvier formation." *J Cell Biol* 162(3): 489-498.

Gatto, C.L., B.J. Walker, and S. Lambert. "Asymmetric ERM activation is required for directed process retraction, migration, and maintenance of polarity in mature Schwann cells." - manuscript reviewed and under revision for *The Journal of Cell Biology.*

# Chapter 1

## Introduction

Myelination

Differences in CNS vs. PNS myelination

Myelinated nerve fiber domain organization

Effect of myelinating glia on axonal properties

Axo-glial interactions and node of Ranvier formation and maintenance

The myelinating Schwann ell

Adaptor proteins in the PNS – ankyrins, ERMs, and EBP50

Thesis aim

Myelination

Myelination is a vertebrate adaptation that involves supporting glial cells, engaged with target nerve cells, concentrically spiraling multi-lamellar sheaths of insulating membrane at precise intervals along the axon (reviewed in Arroyo and Scherer, 2000; Poliak and Peles, 2003; Salzer, 2003). The individual sheaths are known as myelin segments, which completely cover the myelinated axon with the exception of the natural breaks present at either end of abutting, myelinating glial cells. These interruptions are referred to as the nodes of Ranvier. At the nodes, voltage-gated sodium channels (vgscs) become highly localized mediating the continued propagation of the action potential, which originated at the axon hillock/initial segment, down the length of the axon toward its synaptic target (Ritchie and Rogart, 1977; Shrager, 1989).

Why are these specializations critical to our nervous function? Generally, conduction velocity increases proportionately with increasing axonal diameter. The depolarizing, passive spread of current is inversely related to the product of the axial resistance ($r_a$) and membrane capacitance ($c_m$) per unit length of the axon ($r_a c_m$). Resistance decreases proportionately to the square of, and capacitance increases in direct relation to, the axonal diameter. Thus, increasing axonal diameter provides a net decrease in $r_a c_m$ allowing faster action potential propagation. In practice, however, this relationship becomes limiting in nervous system development if the maintenance of a given cranial volume is desirable (reviewed in Kandel et al., 1991).

Myelination aids in resolving this constraint by serving to electrically insulate the underlying region of axonal membrane. Because the capacitance of the myelin membrane is inversely proportional to its own thickness and is oriented as a parallel

capacitor with the axonal membrane, the concentric wraps of the glial cell in myelination cause a decrease in $c_m$ and thus $r_a c_m$. This, in conjunction with the segmental nature of the myelin sheath, provides for the promotion of rapid, saltatory conduction of action potentials and allows for maximal nervous conduction velocities of up to 100 m/sec (Waxman, 1980). In addition, myelination dramatically conserves both space and energy by sparing concomitant increases in axonal caliber that would otherwise be necessary to deliver such rapid nervous impulses. Mathematically modeled, an unmyelinated axon would require an obligate diameter 40-times greater and consume 4000-fold more energy than an equivalently conducting myelinated axon (Garbay et al., 2000). Thus, myelination has been favored evolutionarily as an adaptation to facilitate progressions toward higher order functions and increasing neural complexity.

Differences in CNS vs. PNS myelination

Myelinated fibers can be found in both the central and peripheral nervous systems (CNS and PNS, respectively). Their study is of particular interest in relationship to the host of known debilitating, demyelinating neuropathies, including multiple sclerosis and Charcot-Marie-Tooth disease. Although the functionality of myelin segments in both the CNS and PNS is essentially identical, their generation and some associated properties are specifically divergent.

In the CNS, a single oligodendrocyte is responsible for generating multiple myelin segments, whereas in the PNS, a myelinating Schwann cell (SC) generates only one. Axo-glial interactions at the nodes of Ranvier are maintained by an ancillary cell, the perinodal astrocyte, in the CNS (Black and Waxman, 1988; Raine, 1984), while

further specializations of the SC, the microvilli, fulfill this role in the PNS (Ichimura and Ellisman, 1991; Raine, 1982). (Fig. 1)

The CNS myelin sheath radially organizes the tight junction protein claudin-11/oligodendrocyte specific protein (OSP) (Morita et al., 1999). This four transmembrane protein influences oligodendrocyte proliferation, migration, and differentiation and is not present in the PNS (Bronstein et al., 2000). The SC generates a specialized extracellular matrix (ECM) known as the basal lamina, which contains laminin-2, entactin, type IV collagen, fibronectin, N-syndecan, and glypican (Bunge et al., 1980; Carey et al., 1983; Mehta et al., 1985; Scherer, 1996). The formation of the basal lamina is associated with SC differentiation and required for myelination.

Lastly, the SC myelin segment includes the components of reflexive adherens (Fannon et al., 1995; Menichella et al., 2001) and gap junctions (Miyazaki et al., 1995; Scherer et al., 1995) in the cytoplasmic channel structures, known as Schmidt-Lanterman incisures that connect the inner- and outer-most myelin layers. These channels provide accessible diffusion pathways enabling rapid transport of ions, secondary messenger molecules, and metabolites. Specifically, the calcium-dependent adhesion molecule, E-cadherin, is involved in generating autotypic adherens junctions and is required for the establishment and maintenance of the outer mesaxon. However, tissue-specific gene ablation using Cre/LoxP techniques has demonstrated appropriate nerve functionality in the absence of E-cadherin (Young et al., 2002).

In addition, the gap junction pore-forming protein, connexin 32, is required for normal PNS myelination. Connexin 32 mutations disrupt the path of radial diffusion present in myelinating SCs and are the cause of X-linked Charcot-Marie-Tooth disease

# Figure 1 - Myelination in the CNS vs. PNS

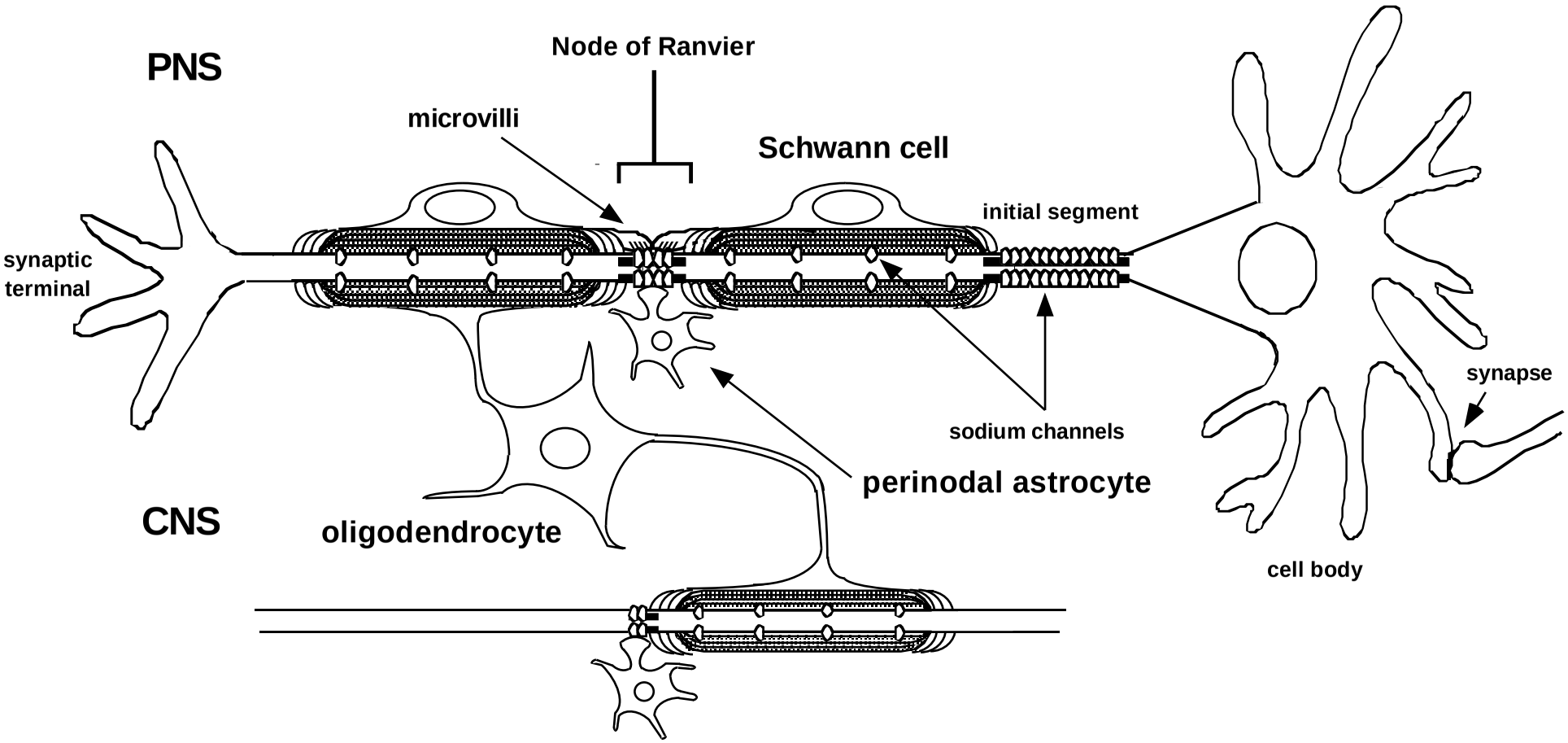

Figure 1 – Myelination in the CNS vs. PNS

Depicted are the interactions between myelinating glia and target axons in the CNS and PNS. As described in the text, a single myelinating oligodendrocyte in the CNS is capable of generating multiple, insulating myelin segments, whereas a given myelinating SC can form only one. The nodes of Ranvier are devoid of myelin, but not glial contact. These contacts are maintained by the perinodal astrocyte in the CNS and microvillar specializations of the SC in the PNS. Such axo-glial interactions may be crucial in the organization and maintenance of the node. As myelination progresses, the vgscs become highly concentrated at the axon initial segment and at the nodes. This facilitates action potential initiation and propagation, respectively, enabling the transmission of electrical stimulation to the axon's synaptic terminal.

(CMTX) (Bergoffen et al., 1993). CMTX involves aberrations in the periaxonal collar and non-compacted myelin regions and both myelin and axonal degeneration. Interestingly, recent evidence indicates an alternate connexin, connexin 47, is expressed in oligodendrocytes and is critical to normal CNS myelination (Menichella et al., 2003; Odermatt et al., 2003). Mice lacking connexin 47 display substantial abnormalities including oligodendrocyte death, thin/absent myelin sheaths, periaxonal disruption, vacuolation, and axonal loss.

Myelinated nerve fiber domain organization

Considerable effort has been focused on defining the morphologic and molecular specializations associated with not only the radial but longitudinal organization of the myelin segments (Fig. 2A). As described above, nodes of Ranvier flank each myelin segment. The intervening myelinated region is referred to as the internode. The length of the internode, and thus the nodal spacing, increases proportionally with respect to the diameter of the underlying axon. The nodes are situated at a distance of approximately 100-times that of the axonal diameter (Friede and Bischhausen, 1980; Friede et al., 1981; Smith et al., 1982a). This suggests that intrinsic axonal determinants govern nodal positioning. However, examination of the hypomyelinating *claw paw* mutant suggests glial signaling involvement. This autosomal recessive mutation delays the onset of PNS myelination (Henry et al., 1991). Sciatic nerves from these animals display prolonged maintenance of an unmyelinated state and atypical patterns of myelin maturation. Initially, myelination generally appears normal but results in drastically shortened internodes (Koszowski et al., 1998). This suggests that the elongation of the myelinating SC determines the internodal length independent of axonal caliber. Definitive

# Figure 2 -Features of myelinated fibers

**A** Longitudinal domain organization along a myelinated nerve fiber

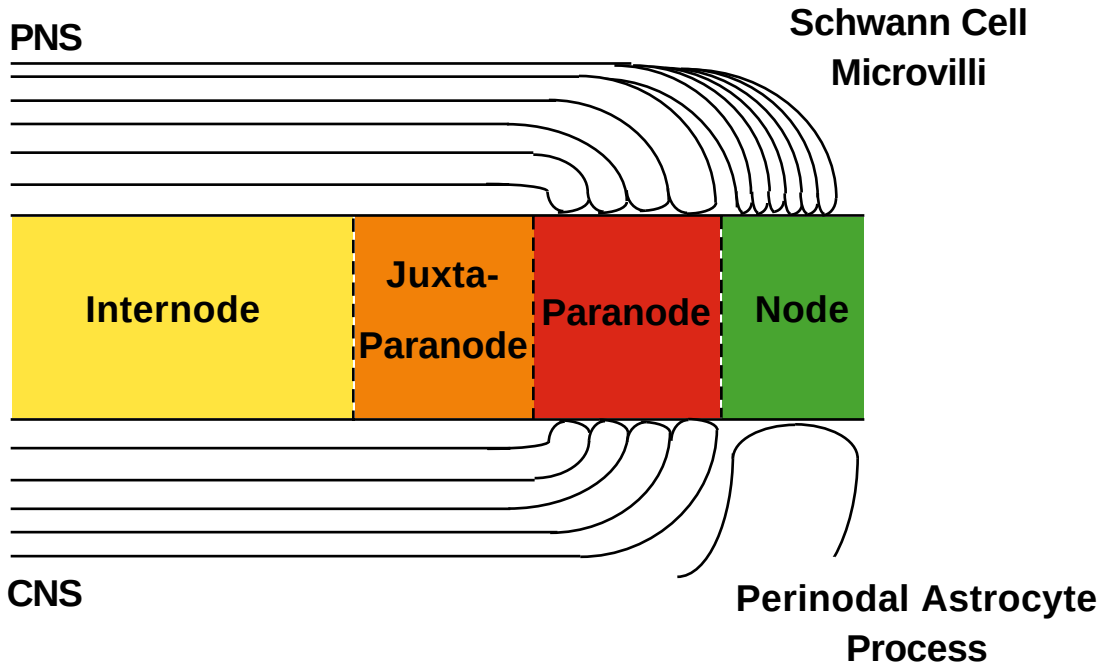


**B** Cross-section through PNS myelinating nerve

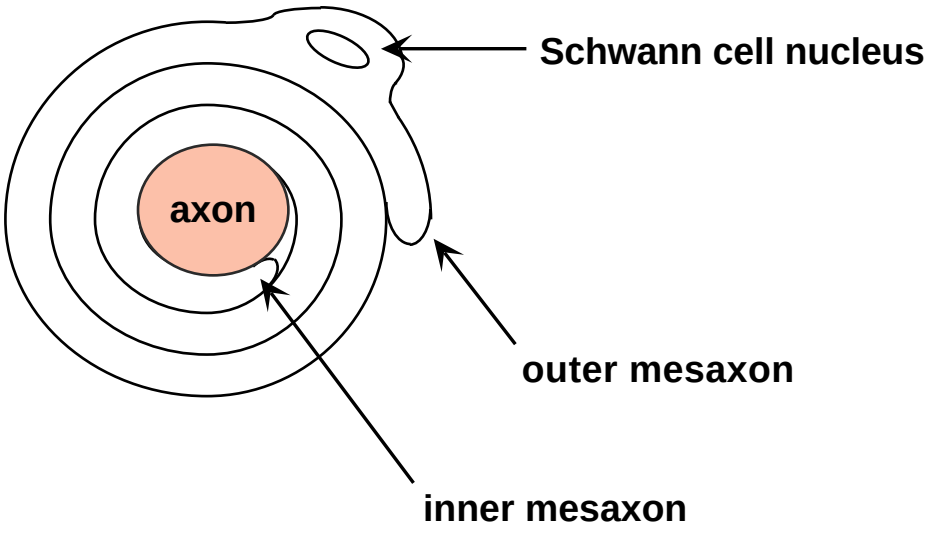

Figure 2 – Features of myelinated fibers

A) Shown is a diagrammatic representation of the longitudinal organization along a myelinated fiber in both the CNS and PNS. The illustration shows a heminodal region in association with either the perinodal astrocyte process or the SC microvilli. Immediately adjacent to the node is the paranode. This region is hallmarked by the presence of cytoplasm-filled glial loops, which are involved in forming tight, septate-like junctions with the associated axonal domain. The next evident domain is the juxtaparanode followed by the most prevalent region of the myelin segment, the internode. B) Illustrated is a cross-section through a PNS myelinated fiber, showing the general positioning of the inner and outer mesaxons. During myelination, the inner lip of the glial cell, the inner mesaxon, advances forming concentric membrane wraps that continue to increase the myelin membrane thickness. Figure adapted with permission from Poliak and Peles, *Nat Rev Neurosci*. 2003 Dec;4(12):968-80.

implication or exclusion of either mechanism controlling internodal length, axonal intrinsic or extrinsic, awaits determination.

Although the mechanisms governing nodal genesis still remain unclear, the nodes are known to be enriched in particular subsets of proteins. As indicated, vgscs become highly localized to the axonal surface of the node (>1200 channels/$\mu m^2$ as compared to <25 channels/$\mu m^2$ along the internode) (Ritchie and Rogart, 1977; Shrager, 1989). These channels undergo a developmental switch from isoform $Na_v1.2$ to $Na_v1.6$, the significance of which is not understood (Boiko et al., 2001; Kaplan et al., 2001). Other axonal proteins found at the nodes include cell adhesion molecules (NrCAM and neurofascin-186 kDa) (Davis and Bennett, 1993; Davis et al., 1996; Lambert et al., 1997), cytoskeletal elements ($ankyrin_G$ and βIV-spectrin) (Berghs et al., 2000; Komada and Soriano, 2002; Kordeli et al., 1995), and a potassium channel ($K_v3.1$ in the CNS and Kcnq2 in the PNS) (Devaux et al., 2003; Devaux et al., 2004).

Considering the glial contribution to the node of Ranvier, contacts are maintained by the SC microvilli in the PNS or the perinodal astrocyte in the CNS. Of the two, the SC microvilli have been better characterized in terms of their molecular constituents. These fine projections have been shown by electron microscopy to emanate from the outer edge of the SC and form an axonally encompassing collar (Waxman and Black, 1987). The microvilli themselves are characterized by the presence of all three of the actin cross-linking family of ERM (ezrin, radixin, moesin) proteins (Melendez-Vasquez et al., 2001; Scherer et al., 2001). In addition, the ERM-binding phosphoprotein 50 kDa (EBP50) is also present (Gatto et al., 2003; Melendez-Vasquez et al., 2001). These components may serve as adaptor molecules linking integral membrane components to

the microvillar cytoskeleton. High-resolution studies have demonstrated filaments, 40-80 nm in length, directly coupling the SC microvilli to the nodal axolemma (Ichimura and Ellisman, 1991). This indicates the potential existence of microvilli-localizing, cognate glial receptors for nodally clustered axonal components. (Fig. 3)

Beyond the node, additional defining structural and molecular detail is discernable along the internode. As the glial cell initiates myelination, it begins to wrap membrane around the circumference of the axon with its inner lip continually advancing (Bunge et al., 1989). The glial surfaces either apposing the ECM or the axon itself are referred to as abaxonal/basal and adaxonal/apical, respectively, and the associated terminations of the spiraling glial cell are known as the outer and inner mesaxons (Fig. 2B). After approximately 1.5 wraps around the axon, a characteristic early, non-compact myelin protein, myelin-associated glycoprotein (MAG), is expressed (Martini and Schachner, 1986; Martini and Schachner, 1988). After multiple turns have been achieved, compaction of these membrane layers begins. The myelin constituent, protein zero ($P_0$), facilitates this compaction. $P_0$ is an abundant, adhesive protein that forms tetramers in *cis*, and these multimers interact homophilically in *trans* bringing the membranes in close apposition (D'Urso et al., 1990). In addition, myelin basic protein (MBP) becomes detectable, which is present only in compact myelin (Sternberger et al., 1978).

As compaction proceeds, the majority of cytoplasm is extruded out toward the lateral borders of the glial wraps forming the paranodal loops adjacent to the node of Ranvier. The paranode itself is distinct in terms of its molecular composition and its proposed functionality. This region's unique character is defined by paranodal/septate-

# Figure 3 - Axo-glial interactions in the PNS

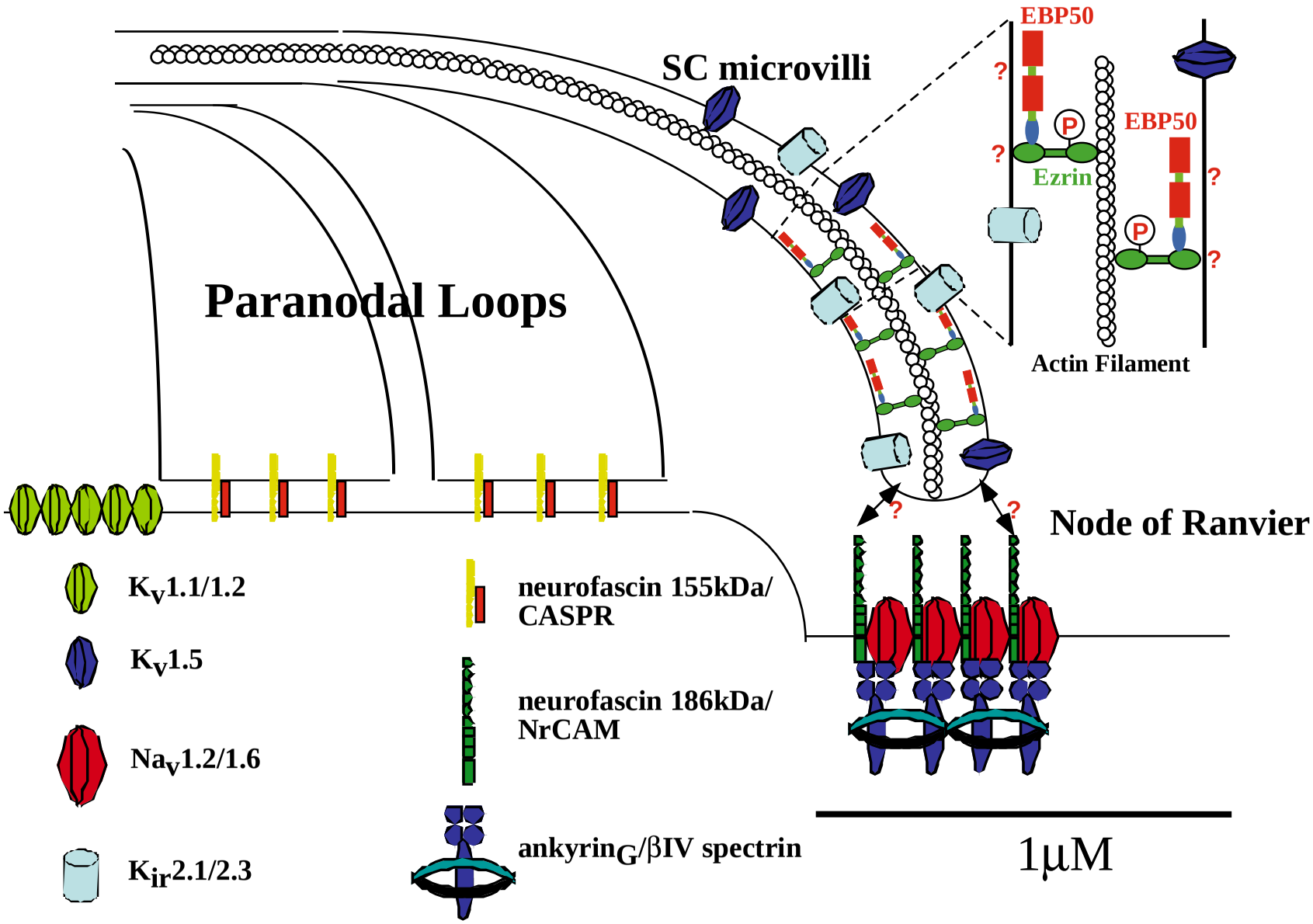

Figure 3 - Axo-glial interactions in the PNS

As indicated in the text, the molecular composition of the nodes of Ranvier and paranodes of myelinated axons is emerging. In the PNS, the myelinating SC maintains contacts at the node via microvilli, which are enriched in actin filaments, ERM family proteins, EBP50, and certain potassium channels. On the axonal side of the node, the glial cell may serve to organize clusters of membrane proteins, such as the cell adhesion molecules, neurofascin 186 kDa and NrCAM, and vgscs of the isotypes 1.2 and 1.6. The underlying axonal cytoskeleton at the node is enriched in ankyrin$_G$ and βIV-spectrin. Adjacent to the node are the non-compacted paranodal loops. These structures are involved in mediating the paranodal, septate-like junctions via interactions between axonally derived contactin/Caspr complexes with glially contributed neurofascin 155 kDa. Immediately beyond the paranode lies the juxtaparanodal region, which marks the lateral border of the compact, myelinated internode and maintains concentrations of the potassium channels, Kv1.1 and 1.2.

like junctions, which are hypothesized to serve as molecular sieves in the membrane restraining the lateral mobility of certain intra-membrane components (Pedraza et al., 2001; Trapp and Kidd, 2000). In addition, the junctions also limit the diffusion of small molecules and ions. As the paranode is situated between the vgsc-enriched node of Ranvier and the potassium channel-enriched juxtaparanode, this functionality is essential to the electrical isolation of these two active domains. The diffusion barriers are maintained by immediate juxtaposition of the axonal and glial membranes (3-5 nm periaxonal space at the paranode vs. 15 nm along the internode (reviewed in Salzer, 2003)) via the interactions of axonal heterodimers of Caspr1/paranodin and contactin with their glial partner, neurofascin 155 kDa (Boyle et al., 2001; Charles et al., 2002; Einheber et al., 1997; Tait et al., 2000).

Caspr is a member of the neurexin superfamily of proteins known to mediate intercellular adhesion and communication. Caspr also contains both a FERM (4.1, ezrin, radixin, moesin) and SH3 domain (Peles et al., 1997). Thus, it is situated to mediate the translation of extracellular events to the underlying cytoskeleton and participate in organizing responsive signaling complexes at the paranodal membrane. The interaction of Caspr with contactin, a glycosyl-phosphatidylinositol (GPI)-linked glycoprotein, is critical for its appropriate processing and targeting (Bonnon et al., 2003; Gollan et al., 2003). These *cis*-interactors complex heterophilically with the glial cell adhesion molecule, neurofascin 155 kDa, via the direct binding of contactin and neurofascin (Charles et al., 2002; Gollan et al., 2003) (Fig. 3). This was demonstrated by the over-expression of Caspr inhibiting the interaction. Inhibition resulted from the biosynthetic association of Caspr with contactin forcing the expression of a low molecular weight,

endoglycosidase H-sensitive isoform of contactin at the cell surface. This low molecular weight variant remains associated with Caspr but is unable to bind neurofascin 155 kDa (Gollan et al., 2003).

Advances in the field will require further dissection of the exact functionality of the junctions formed by these intermolecular associations. However, their proposed role as diffusional barriers has been well documented. This is best evidenced by analysis of mutations that result in disrupted paranodal regions, which include the engineered contactin and Caspr1 null mice (Bhat et al., 2001; Boyle et al., 2001). The nerves of these animals display elongated nodes of Ranvier, as indicated by diffuse vgsc clusters. In addition, the paranodes maintain the irregular appearance of potassium channels (Kv1.1 and 1.2), Caspr2, and the GPI-linked cell adhesion molecule TAG-1. These proteins are normally restricted to the adjacent juxtaparanodal region (Arroyo et al., 2001; Poliak et al., 1999). Other mutations impairing paranodal development include the CGT (UDP-galactose ceramide galactosyl-transferase) and CST (cerebroside sulfotransferase) targeted gene disruptions. These enzymes are necessary for the formation of myelin glycolipids, including galactocerebroside (GalC) and sulfatide. These animals also display a loss of lateral diffusional control in their myelinated fibers, and their aberrant phenotypes specifically implicate glycolipid synthesis in junctional complex assembly (Honke et al., 2002; Poliak et al., 2001).

Effect of myelinating glia on axonal properties

Axo-glial interactions not only serve to physically specify regional boundaries but also allow the myelinating glial cells to exert marked biochemical and physiological influences on their associated axon. For example, increased axonal diameter is promoted

along the length of the compact, myelinated segment, with caliber reduced by as much as 80-85% in paranodal and nodal regions (Berthold, 1996; Sward et al., 1995). Further, these alterations in axonal diameter are directly linked to glial-induced cytoskeletal rearrangements.

The status of the axonal neurofilament network significantly influences axonal caliber and is itself influenced by myelination status. Increased neurofilament phosphorylation allows for enhanced separation, providing increases in axonal diameter. Neurofilaments residing in either non-compacted or unmyelinated regions (i.e. paranodes and nodes, respectively) are reduced in total amount, more ordered, and less phosphorylated (de Waegh et al., 1992; Martini, 2001; Starr et al., 1996). The functional consequence of these factors is axonal constriction. In accordance with these findings, along the myelinated internodal region, neurofilament phosphorylation and axonal caliber are increased. Transgenic mice, one of which utilizes the $P_0$ promoter to drive diptheria toxin production in myelinating SCs, implicate the direct influence of the myelinating glial cell on these factors. These animals display severe hypomyelination that is coupled with dramatic decreases in neurofilament phosphorylation and axonal diameter (Cole et al., 1994).

The myelinating glial cell also affects the axonal microtubule cytoskeleton, which again is best demonstrated by examining several available hypomyelinating mutants. The PNS myelin mutant *trembler* is deficient in a compact myelin component, the peripheral myelin protein 22 kDa (PMP22). Demyelinated segments in these mice exhibit decreases in axonal caliber, depressed neurofilament phosphorylation, and microtubule cytoskeleton modifications. The stability of the *trembler* axonal microtubule network is

decreased and the composition and phosphorylation of axonal microtubule-associated proteins, including tau, MAP1A, and MAP1B, are altered (Kirkpatrick and Brady, 1994). In the CNS myelin mutant *shiverer*, which is deficient in MBP, microtubule stability is reduced. However, microtubule density is increased, as a result of increased tubulin expression (Kirkpatrick et al., 2001).

Axo-glial interactions and node of Ranvier formation and maintenance

The effect of the glial cell on certain axonal properties, including caliber via cytoskeletal modification, remains largely undisputed. However, one of the most significant controversies lies in whether axo-glial interactions are required for the formation and maintenance of the nodes of Ranvier. Is node formation glial cell-guided, or do axonally-derived intrinsic determinants govern this process? Examined in both the CNS and PNS, contradictory findings leave these key questions unsatisfactorily answered.

The hypothesized dependence of nodal development on direct glial association has been well demonstrated. Using vgsc clustering as an indicator of nodal genesis, vgsc aggregates have been shown to faithfully arise in close proximity to MAG-positive SC processes (Vabnick et al., 1996). Transgenic mouse models exploiting the $P_0$ promoter have shown that adherence of SCs is required for vgsc clustering into focal nodal regions, and these SCs must have reached a committed myelinating stage (Vabnick et al., 1997). In addition, remyelination studies in the induced PNS disease state of Experimental Allergic Neuritis (EAN), which is used as a model for immune-mediated inflammatory demyelinating diseases like Guillan-Barre syndrome and multiple sclerosis, demonstrate that vgsc reorganization depends upon SC positioning (Novakovic et al., 1998). Studies

in cultured dorsal root ganglia (DRGs) demonstrate the preclusion of vgsc and ankyrin$_G$ clustering in the presence of conditioned media isolated from myelinating cultures. The absence of clusters was also noted on suspended axonal bundles, or fascicles, despite their close proximity to other myelin segments (Ching et al., 1999). Further, the MBP-TK transgenic mouse, which undergoes specific oligodendrocyte ablation upon FIAU (1-(2-deoxy-2-fluoro-β-δ-arabinofuranosyl)-5-iodouracil) treatment, retains axonal nodal component protein levels in the complete absence of their clustering (Mathis et al., 2001).

Alternatively, compelling evidence also indicates a glial-independence associated with node formation. Studies of lysophosphatidyl-choline treated, demyelinated axons demonstrate foci of directed current prior to remyelination, indicating vgsc reorganization in the absence of axo-glial interactions in the PNS (Smith et al., 1982b). The *dystrophic* mouse of the strain 129/ReJ-Lama$^{2dy}$, which is deficient in the expression of merosin (laminin α2), organizes vgsc clustering in amyelinated regions that implicate SC independent events (Deerinck et al., 1997). CNS studies indicate that soluble oligodendrocyte-derived factors promote node formation in cultured retinal ganglion cell axons (Kaplan et al., 1997). Further, in the *jimpy* mutant mouse, which is altered in its myelin proteolipid protein (PLP) expression, oligodendrocytes spontaneously degenerate, but nodal clusters of vgscs and ankyrin$_G$ are still observed (Mathis et al., 2001).

<u>The myelinating SC</u>

As this body of work will focus on the specialized axo-glial contacts maintained in the PNS, we shall concentrate on the myelinating SC. SCs are derived from multi-potent neural crest cells, which arise from the neuroepithelium of the closing neural tube and begin their lateral and ventral migratory streams at embryonic day 9-10 (E9-10) in

the rat (reviewed in Lobsiger et al., 2002; Mirsky and Jessen, 1999). By E12-14, these cells have become lineage specified, with certain populations directed toward gliogenesis by β-neuregulin and Notch signaling. These cells serve as the SC precursors (Jessen and Mirsky, 1991; Jessen and Mirsky, 1997; Jessen and Mirsky, 1998). Flattened, markedly migratory, and highly mitotic, SC precursors can be identified in association with fascicles of extending axons of the PNS (Fig. 4A). Their molecular signature is defined by the expression of the low-affinity neurotrophin receptor p75, the cell adhesion molecule L1, the intermediate filament protein nestin, and the growth-associated protein 43 (GAP43) (Jessen et al., 1994; Jessen and Mirsky, 1998; Stewart et al., 1992). They also maintain low levels of $P_0$ (Bhattacharyya et al., 1991), PMP22 (Hagedorn et al., 1999; Pareek et al., 1993), and the transcription factor 0ct-6/SCIP (Blanchard et al., 1996; Monuki et al., 1989). Further, SC precursors will apoptose if deprived of axonal contact without introducing exogenous trophic support due to the lack of discrete autocrine survival loops (Jessen and Mirsky, 1999).

At E16-16.5, SC precursors undergo differentiation into committed early/ immature SCs (Jessen et al., 1994). These bipolar cells are distinguished by the expression of the small calcium binding protein, S100. In addition, they present the sulfoglycolipid antigen 04 (Mirsky et al., 1990), express the intermediate filament protein GFAP (glial fibrillary acidic protein) (Jessen et al., 1990), and upregulate the transcription factors, Oct-6 and Krox20 (Arroyo et al., 1998; Lobsiger et al., 2001). In contrast to the SC precursors, the early SCs are able to fully withstand axonal deprivation (Jessen and Mirsky, 1999). Further, these early SCs continue to divide, with a mitotic

# Figure 4 - Schwann cell development and differentiation

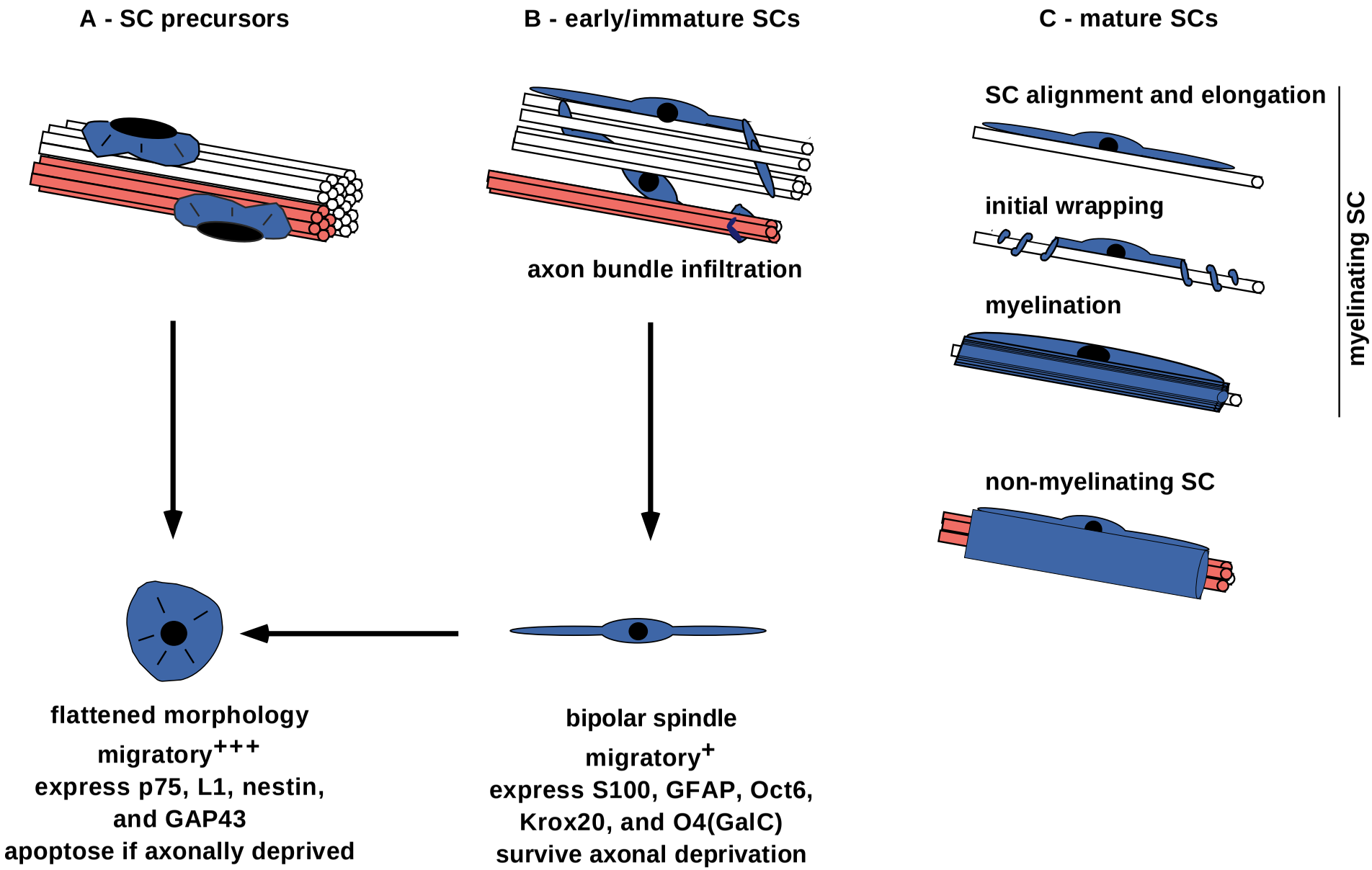

Figure 4 – SC development and differentiation

Detailed here are the developmental stages leading to the differentiation of the mature SC. A) Upon encountering bundles/fascicles of axons, the neural crest-derived SC precursors have a flattened morphology and are highly migratory (E12-14 in rat). These cells can be isolated from their axonal partners, however, due to a lack of autocrine survival loops will apoptose shortly thereafter. B) The SC precursors transition to early/immature SCs assuming their typical bipolar spindle shape (E16-16.5). These S100-reactive cells are less migratory than the SC precursors; however, they actively infiltrate the axon bundle initiating axon sorting and engagement. At this developmental stage, SCs may be deprived of axonal contact to permit isolated SC culture. Of note, there is a reversibility of this early bipolar phenotype *in vitro*. The reversion of these cells to the precursor morphology is highly dependent upon culture density and passaging frequency. C) The mature SCs can assume either a myelinating or non-myelinating role in the peripheral nerve (P1-). Initiation of myelination involves the 1:1 association of the SC with its target axon, SC elongation, and formation of the initial membrane wraps around the axon. Having achieved this positioning, the SC then commences the myelination program. However, not all SCs are destined to myelinate. Non-myelinating SCs interact with small bundles of axons (shown here in pink) and ensheathe them with simple membrane extensions.

peak at E19-20, and infiltrate axon bundles preparing to assume their terminally differentiated state (Stewart et al., 1993) (Fig. 4B).

Neonatally, SC maturation culminates with the generation of two functional categories of SCs, myelin- and non-myelin forming (reviewed in Mirsky and Jessen, 1996). Myelinating SCs segregate larger caliber axons (>1 μm diameter) until achieving the appropriate 1:1 relationship, as each SC will establish only one myelin segment. Basal lamina formation and myelin deposition then commence in response to presently unidentified inductive cues. The non-myelin forming SCs also establish a basal lamina but only ensheathe and separate groups of smaller diameter axons with simple, membrane extensions (Fig. 4C).

Adaptor proteins in the PNS – ankyrins, ERMs, and EBP50

Myelination involves morphologic and molecular specializations of both the myelinating glial cell and its target axon. These molecular alterations occur at the membranes of the axo-glial interface and the underpinning cytoskeletal network. Here, we will discuss the importance of certain adaptor proteins in PNS myelination that will be of particular relevance in the presented studies.

Ankyrins

Crucial to the functionality of the axonal cytoskeleton is the regulated expression of the ankyrins. Ankyrins are membrane adaptor proteins that immobilize integral proteins linking them to the spectrin-based membrane skeleton (reviewed in Bennett and Chen, 2001; Bennett and Lambert, 1999). Ankyrins are modular proteins that maintain several conserved domains, including $NH_2$-terminal membrane-binding ANK repeats (89-95 kDa), a spectrin-binding domain (62 kDa), and a COOH-terminal death domain (12

kDa) (Lambert et al., 1990; Lux et al., 1990; Otto et al., 1991). The ANK repeats themselves are 33-amino acid repeats, of which there are 24 tandemly arrayed in the ankyrins. These 24 ANK repeats are further structured such that four globular subdomains of six repeats each are generated (Michaely and Bennett, 1993). The largest ankyrin isoforms are selectively found in the axons of CNS and PNS neurons and contain considerable insertions separating the spectrin-binding and death domains. These variable, filamentous tail regions may facilitate interactions in a tissue- and isoform-specific manner and, if fully extended, could be as long as 0.5 μm. (Fig. 5)

The ankyrin family of proteins is encoded by three distinct genes, ANK1, ANK2, and ANK3. The corresponding polypeptides are referred to as ankyrin$_R$, ankyrin$_B$, and ankyrin$_G$, respectively. Various isoforms of these proteins are often present due to developmentally regulated, tissue-specific, alternative mRNA processing (Fig. 5).

The multi-valency of ankyrin (Michaely and Bennett, 1995) allows it to take part in the assembly of specialized regions of the plasmalemma implicated in processes such as axon guidance and the initiation of action potentials. To this end, ankyrins link a variety of proteins to the spectrin-based membrane skeleton. These include cell adhesion molecules (Bourrguignon et al., 1995; Davis and Bennett, 1993; Kalomiris and Bourguignon, 1988; Zhang et al., 1998), ion channels and exchangers (Li et al., 1993; Srinivasan et al., 1988), and calcium-release channels (Bourguignon and Jin, 1995; Bourguignon et al., 1993).

Sequence motifs that mediate ankyrin-membrane protein interactions have begun to emerge. A 5-amino acid sequence (FIGQY) is obligatory and phosphorylation-state dependent for the ankyrin binding of the immunoglobulin (Ig)/ fibronectin III (FNIII)

# Figure 5 - Domain structure of ankyrin isoforms

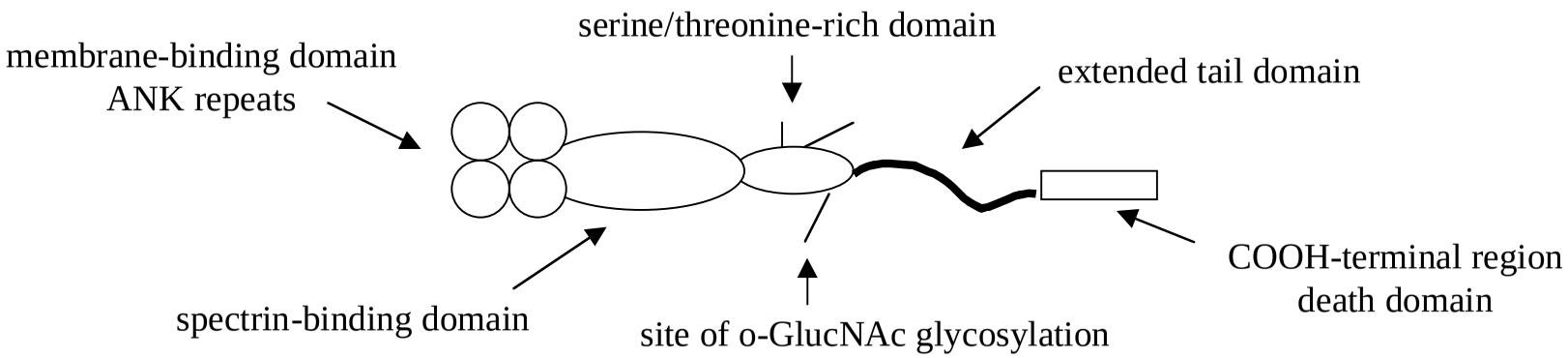


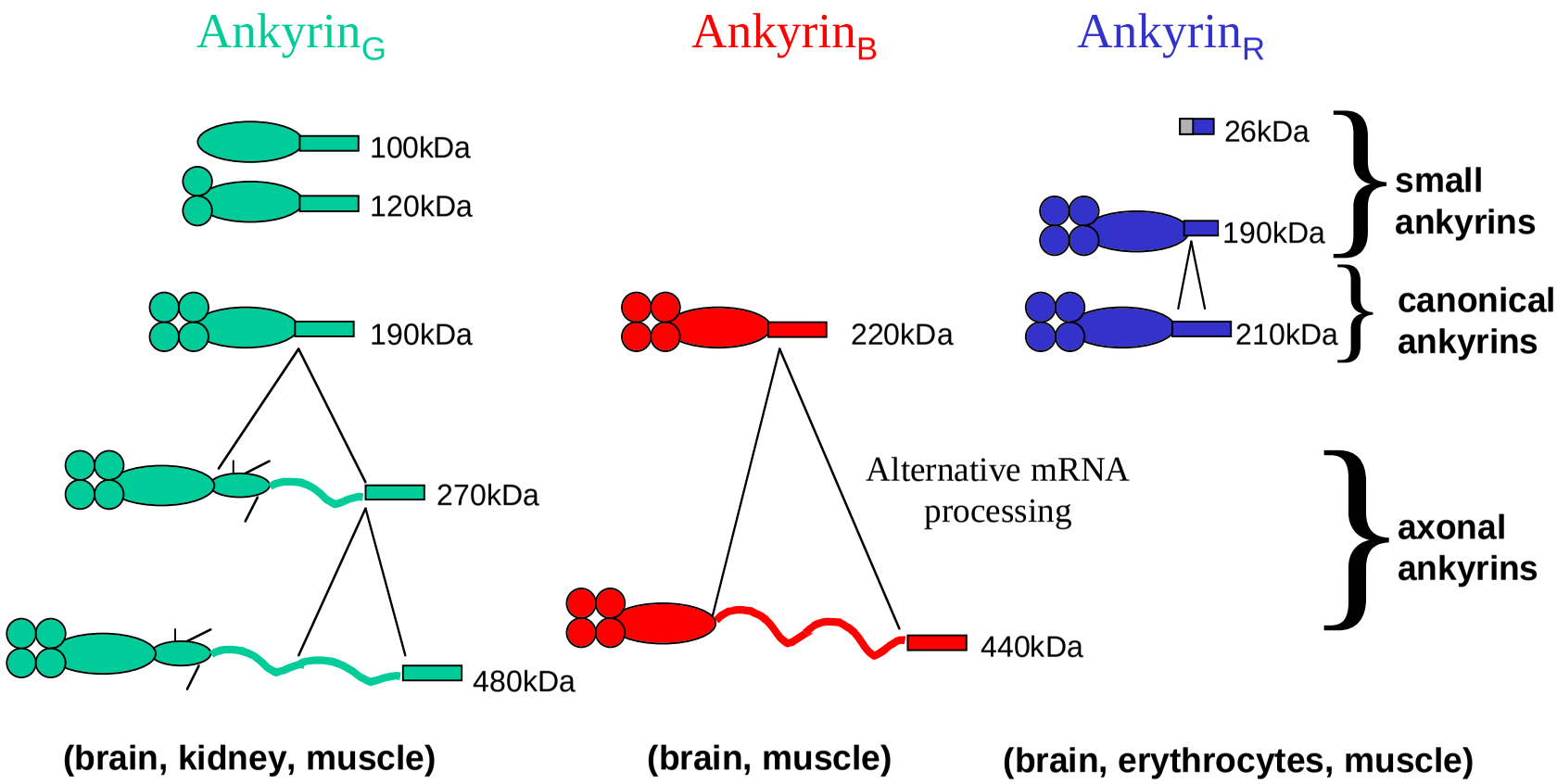

Figure 5 – Domain structure of ankyrin isoforms

Illustrated is the generalized domain structure of the ankyrin family of membrane adaptor proteins. Ankyrins maintain several conserved domains, including $NH_2$-terminal membrane-binding ANK repeats (89-95 kDa), a spectrin-binding domain (62 kDa), and a COOH-terminal death domain (12 kDa). Variable domains often utilized result from alternative mRNA processing and include an o-GlucNAc-glycosylated serine/threonine-rich region and a filamentous, extended tail domain. The ankyrin family is the product of three distinct genes with their resulting polypeptides known as $ankyrin_G$, $ankyrin_B$, and $ankyrin_R$. Shown is the organization and domain usage of the various ankyrin isoforms. While ubiquitously expressed, the ankyrins are specifically enriched in brain, kidney, muscle, and erythrocytes, as indicated.

family of neural cell adhesion molecules, including L1, NrCAM, and neurofascin (Zhang et al., 1998). Further, a highly conserved 9-amino acid motif ((V/A)P(I/L)AXXE(S/D)D) has recently been identified, which confers ankyrin binding to the α-subunit of vgscs (Lemaillet et al., 2003). However, the specificity of interactions between various isoforms of ankyrin and their membrane-associated binding partners remains unclear.

ERMs

ERM (ezrin, radixin, moesin) proteins are critical in the formation of specialized plasma membrane domains. In particular, ERMs are highly enriched in protrusive structures, like microvilli and membrane ruffles, where they link the cell membrane to the actin cytoskeleton. These three proteins are very closely related, sharing 75-78% overall identity, and are members of the band 4.1 super-family. As such, the ERMs contain the shared $NH_2$-terminal FERM (4.1, ezrin, radixin, moesin) domain, which is 32% identical to the first 300 residues of the founding family member, erythrocyte band 4.1 (reviewed in Bretscher et al., 2000; Bretscher et al., 2002; Bretscher et al., 1997). In band 4.1, this domain connects the actin/spectrin cytoskeleton to the membrane protein glycophorin C (Anderson and Lovrien, 1984; Marfatia et al., 1995; Marfatia et al., 1994) and confers membrane-anchoring properties to the ERM family.

The ERM proteins bind integral membrane proteins, i.e. CD44 (Tsukita et al., 1994), and other adaptor molecules, i.e. EBP50 (Reczek et al., 1997), via their $NH_2$-terminal regions and to actin through their COOH-terminal domains (Pestonjamasp et al., 1995; Turunen et al., 1994). However, the capacity of the ERMs to engage in these bifunctional, cross-linking interactions is dependent upon the relief of their intrinsic conformational regulation and their phosphorylation state. These proteins are maintained

in a dormant, "closed," non-phosphorylated state when the ERMs' $NH_2$-terminal 296 residues (co-incident with the FERM domain) interact with the COOH-terminal 110 residues (amino acids 467-577 in ezrin). These self-associating domains are known as the $NH_2$- and COOH-ERM association domains (N-ERMAD and C-ERMAD, respectively) and mediate both intra- and inter-molecular, high affinity interactions (Gary and Bretscher, 1995). (Fig. 6)

Activation of these proteins and the unmasking of their membrane- and actin-binding regions then require the physical separation of the ERMAD domains and stabilizing phosphorylation. First, ERMs interact with phosphatidylinositol (4,5)-bisphosphate (PIP2). PIP2 binds to the N-ERMAD region and suppresses the intra-molecular auto-inhibition (Niggli et al., 1995). This was demonstrated by the enhanced binding of full-length radixin to the cytoplasmic tail of CD44 (Hirao et al., 1996) and of ezrin to ICAM-1 and –2 (Heiska et al., 1998) in the presence of this phosphoinositide. However, PIP2-ERM binding is not itself sufficient to promote ERM activation, suggesting that PIP2 binding may induce a conformational shift toward an "open" state that renders the ERM proteins more susceptible to phosphorylation.

The recognized, activating ERM phosphorylation site is that of a conserved COOH-terminal threonine residue (ezrin T567, radixin T564, and moesin T558), originially identified in moesin during platelet activation by thrombin (Nakamura et al., 1995). The phosphorylated, active versions of these proteins mediate the organization of the cortical actin-based cytoskeleton and are specifically concentrated in microvilli and other cell surface structures (Yonemura and Tsukita, 1999). Phosphorylation at this key threonine suppresses N-/C-ERMAD interactions (Matsui et al., 1998) and is

# Figure 6 - ERM and EBP50 structure and function

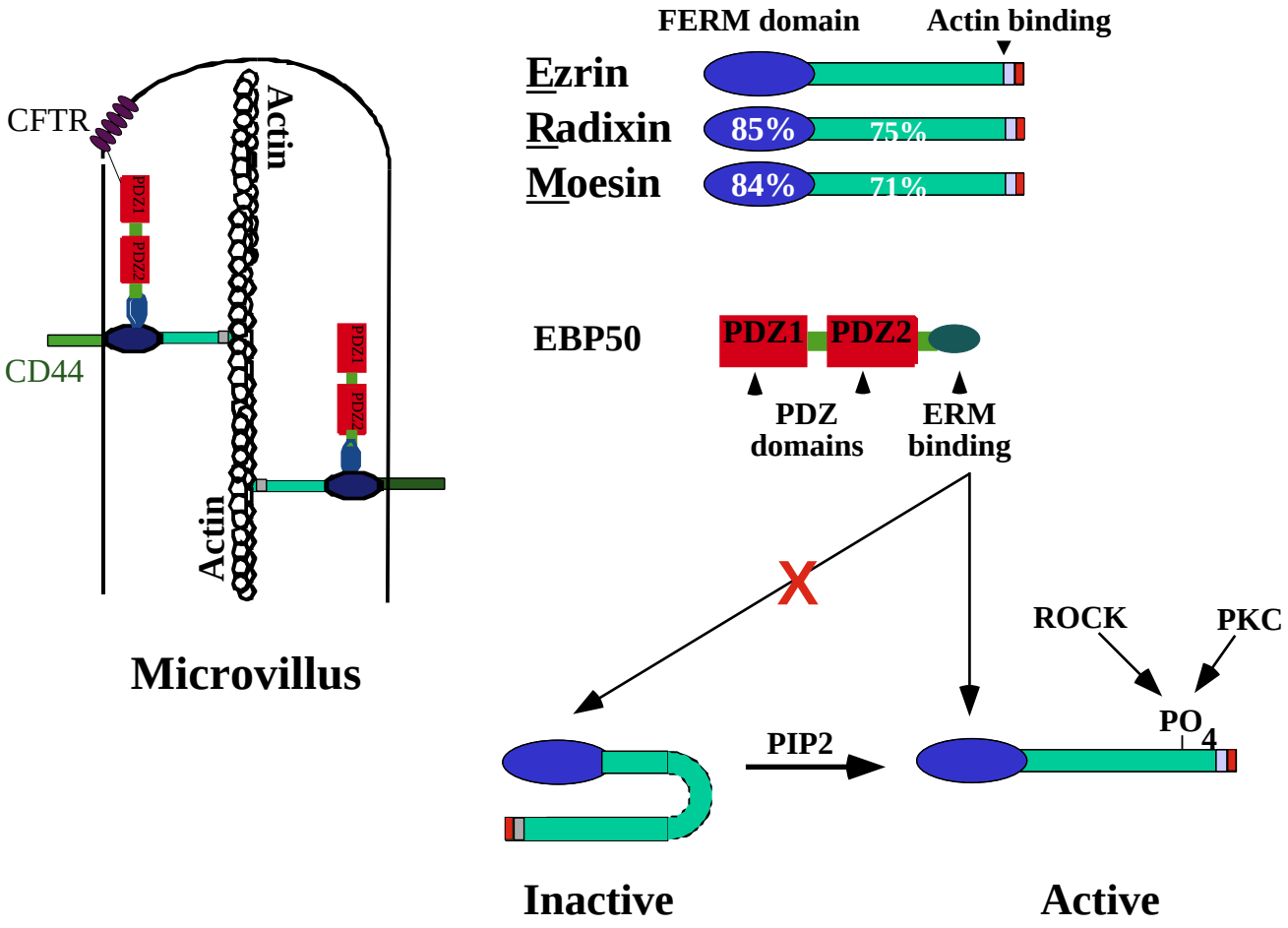

Figure 6 – ERM and EBP50 structure and function

A prototypical microvillus is shown detailing the interactions between core actin filaments, ERMs, EBP50, and integral membrane proteins. This schematic demonstrates that the ERM-membrane linkages may be direct, as with CD44, or indirect via EBP50, as with the CFTR. Also detailed is the structure of the ERM family proteins harboring globular $NH_2$-terminal (FERM) domains, α-helical central regions, and charged COOH-terminal domains. The identity of these regions in radixin and moesin are given with respect to ezrin. The domain organization of EBP50 is also shown, detailing its two PDZ domains and its COOH ERM-binding region. As described in the text, EBP50 will only interact with activated, phospho-ERMs. A proposed mechanism of ERM activation suggests a two-stage process whereby PIP2 alleviates the intrinsic conformational inhibition achieved by N- and C-ERMAD interaction allowing for COOH-terminal threonine phosphorylation by either ROCK or PKC.

accomplished by at least three different kinases, Rho-kinase (ROCK) (Matsui et al., 1998; Tran Quang et al., 2000), protein kinase Cα (PKCα) (Ng et al., 2001), and PKCθ (Simons et al., 1998). The combination of electrostatic and steric effects induced by T567/T564/T558 phosphorylation weakens the affinity of the $NH_2$- and COOH-terminal regions for one another enabling the unmasking of the functional ERM domains (Pearson et al., 2000).

EBP50

While activated ERM proteins have been shown to participate in direct membrane-cytoskeleton cross-linking, ERM-binding adaptor proteins may also be employed to accomplish these linkages indirectly. The ERM-binding phosphoprotein 50 kDa (EBP50)/NHE3 regulatory exchange factor (NHERF) is one such scaffolding protein, originally identified in the renal brush border, placental microvilli, and brain (Reczek et al., 1997; Weinman et al., 1993). EBP50 is a 357-residue polypeptide that contains two PDZ (PSD-95/DlgA/ZO-1) domains. In addition, the COOH-terminal 30 amino acids of EBP50 comprise an ERM-interacting region that tightly binds the N-ERMAD of activated, phospho-ERMs. (Fig. 6)

EBP50 binds a multitude of membrane proteins via its PDZ domains, which recognize specific consensus sequences at the extreme COOH-termini of their targets. These consensus sequences have been defined as -X-S/T-R/Y-L for PDZ1, with the experimentally determined optimal sequence being –D-T-R-L, and -S-S/T-W-L for PDZ2 (Wang et al., 1998). Containing such sequences, EBP50 interacts with, apically targets, and aids in maintaining the localization of the β2-adrenergic receptor (Hall et al., 1998a; Hall et al., 1998b), platelet-derived growth factor receptor (Maudsley et al., 2000), and

cystic fibrosis transmembrane receptor (CFTR) (Short et al., 1998; Wang et al., 1998). EBP50 has also been implicated in the regulation and intracellular trafficking of its associated proteins. Thus, EBP50 could mediate the recruitment and retention of integral membrane proteins to areas enriched in activated ERMs, such as the microvilli.

Thesis aim

As previously indicated, this thesis will examine the axo-glial contacts maintained by the SC microvilli, hypothesizing that their establishment and stability are in fact vital to appropriate myelination. Pursuant to this end, we will explore several facets of PNS myelination, including molecular alterations in axonal and SC composition upon the induction of myelination, axo-glial interactions involved in node of Ranvier formation and maintenance, myelin segment generation and maturation, and SC motility. These studies will shed new light on the dramatic events associated with initiating peripheral myelination and the dynamics of the myelinating SC.

# Chapter 2

## Methodologies

DRG and SC Culture:
Maintenance
Transfection
Retroviral Infection
Immunostaining
Live Cell Imaging

Teased Sciatic Nerve Fibers

EBP50 Construct and Antibody Generation

Presented is a detailed accounting of the methodologies and manipulations that were employed to enable the study of events in PNS myelination. Of note, our primary experimental system centers on myelinating, explanted dorsal root ganglia (DRGs). DRGs contain the cell bodies of peripheral sensory neurons that serve as conduits between the periphery and spinal cord. Also within the DRG are specialized glial cells known as satellite cells, which encapsulate the somal region of the sensory neurons (Wood, 1976). The satellite cells retain a multi-potency that allows them to be differentiated *in vitro* into myelinating cells that are functionally and phenotypically indistinguishable from SCs (Hagedorn et al., 2000a; Hagedorn et al., 2000b). This glial conversion is convincingly demonstrated by the satellite cells responding to axonal regeneration and outgrowth in DRG explants by the specific expression of the SC-restricted transcription factor, Krox20 (Murphy et al., 1996). (For purposes of clarity then, DRG-originating glial cells in the *in vitro* explants will henceforth be referred to as SCs.) This culture system permits the association of tissue-endogenous, myelinating glial cells with target axons allowing for a physiologic approximation of PNS developmental specialization.

DRG Explant and SC Cultures

DRG explants were cultured essentially as previously described (Howe and McCarthy, 1998). Spinal cords and associated DRGs were dissected out of euthanised Wistar rat embryos (E16) (Charles River, North Wilmington, MA) and rinsed in Hank's Balanced Salt Solution (HBSS) with calcium (1.2 mM) and magnesium (0.8 mM) (Sigma-Aldrich, St. Louis, MO) supplemented with 5% fetal bovine serum (FBS), 50 U/mL penicillin, and 50 μg/mL streptomycin. Ganglia were trimmed of spinal roots,

rinsed with HBSS (no serum), removed, and plated into standard feed (Basal Eagle's Medium (BME) (Sigma) including ITS+ supplements (Discovery Labware, Inc., Bedford, MA), 0.2% BSA, 10 mM HEPES, 498 mg/dL D-glucose, 100 ng/mL 2.5S NGF (Discovery Labware, Inc.), 50 U/mL penicillin, and 50 μg/mL streptomycin). Coverslips (Carolina Biologicals, Burlington, NC) were coated with 0.4 mg/mL Matrigel in BME (Discovery Labware, Inc.) and 10 μg/mL poly-D-lysine (Sigma) then maintained on Teflon circles (American Durafilm, Holliston, MA). After approximately 21 days, cultures were supplemented with 15% FBS and 50 μg/mL ascorbate to induce myelination (Eldridge et al., 1987). Cultures were incubated at 37°C in humidified 5% $CO_2$/95% room air with regular feeding every other day. In some instances, media also included various combinations of lysophosphatidic acid (LPA) (1 μM) (Sigma) and the Rho-kinase inhibitor, Y-27632, (2-20 μM) (Calbiochem-Novabiochem Corp., San Diego, CA). (Fig. 7)

Isolated SCs were cultured according to the Brockes Method (Brockes et al., 1979). P1 rat pups were euthanized and their sciatic nerves removed. The nerves were then incubated with 0.1% collagenase (Sigma) in L-15 for 30 minutes at 37°C followed by 0.1% collagenase with 0.25% trypsin for 30 minutes 37°C. After rinsing with DMEM+10% FBS the nerves were triturated and plated into the same medium in an untreated 100 mm culture dish. The next day $10^{-5}$ M 1-(β-D-arabinofuranosyl)cytosine (AraC) (Calbiochem) was added. After three days of this anti-mitotic treatment, the AraC was washed out and the cells were allowed to recover for 24 hours in DMEM+10% FBS. Anti-Thy1.1 (clone TN-26) (1:100 in DMEM) and rabbit complement sera HLA-ABC (Sigma) (1:1 in DMEM) treatment followed to remove residual fibroblasts.

# Figure 7 – Model - DRG culture establishment

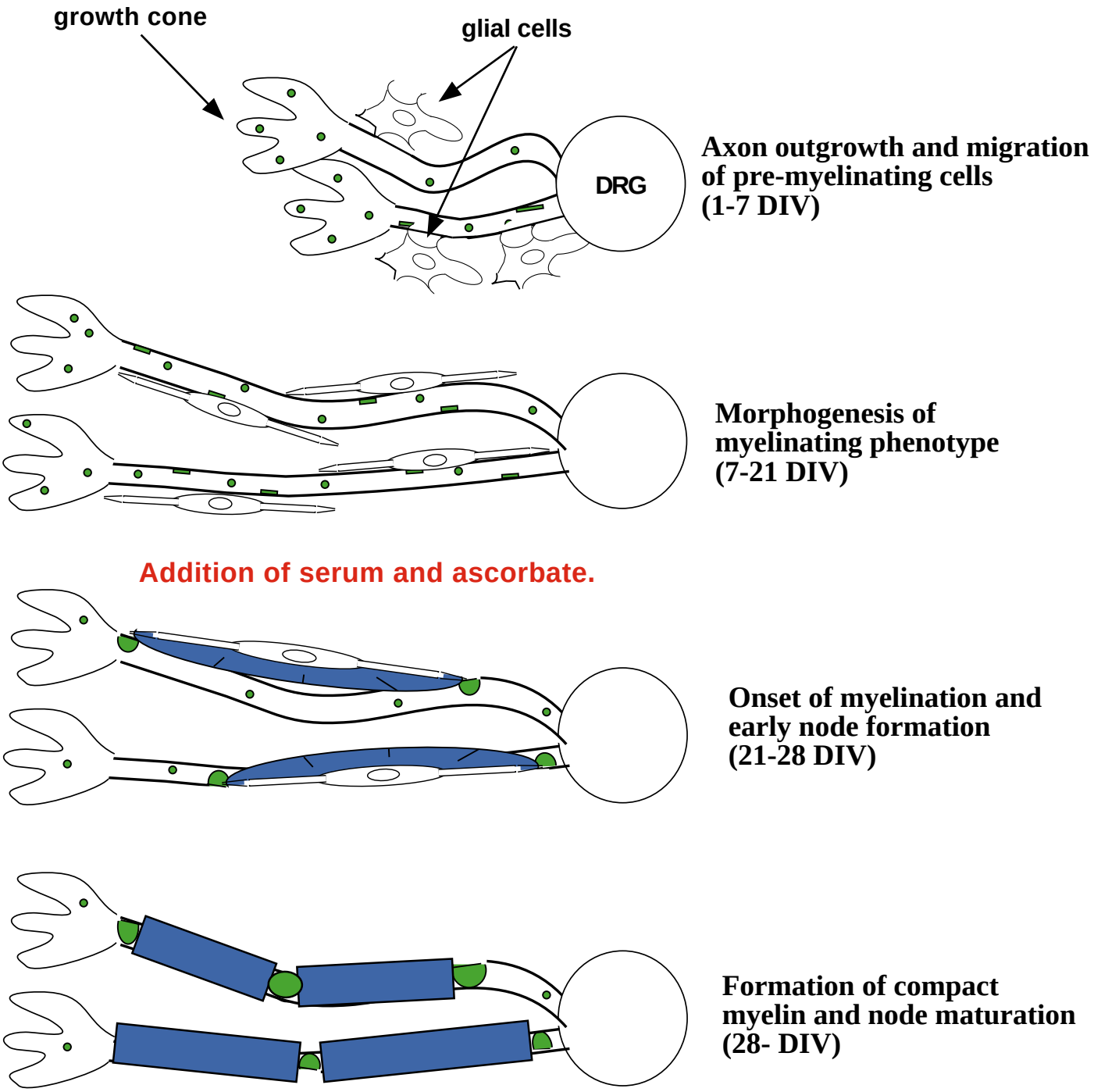

Figure 7 – Model - DRG culture establishment

These studies employ DRG explants as models for myelination and node formation. DRGs are removed from the spinal cords of E16 rat embryos. Upon plating, a rapid phase of axonal outgrowth triggers the migration and proliferation of a pre-myelinating glial population. These cells undergo differentiation toward a myelinating phenotype, including the assumption of a markedly bipolar morphology. Myelination is induced upon the introduction of serum and ascorbate to the culture media. As the cultures are allowed to mature, molecular markers indicating myelination and node formation are readily detected.

Cultures were then maintained in Primaria tissue culture flasks (Becton Dickinson, Franklin Lakes, NJ) with twice weekly feeding of DMEM+10% FBS. Expansion could be facilitated by the addition of 4 μM forskolin and 20 μg/mL bovine pituitary extract (Sigma). However, this treatment converted the cells from their bipolar spindle shape to a flattened, more fibroblastic looking morphology. Thus, expediting SC expansion was not routinely performed.

Explant Transfection

Explants were transfected using Lipofectamine PLUS (Invitrogen, Grand Island, NY). Cultures were treated for 24 hours prior to transfection with media of choice (Pedraza and Colman, 2000). One microgram of DNA per coverslip was used, and the DNA/PLUS (3.5 μL)/Lipofectamine (2.8 μL) complexes were incubated with the cultures for 3-4 hours in unsupplemented BME. The transfection mixture was then removed. The cultures were rinsed once with BME and returned to the appropriate medium.

Explant Retroviral Infection

Retroviruses were generated using ecotropic Phoenix cells (a gift of Gary Nolan, Stanford Univeristy School of Medicine, Stanford, CA). These cells were treated with selective feed, DMEM containing 10% FBS, 200 μg/mL hygromycin and 2 μg/mL diptheria toxin (Sigma), for 1 week and then allowed to recover in DMEM+10% FBS for 1 week prior to transfection with retroviral construct of interest [herein, either MSCV2.2-ires-GFP (gift of Stephen Jones, University of Massachusetts Medical School, Worcester, MA) or pBMN-ires-GFP (gift of G.N.)]. These cells were seeded in 100 mm culture dishes such that they would be 70% confluent upon transfection. Using 20 μg DNA/32.5 μL PLUS reagent/67.5 μL Lipofectamine, cultures were transfected overnight in

unsupplemented DMEM. The next day, the medium was replaced with 8 mL of DMEM+10% FBS. Cultures were allowed to produce viral particles for 48 hours. Culture supernatant was then harvested and either spun for 5 minutes at 500 g or passed through a 0.45 µm filter to remove cellular debris. Virus-containing media were aliquoted, flash frozen, and stored at –80°C.

For DRG infection, three consecutive days of retroviral exposure (d3-5 *in vitro*) were allowed. DRG explants were incubated with 1 mL retroviral medium supplemented with 4 µL Lipofectamine for 4 hours. Coverslips were then rinsed twice with unsupplemented BME and returned to standard feed.

DRG Explant and SC Immunostaining

For explant staining, which included probing for myelin components, explants were fixed for 10 minutes at 4°C in 4% paraformaldehyde/4% sucrose in PBS, pH 7-7.4. After washing with PBS, cultures were blocked with 10% BSA in PBS+0.2% triton X-100 (PBS-T) for 1 hour at 37°C. Primary antibodies were then diluted in 2% BSA in PBS-T and incubated for 1-2 hours at 37°C. Coverslips were washed with PBS-T; secondary antibodies, also diluted in 2% BSA in PBS-T (1:1000), were then added and incubated for 1 hour at 37°C. After washing with PBS-T followed by PBS alone and a water rinse, coverslips were mounted using Vectashield mounting medium (Vector Labs, Burlingame, CA). General DRG immunostaining, which did not include any processing for myelin component detection, involved explant fixation for 10 minutes at 4°C in 4% paraformaldehyde/4% sucrose in PBS, pH 7-7.4. After washing with PBS, a 7 minute permeablization using PBS-T followed. After washing with PBS, cultures were blocked with 10% BSA in PBS for 1 hour at 37°C. Primary antibodies were then diluted in 2%

BSA in PBS and incubated for 1-2 hours at 37°C. Coverslips were washed with PBS; secondary antibodies, also diluted in 2% BSA in PBS (1:1000), were then added and incubated for 1 hour at 37°C. After washing with PBS and a water rinse, coverslips were mounted using Vectashield mounting medium. SCs were processed similarly with the exception of fixation for 20 minutes at room temperature.

Using Plan Neofluar, 40X and 100X, N.A. 1.3, oil and Plan Apochromat, 63X, N.A. 1.4, oil objectives, images were captured at room temperature with IPLab Spectrum 3.1 (Signal Analytics Corporation, Vienna, VA) software on an upright Axioplan microscope (Carl Zeiss, Germany). A Sensys digital camera (Photometrics Limited, Tucson, AZ) was used. Images were imported into Adobe Photoshop 4.0 (Adobe Systems, Inc., San Jose, CA) and adjustments of contrast and brightness were made when necessary to approximate the original IPLab images. Further, Adobe Photoshop and Canvas 5 (Deneba/ACD Systems, Inc., Saanichton, BC) were used to generate multi-panel composites and final figures. Quantitative analysis was performed where indicated, and p-values associated with unpaired Student's t-tests are reported where appropriate.

Sources of primary antibodies are as follows: anti-α-tubulin – Sigma; anti-ankyrin$_B$ (Chan et al., 1993); anti-ankyrin$_G$ (Lambert et al., 1997); anti-βIV spectrin – gift from Masayuki Komada, Tokyo Institute of Technology, Japan (Komada and Soriano, 2002); anti-EBP50 as described herein (Gatto et al., 2003); anti-ERM(20109W) – gift from Elizabeth Luna, University of Massachusetts Medical School, Worcester, MA; anti-ERM and anti-phospho-ezrin(Thr567)/radixin(Thr564)/moesin(Thr558) – Cell Signaling Technology, Inc., Beverly, MA; anti-MAG – Chemicon International, Temecula, CA; anti-MBP – Boehringer Mannheim/Roche Diagnostics, Indianapolis, IN; anti-N-cadherin

- BD Transduction Laboratories, Mississauga, ON, Canada; anti-neurofascin (Lambert et al., 1997); anti-neurofilament (SMI312) – Sternberger Monoclonals, Inc., Lutherville, MD; Alexa-Fluor 594 phalloidin – Molecular Probes, Eugene, OR; anti-RhoA – Santa Cruz Biotechnology, Inc., Santa Cruz, CA; anti-T7 – Novagen, Madison, WI; and anti-VSVG - Roche Applied Science, Indianapolis, IN. All secondary antibodies were purchased from Molecular Probes.

Live Cell Imaging

Technical expertise and useful discussion regarding live cell imaging were generously provided by Joshua Nordberg and Greenfield Sluder (University of Massachusetts Medical School, Worcester, MA). Explants or dispersed SCs were either grown on 22 mm square coverslips (Carolina Biologicals) or in 30 mm Rose dishes (World Precision Instruments, Sarasota, FL) and treated as indicated. Preparations were then mounted for imaging on a DMIRE 2 inverted microscope (Leica Microsystems, Allendale, NJ) in a 37°C heated plexiglass environmental chamber. Image acquisition using a PL Fluotar, 25X, 0.75 N.A., oil objective and an ORCA ER extended range cooled CCD camera (Hamamatsu, Bridgewater, NJ) was performed using OpenLab 3.0.9 software (Improvision, Lexington, MA). Image processing was performed with OpenLab to adjust contrast when necessary and generate video files. Further processing to allow video frame rotation was performed with NIH Image 1.62 (developed at the U.S. National Institutes of Health and available on the Internet at http://rsb.info.nih.gov/nih-image/). For still frame composite generation, individual frames were exported from OpenLab and imported into Adobe Photoshop. Final figure preparation and migration distance measurements were performed using Canvas 5. Quantitative analysis was

performed where indicated, and p-values associated with unpaired Student's t-tests are reported where appropriate.

Teased Sciatic Nerve Fiber Preparation and Immunostaining

Protocols and extensive discussion regarding teased sciatic nerve fiber preparations were kindly provided by Steven Scherer (Hospital of the University of Pennsylvania, Philadelphia, PA) and Peter Shrager (University of Rochester Medical Center, Rochester, NY). Sciatic nerves were dissected from appropriately staged, euthanized Wistar rats and fixed on ice for 30 minutes-2 hours using 4% paraformaldehyde in PBS (pH 7.4). Nerves were transferred to PBS and cut, with the outer perineurial sheath on, into segments approximately 0.5 cm long. Nerves were then desheathed by grasping one end and slitting the perineurium with a 30-gauge needle. Using the fine needle, segments were subdivided into fascicles of nerve fibers. Several small fascicles were transferred to a drop of PBS onto a Vectabond (Vector Labs) or Cell-Tak (Discovery Labware, Inc.) treated slide and air dried overnight at room temperature.

Sciatic nerve fibers were permeablized by immersion in -20°C acetone for 10 minutes and then rehydrated with PBS. Blocking solution (5% goat serum in PBS, 0.02% sodium azide, and 0.1% Triton) was applied for at least 60 minutes at room temperature. Fibers were then incubated with primary antibody diluted in the blocking solution in a humidified chamber for 24 hours at 4°C. Slides were washed with PBS, and secondary antibody (diluted 1:200 in blocking solution) was then applied for 60 minutes at room temperature. Slides were rinsed with PBS and allowed to air dry. Using Vectashield as a mounting medium, slides were coverslipped and sealed for microscopy.

cDNA Constructs

An EBP50 p3xFLAG-CMV7 cDNA was kindly provided by R. Brian Doctor (University of Colorado Health Sciences Center, Denver, CO). A full length EBP50 fragment was generated using this construct as a template via PCR introducing 5' EcoRI and 3' BamHI sites for subcloning. This fragment was digested as indicated for introduction into a C2-GFP vector (Clontech, Palo Alto, CA) generating full length EBP50-GFP. For the deletion of the ERM-binding domain, the EBP50 fragment was subcloned into pBTM. The COOH-terminal 70 amino acids were removed, and EBP50-70 was liberated from pBTM by EcoRI/BglII treatment. This fragment was inserted into C2-GFP generating EBP50-70-GFP. A third EBP50 variant lacking its two PDZ-binding domains was generated as follows. EBP50-GFP was EcoRI/BamHI digested to release an EBP50 fragment that was subcloned into pBS for site-directed mutagenesis to allow SacI flanking of PDZ2. After re-introducing this fragment into pBTM, SacI and XhoI/SalI treatment removed both PDZ1 and PDZ2. EcoRI/BamHI treatment then released this fragment for the generation of EBP50-PDZ1+2-GFP. VSVG (vesicular stomatis viral G protein)-tagged wild-type and FERM domain ezrin constructs were generous gifts of Monique Arpin (Institut Curie, Paris, France), and Michael Czech (University of Massachusetts Medical School, Worcester, MA) kindly supplied PLCδ-PH-GFP cDNA. T7-tagged Kv1.5 constructs were generous gifts of David Fedida (University of British Columbia, Vancouver, BC, Canada).

EBP50 Antibody

An antibody against EBP50 was raised in rabbits for the following study (Covance, Denver, PA). A recombinant EBP50-GST fusion was generated using the

pET-41a+ vector (Novagen) expressed in bacteria, purified, and used as the immunogen. For antisera purification, His-tagged EBP50 (generated using pET-28b+ (Novagen)) was isolated using a Talon kit (Clontech, Palo Alto, CA). This fusion protein was then coupled to CNBr-Sepharose (Amersham Pharmacia, Piscataway, NJ) and used as an antibody trap in column-based, batch purification. After applying serum to the prepared column, it was washed sequentially with PBS, PBS/0.5 M NaCl, 2 M urea/0.1 M glycine/20% triton X-100, and PBS. Antibody was eluted from the column using 4 M $MgCl_2$. Eluted antibody was then dialyzed against PBS, followed by 50% glycerol in PBS, and stored at -20°C. Antibody concentration was determined by absorbance analysis, with an OD of 1.28 at 280 nm approximately equivalent to 1 mg/mL.

# Chapter 3

## DRG culture establishment and characterization defining the differential localization of ankyrinB/ankyrinG in specifc axonal populations

Myelin segment and node of Ranvier formation

Ankyrin expression in early DRG growth cones

Ankyrin$_B$/ankyrin$_G$ restriction in pre-myelinated axons based on axonal caliber

Differential ankyrin$_B$/ankyrin$_G$ localization in teased sciatic nerve fibers

Introduction

As we have discussed, the initiation and maintenance of myelination requires considerable investment from both the myelinating glial cell and the chosen axon. As molecular and morphologic alterations are effected at the axonal plasma membrane, coordinated modifications of the associated cytoskeleton are necessary. Of significant importance in myelination are the regulated expression, targeting, and retention of the ankyrins. Recall that ankyrins are membrane adaptor proteins that immobilize integral proteins linking them to the spectrin-based membrane skeleton (reviewed in Bennett and Chen, 2001; Bennett and Lambert, 1999), including cell adhesion molecules (Bourrguignon et al., 1995; Davis and Bennett, 1993; Kalomiris and Bourguignon, 1988; Zhang et al., 1998), ion channels and exchangers (Li et al., 1993; Srinivasan et al., 1988), and calcium-release channels (Bourguignon and Jin, 1995; Bourguignon et al., 1993),

Specific ankyrin isoforms localize to axonal domains and are required for appropriate neural functionality. The most abundant ankyrins present in CNS and PNS axons include the 440 kDa ankyrin$_B$ and the 480/270 kDa ankyrin$_G$. The 440 kDa ankyrin$_B$ employs similar exon usage as compared to the alternatively spliced 220 kDa isoform with the additional inclusion of a 220 kDa tail region separating the spectrin-binding domain and the COOH-terminal region (Chan et al., 1993) (Chapter 1, Fig. 5). Moreover, the 440 kDa ankyrin$_B$ is generally restricted to pre- and unmyelinated axons (Chan et al., 1993; Kunimoto et al., 1991) where it co-localizes diffusely with the cell adhesion molecule, L1. The domain usage in ankyrin$_G$ 480 kDa is similar to that of the 440 kDa ankyrin$_B$ with the addition of a serine/threonine enriched (35%), o-GlcNAc glycosylated region (residues 1478-1908) immediately after the spectrin binding domain

(Chapter 1, Fig. 5) (Kordeli et al., 1995; Zhang and Bennett, 1996). Ankyrin$_G$ 480/270 kDa localizes with the vgsc to axon initial segments and to the nodes of Ranvier with the vgsc and cell adhesion molecules, neurofascin and NrCAM, in myelinated fibers (Kordeli et al., 1995; Lambert et al., 1997).

Despite their axonal association and structural and biochemical similarities, ankyrin$_B$ and ankyrin$_G$ are not functionally redundant and maintain distinct physiologic roles. Examining the phenotypes of ankyrin$_B$ and ankyrin$_G$ knockout mice provides the best demonstration of the ankyrins' non-overlapping roles in neural development and function. Ankyrin$_B$ null mice display lateral ventricle dilation, loss of L1 from long fiber tracts in the brain and spinal cord, and severe optic nerve degeneration (Scotland et al., 1998). This mutation is lethal in the early neonatal period with resultant death by P21. Alternatively, a cerebellum-specific deletion of ankyrin$_G$ results in viable, fertile animals with no obvious neurologic defect until P16-17. This disruption of ankyrin$_G$ expression leads to a progessive ataxia including abnormal gait, tremor, and generally reduced locomotion (Zhou et al., 1998). In addition, the localization of vgscs to the initial segments of granule cell neurons is compromised, and the action potential firing capacity of the Purkinje neurons is severely impaired, leading to degeneration.

Studies in sciatic nerve and dispersed DRG cultures suggest that ankyrin$_B$ and ankyrin$_G$ isoforms are present in the same axons and may be coordinately regulated during myelination. Ankyrin$_B$ is believed to be down-regulated at the onset of myelination in a fashion similar to that of its binding partner, L1. This was initially observed in optic nerve studies where ankyrin$_B$ (and thus L1) was lost upon expression of the myelin protein, MBP (Bartsch et al., 1989; Chan et al., 1993). Accordingly, upon

myelination, ankyrin$_G$ becomes redistributed from a continuous localization along the axon to clusters at sites of nodal development. This ankyrin$_G$ reorganization occurs concomitantly with its interacting proteins neurofascin, NrCAM, and the vgsc (Chan et al., 1993; Kordeli et al., 1995; Kunimoto, 1995; Kunimoto et al., 1991; Lambert et al., 1997). (Fig. 8)

The data concluding ankyrin$_B$ and ankyrin$_G$ to be co-localized in pre-/unmyelinated axon tracts are puzzling (Lambert et al., 1997; Zhang and Bennett, 1998). While areas of overlapping ankyrin$_B$ and ankyrin$_G$ immunoreactivity are apparent, there is no mention or attempt to address the more substantial, mutually exclusive staining patterns that are also observed. As this could be of significant physiologic relevance, we examined ankyrin$_B$ and ankyrin$_G$ expression in PNS cultures derived from DRG explants allowing the distinct visualization of individual axons. Interestingly, ankyrin$_B$ and ankyrin$_G$ exhibited differential localizations to specific axonal populations. This was evident as early as one day *in vitro* in early DRG growth cones and persisted over time. In mature pre-myelinated cultures, a clear correlation between axon caliber and ankyrin expression, as detected by immunofluorescence, was identified. These observations indicate that distinct populations of axons emanate from the DRG, and contrary to previous findings, axons destined for myelination and node formation may express a distinct complement of peripheral, and by association integral, membrane proteins as compared to those observed in non-myelinated axons. These distinguishing features may play a role in the selection of axons for myelination.

# Figure 8 - Model – Myelination and proposed molecular rearrangements

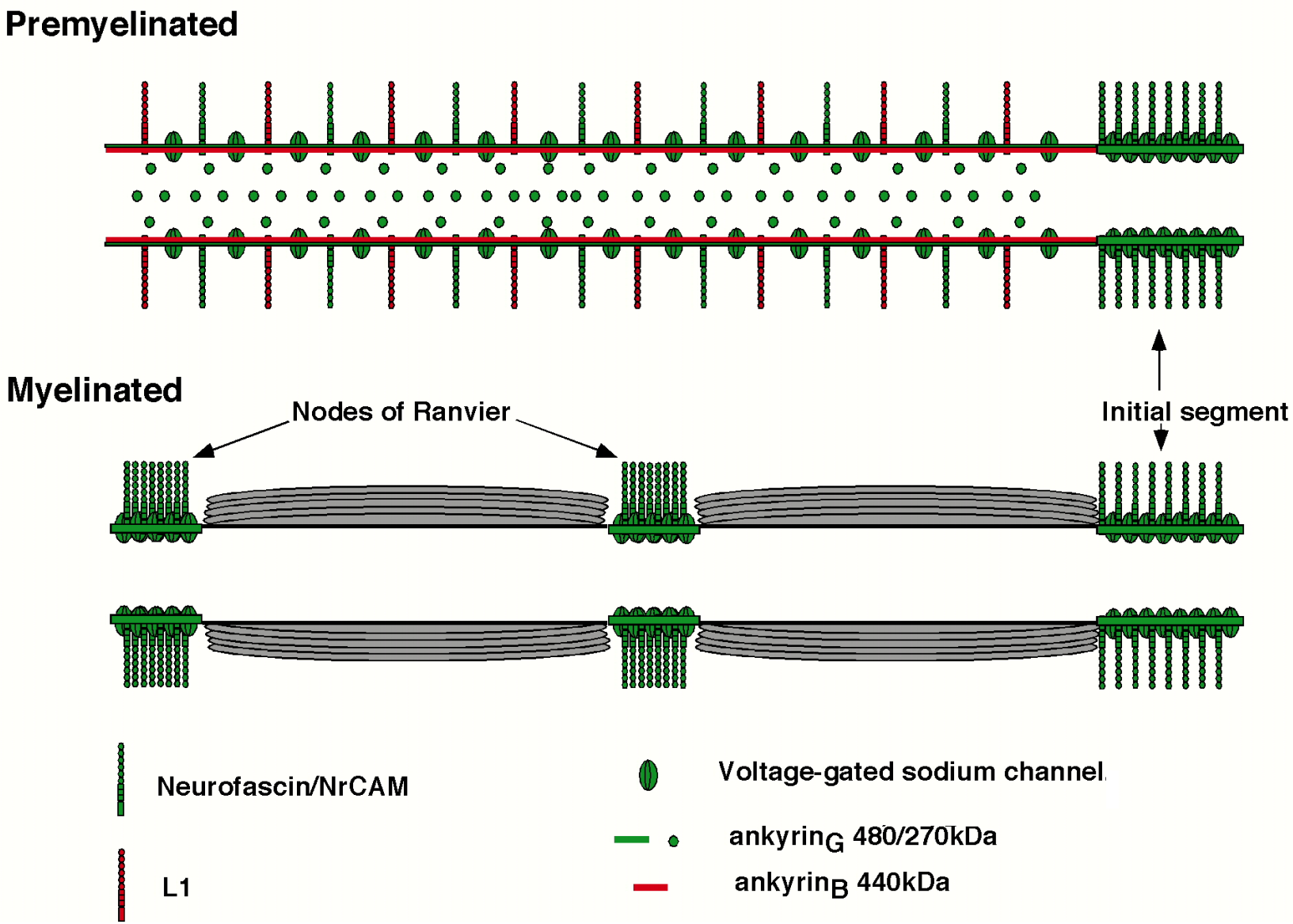

Figure 8 - Model – Myelination and proposed molecular rearrangements

Several studies suggest coordinate regulation of certain membrane-associated elements during myelination. It is proposed that in premyelinated axons, the cytoskeletal components, ankyrin$_B$ and ankyrin$_G$, cell adhesion molecules, L1, NrCAM, and neurofascin, and vgscs are maintained in a continuous distribution along the axon. Then, ankyrin$_B$ is down regulated at the onset of myelination in a fashion similar to L1. In contrast, upon myelination ankyrin$_G$ becomes redistributed and clustered at sites of nodal development with neurofascin, NrCAM, and vgscs.

## Results

### Myelin segment and node of Ranvier formation

DRG explants were established to examine PNS development, in particular to resolve ankyrin expression patterns in pre-myelinated axons. This culture system allowed the distinct visualization of individual axons in association with endogenous glial cells and could be maintained in a pre-myelinating state by culture condition manipulation. Upon the adhesion of the isolated DRGs to the prepared coverslips, neurite outgrowth proceeded with the elaboration of growth cones, which directed axonal extension. This rapid axonal outgrowth provided mito- and motogenic stimuli prompting SC proliferation and migration along the axons (Chapter 2, Fig. 7 and Video 1). Once the length of the axons were fully lined by closely associated SCs, this system allowed for the precisely controlled induction of myelination upon the addition of serum and ascorbate to the culture medium (Eldridge et al., 1987). This was evidenced by the identification of mature myelin segments, as detected by MBP immunoreactivity after 14 days induction [35 total days in culture/14 days post induction of myelination with serum and ascorbate (d35/M14)] (Fig. 9).

Sciatic nerve studies have demonstrated that as nodal development ensues, the formation of mature nodes of Ranvier involves the fusion of paired clusters of nodal components, which form at the tips of adjacent myelinating SCs in the PNS (Lambert et al., 1997). We were able to detect maturing compact, hemi-, binary, and broad nodes, detected via ankyrin$_G$ staining (Figs. 9A, B). Futher, this explant culture system allowed visualization of multiple nodal specializations along a substantial length (>500 μm) of an individual axon (Fig. 9B).

# Figure 9 - Node of Ranvier and myelin segment formation in DRG explants

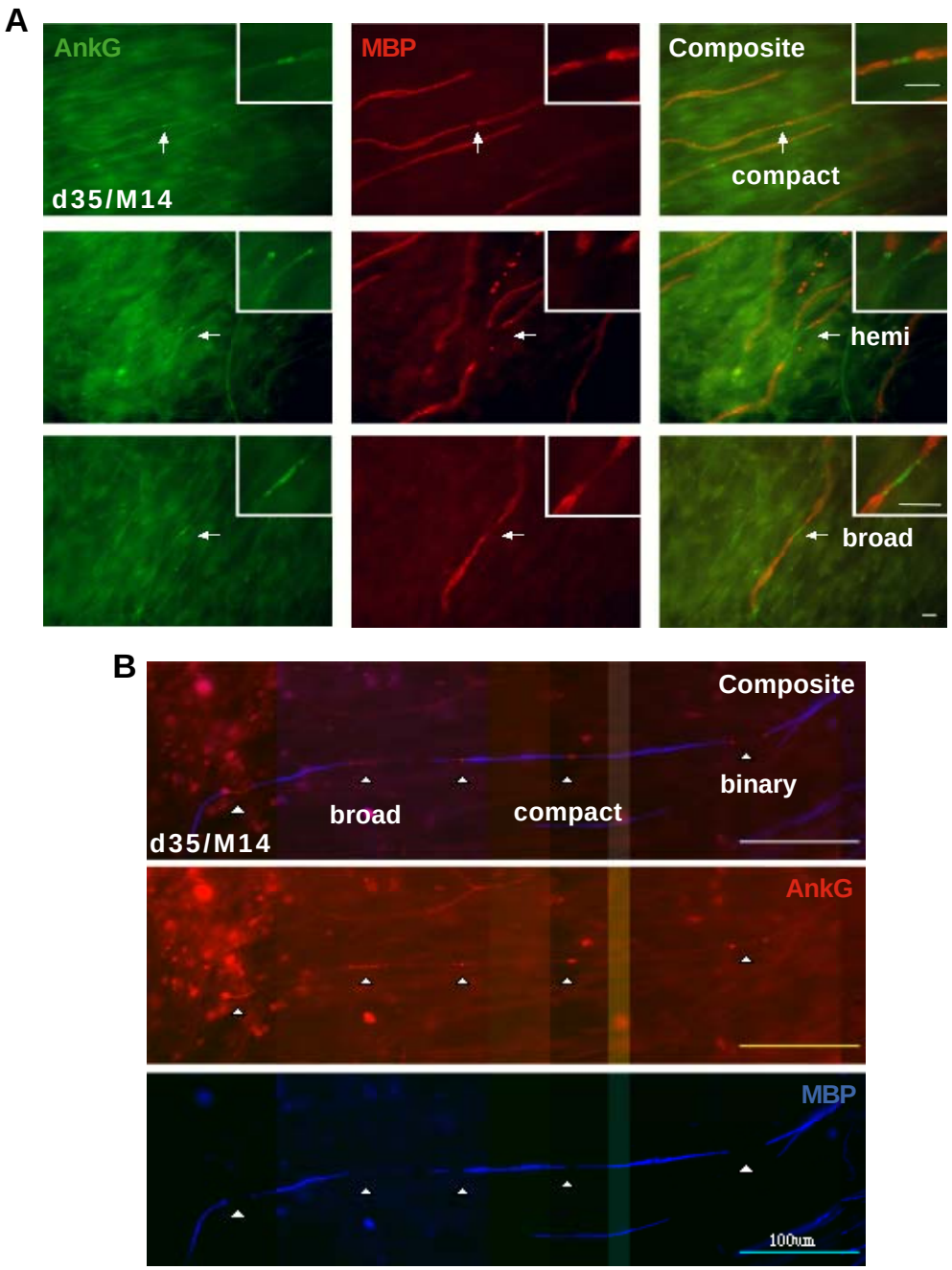

Figure 9 - Node of Ranvier and myelin segment formation in DRG explants

A) Ankyrin$_G$ (green) and MBP (red) staining were used to demonstrate nodes of Ranvier and myelin segments, respectively, after 35 days in culture and 14 days induction with serum and ascorbate (d35/M14). Composite images show mature compacting, hemi-, and broad nodes (arrows), with magnified views shown as insets. B) Ankyrin$_G$ (red) and MBP (blue) staining demonstrate numerous myelin segments and associated nodes along one individual axon over a considerable distance (>500 μm). Arrowheads indicate broad, binary, and mature, compacting nodes. Scale bar=10 μm, unless otherwise indicated.

As has been described, node formation not only includes the clustering of the cytoskeletal element ankyrin$_G$, but also the axonal cell adhesion molecules, neurofascin and NrCAM. In mature myelinated cultures (d67/M46), nodal clusters of neurofascin were readily identified in co-localization with ankyrin$_G$. Further, on rare occasion when a DRG cell body was separated from the explant proper, visualization of the axonal initial segment, which is also enriched in ankyrin$_G$, was possible (Fig. 10). In addition, the first hemi-node indicating the start of the myelinated region of the axon was also visible. An associated neurofascin cluster at the distal region of the ankyrin$_G$-stained initial segment defined its border.

These findings indicate that stages of nodal development described *in vivo* were well represented in these *in vitro* cultures. As these discrete, well-defined molecular rearrangements were clearly evident, we were confident then to examine the predicted regulation and expression of the axonal ankyrins in this system.

Ankyrin expression in early DRG growth cones

We first examined the ankyrin$_B$ and ankyrin$_G$ distributions in DRG growth cones. At d1, ankyrin staining revealed that early axons and their associated growth cones were reactive to both ankyrins, but not to the same extent (Fig. 11). Individual growth cones qualitatively more reactive to ankyrin$_B$, ankyrin$_G$, or a combination of both were readily identified. These results suggest that both ankyrins may have roles in growth cone elaboration and neurite extension. Further, their differential localization may be the first molecular indication of an inequality and distinguishing feature associated with the axons originating from the DRG explant.

# Figure 10 - Node of Ranvier and initial segment formation in DRG explants

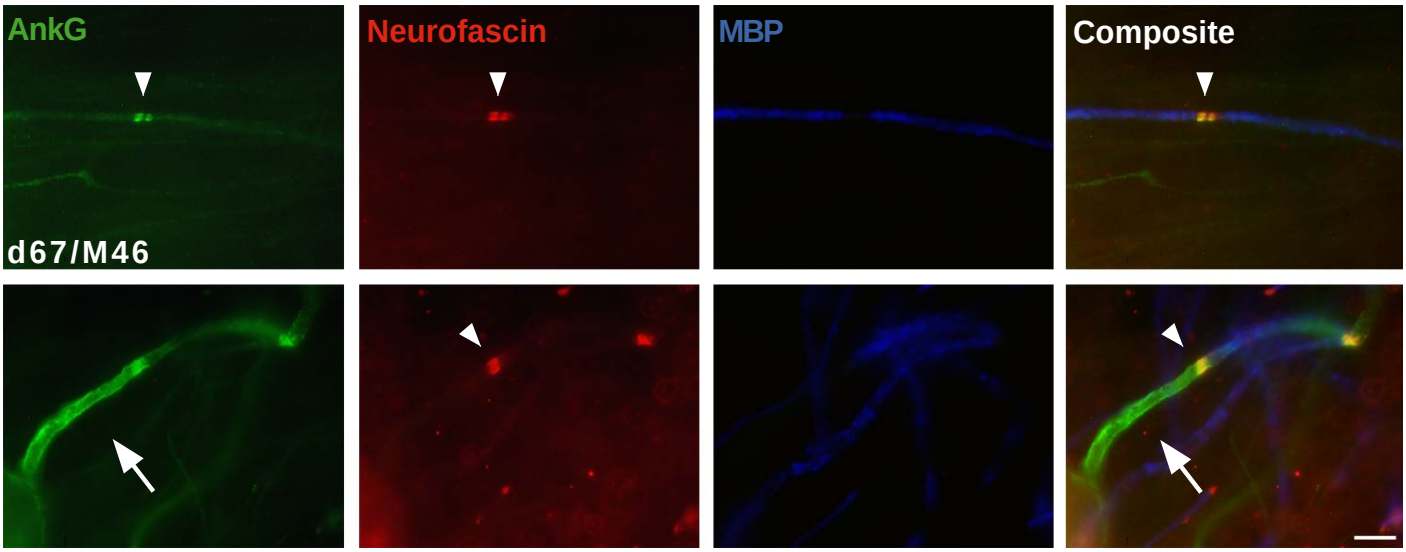

Figure 10 - Node of Ranvier and initial segment formation in DRG explants

Immunocytochemistry was performed using antibodies against ankyrin$_G$ (green), neurofascin (red), and MBP (blue) in a mature, myelinated culture (d67/M46). The top row of panels illustrates the formation of ankyrin$_G$ and neurofascin-positive nodal clusters (arrowheads) adjacent to the distal tips of the myelinating SCs. The bottom row of panels demonstrates ankyrin$_G$ localization to a DRG axonal initial segment (arrows). The neurofascin cluster immediately apposing the ankyrin$_G$ initial segment staining indicates the first nodal region of the myelinated axon. Scale bar=10 μm.

# Figure 11 - AnkyrinB and ankyrinG present in early DRG growth cones

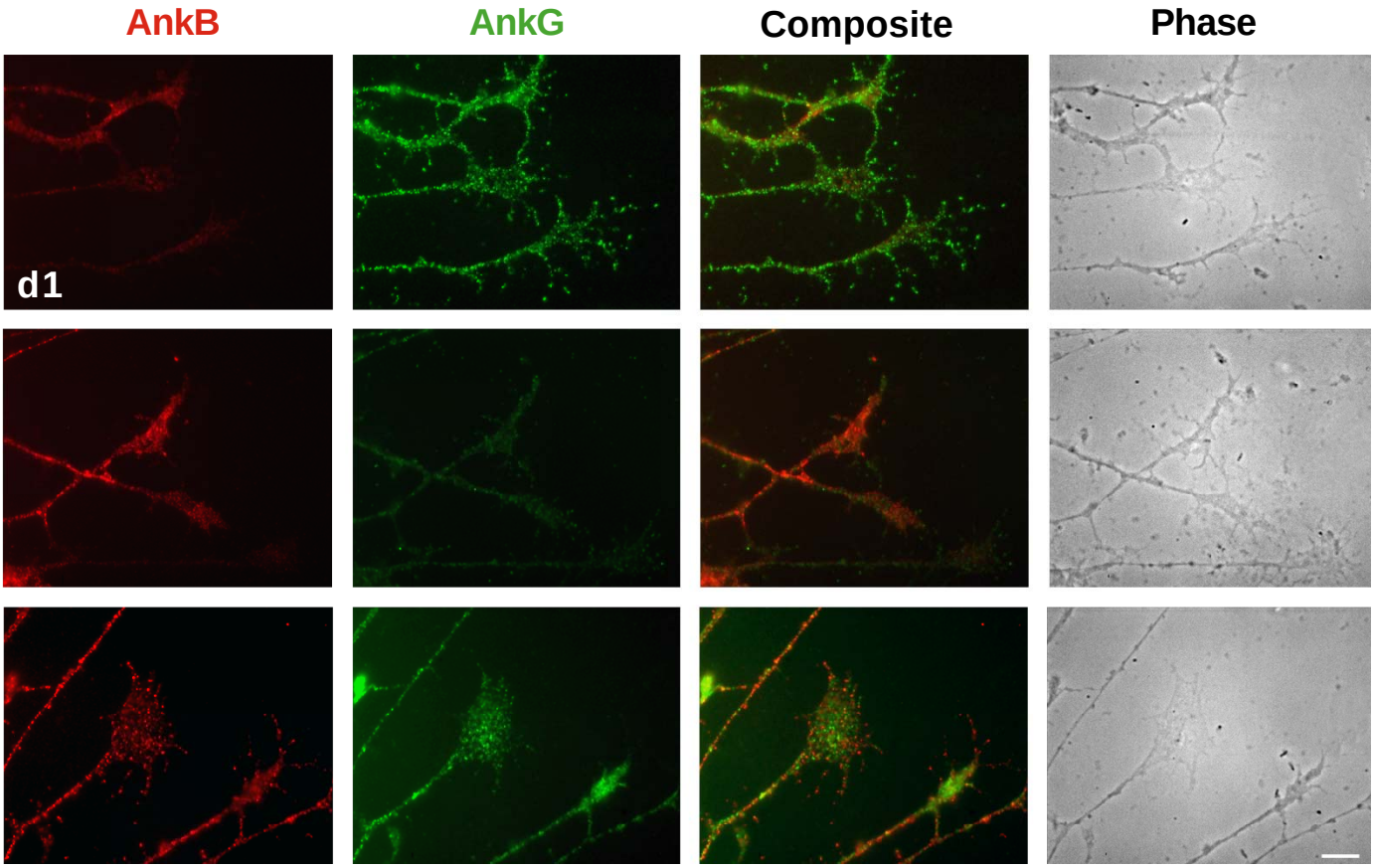

Figure 11 - AnkyrinB and ankyrinG present in early DRG growth cones

Explants (d1) were stained with antibodies against ankyrin$_B$ (red) and ankyrin$_G$ (green). This revealed different populations of axons extending from the body of the DRG. Axons and growth cones were qualitatively more reactive to ankyrin$_B$, ankyrin$_G$, or a combination of the two. Scale bar=10 μm.

AnkyrinB/ankyrinG restriction in pre-myelinated axons based on axonal caliber

As variable immunoreactivity to ankyrin$_B$ and ankyrin$_G$ was detectable as early as d1 in culture, a time course examining the localizations of these proteins was performed. Upon the examination of pre-myelinated explants from d5, 8, 14, and 28, the differential localization of the ankyrins to distinguishable, separate populations of axons was maintained (Fig. 12).

Quantitative evaluations of the observed differential localization were undertaken in mature standard cultures. At d35, pre-myelinated explants still maintained discrete ankyrin localizations (Fig. 13A). The equivalent myelination-induced stage (d35/M14) displayed clear nodal development, mature myelin segment formation, and distinct ankyrin staining patterns for both ankyrin$_B$ and ankyrin$_G$ in other pre- and/or non-myelinated axons. This was in contrast to previous findings that ankyrin expression was altered during myelination, with ankyrin$_B$ being down-regulated in myelinated axons and retained in unmyelinated axons while ankyrin$_G$ disappeared from unmyelinated axons (Lambert et al., 1997).

Interestingly, there was a distinct correlation between the ankyrin preferentially expressed and apparent axonal diameter in mature pre-myelinating explants (d41). 57.6% of the total population of axons was reactive for only ankyrin$_B$, 41.1% for only ankyrin$_G$, and 1.3% for both. Further, 94% of the ankyrin$_B$-positive axons range in caliber from 0.33-0.83 μm, whereas 64% of the ankyrin$_G$-positive axons range from 1-1.65 μm (Fig. 13B). In addition, the axonal caliber was considered in terms of only the 1 μm size requirement for PNS myelination. Of the total axons measuring less than 1 μm in diameter, 80% were immunoreactive for ankyrin$_B$. Of the axons greater than or equal

# Figure 12 - AnkyrinB and ankyrinG differentially localize in pre-myelinated DRG axons

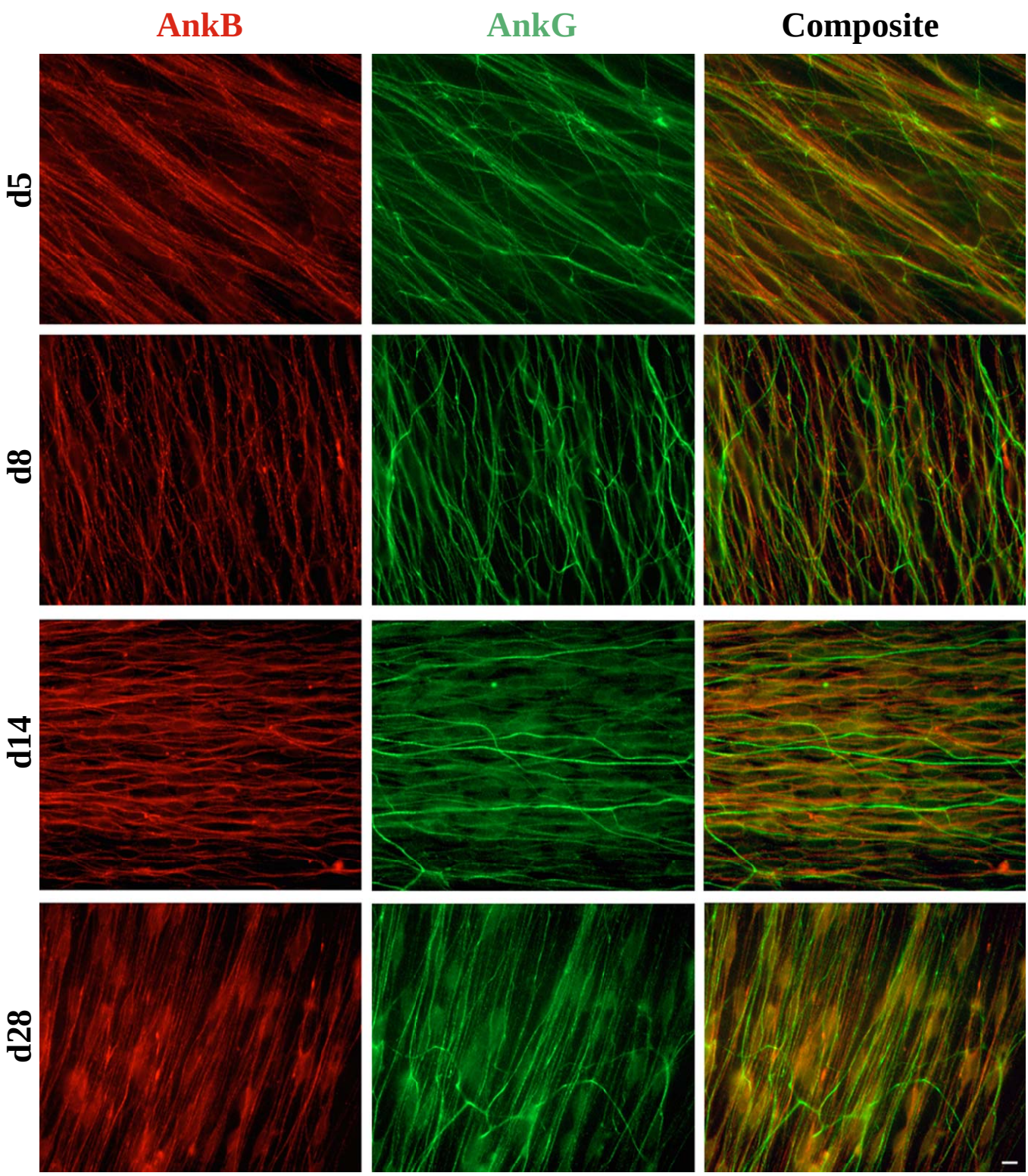

Figure 12 - AnkyrinB and ankyrinG differentially localize in pre-myelinated DRG axons

A time course of pre-myelinated explants (d 5, 8, 14, and 28) was examined for ankyrin localization. The staining patterns define axonal populations that differ in their ankyrin$_B$ (red) and ankyrin$_G$ (green) reactivity. Scale bar=10 μm.

# Figure 13 - Differential ankyrin localization correlates with axonal caliber

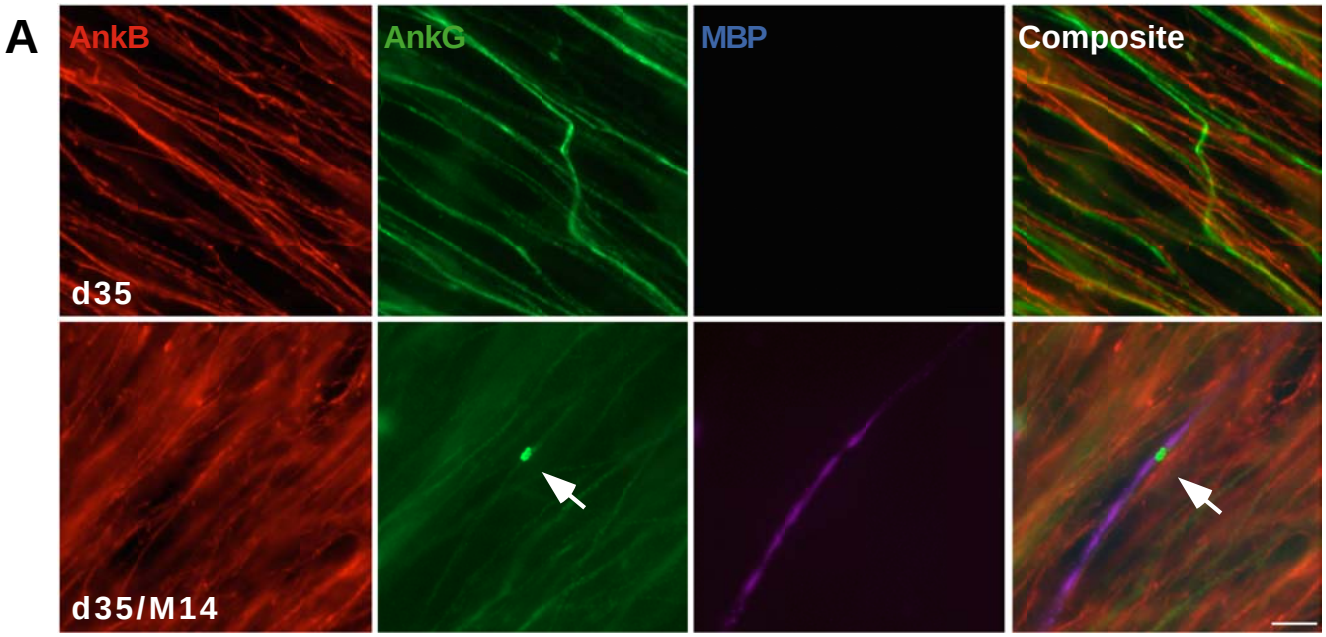


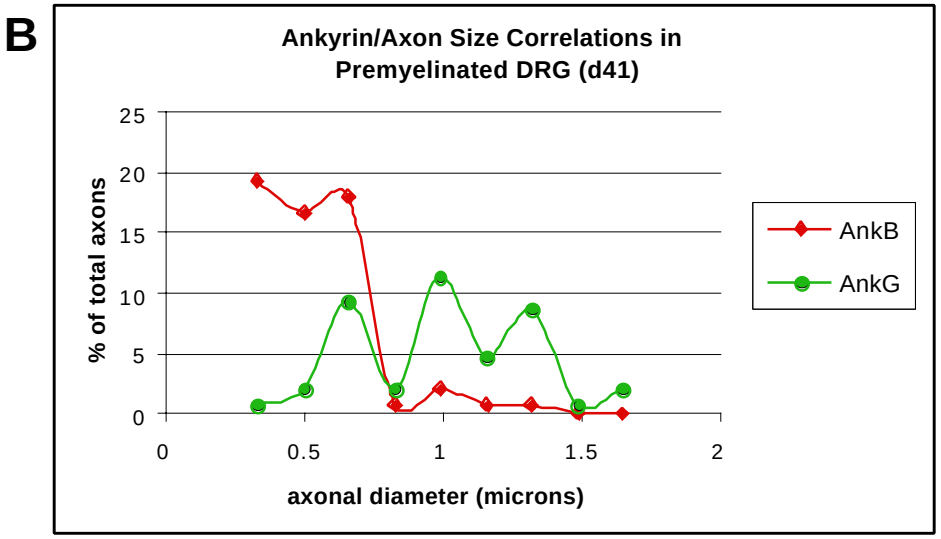


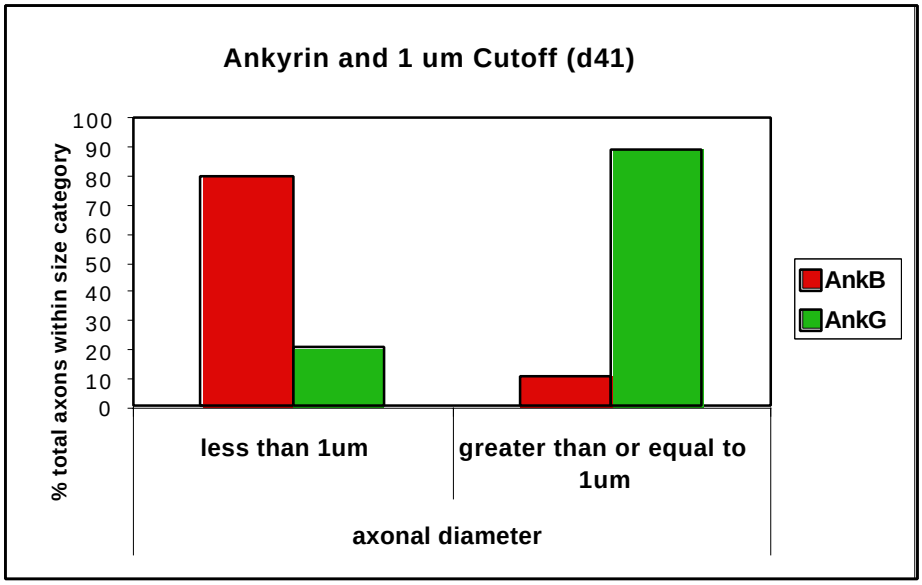

Figure 13 - Differential ankyrin localization correlates with axonal caliber

As there appeared to be a link between axonal diameter and ankyrin expression/reactivity, we examined the nature of this correlation. A) d35 pre-myelinated or d35/M14 myelinated explants were stained for ankyrin$_B$ (red), ankyrin$_G$ (green), and MBP (blue). Arrows denote nodes of Ranvier. Scale bar=10 μm. B) In a mature pre-myelinated culture (d41), 151 discretely individual axons were counted. Presented is a quantification of the relationship of ankyrin expression (B/G) and axonal diameter. 57.6% of the total population of axons was reactive for only ankyrin$_B$, 41.1% were reactive for ankyrin$_G$, and 1.3% were reactive for both. Further, 94% of the ankyrin$_B$-positive axons range in caliber from 0.33-0.83 μm, whereas 64% of the ankyrin$_G$-positive axons range from 1-1.65 μm. C) To examine the ankyrin expression pattern seen in axons likely to be myelinated, axonal diameters were classed in relation to the 1 μm size cut-off generally associated with PNS myelination. Of the total axons measuring less than 1 μm in diameter (103:151), 80% were immunoreactive for ankyrin$_B$, whereas in axons greater than or equal to 1 μm (41:151) in diameter, 89% were reactive for ankyrin$_G$.

to 1 μm in diameter, 89% were reactive for ankyrin$_G$ (Fig. 13C). These results strongly suggest a link between the axonal caliber that generally meets the PNS requirement for myelination and ankyrin expression, as detected by immunofluorescence. Thus, the ankyrin profile of an axon may be a distinguishable feature in terms of its predetermined myelination status.

Differential ankyrinB/ankyrinG localization in teased sciatic nerve fibers

As a considerable disparity was seen as to the ankyrin localization in the *in vitro* DRG explant culture system as compared to reported findings in sectioned sciatic nerve (Lambert et al., 1997), we extended our recent findings to another *in vivo* alternative. As myelination is primarily a post-natal event in the PNS (reviewed in Garbay et al., 2000), sciatic nerve teased fibers from neonatal animals were examined. P4 sciatic nerves revealed variant axonal tracts that stained, in a mutually exclusive manner, for either ankyrin$_B$ or ankyrin$_G$ (Fig. 14). These results suggest that there may indeed be *in vivo* physiological relevance to the observed *in vitro* differential ankyrin localization.

# Figure 14 - Ankyrin localization in teased sciatic nerve fibers

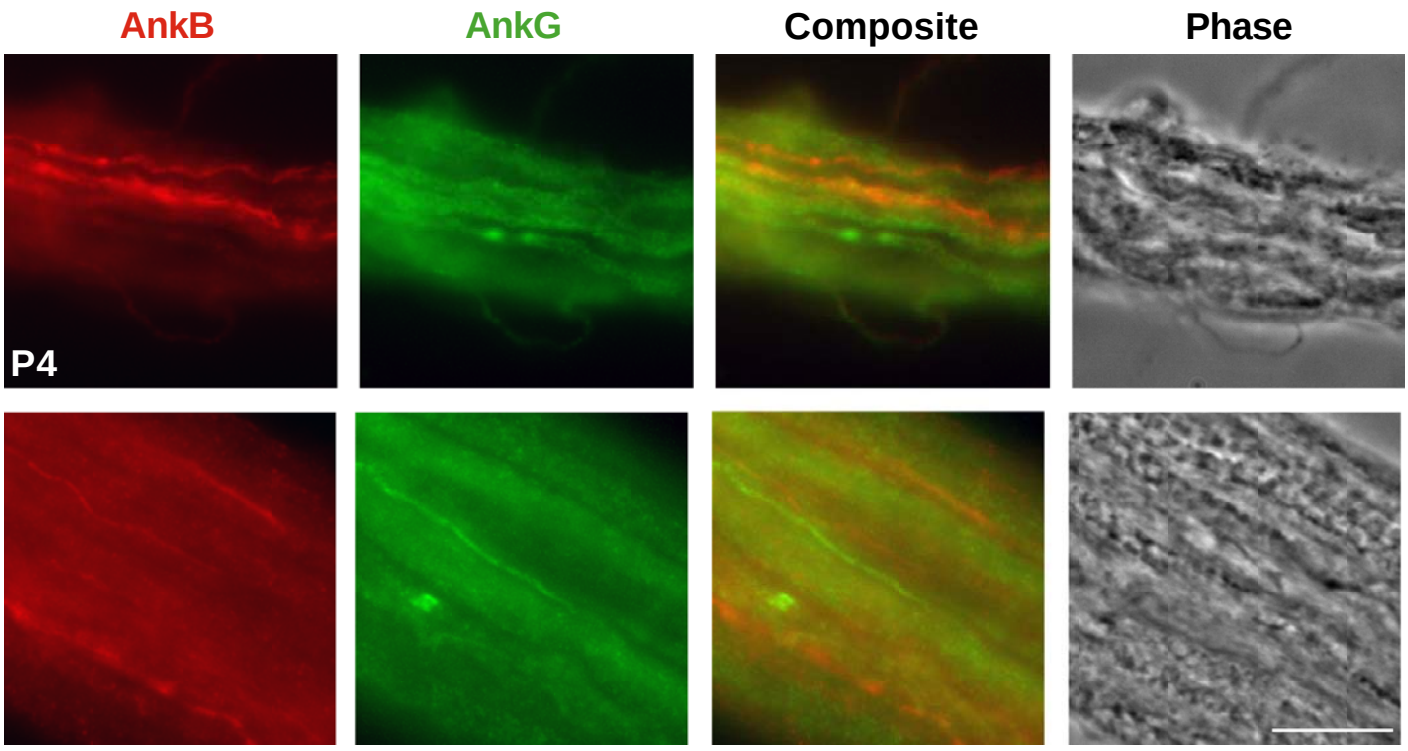

Figure 14 - Ankyrin localization in teased sciatic nerve fibers

Sciatic nerves were removed from P4 rat pups, fixed, separated, and stained. Preliminary results indicate that in pre-myelinated tissue, ankyrin$_B$ (red) and ankyrin$_G$ (green) are differentially localized in distinct axonal tracts. Scale bar=10 μm.

Discussion

This study demonstrates that the *in vitro* DRG explant culture system allows visualization of precise events in PNS myelination. This system supports the study of both axonal and SC development. Myelin segment formation is well represented, and the organization of the associated nodes of Ranvier is comparable to *in vivo* findings. Having established the appropriateness of this system for further PNS myelination-based studies, predicted myelination-dependent molecular rearrangements were examined and characterized.

We have exposed the differential localization of ankyrin isoforms in axons of variable caliber. Those axons of an appropriate apparent size ($\geq$1 μm in diameter) for myelination were shown to be specifically reactive for ankyrin$_G$, while smaller caliber axons were more frequently reactive for ankyrin$_B$. Our results sharply contrast with previous findings that indicated ankyrin$_G$ 480/270 kDa and ankyrin$_B$ 440 kDa were co-expressed together at significant levels prior to myelination and continuously co-distributed along the length of the axon (Lambert et al., 1997).

The striking difference in the cytoskeletal composition of sub-populations of pre-myelinating axons in PNS cultures may have significant implications in terms of inherent, axonal properties. In particular, the presence of a specialized cytoskeleton may translate into a distinct repertoire of membrane-associated proteins. As axonal ankyrin-binding membrane proteins, such as neurofascin, have shown no *in vitro* biochemical discrimination between ankyrin$_B$ and ankyrin$_G$ isoforms (Davis and Bennett, 1993), our evidence promotes the concept of wholly restricted ankyrin expression serving to drive particular membrane protein presentation in the PNS. Alternatively, the differential

ankyrin distribution may reflect a previously unknown step in pre-myelinated axonal commitment.

This qualitative observation requires diligent biochemical confirmation by mRNA and protein expression analysis. Also remaining to be determined in a continuation of this work is whether a coordinated differential membrane composition is associated with axons of variable caliber and the differential ankyrin expression. This could lead to the identification of target molecules that trigger axo-glial recognition cascades either initiating SC myelination (in association with ankyrin$_G$) or promoting ensheathement and maintenance of a non-myelinating SC pheontype (in association with ankyrin$_B$).

For example, one proposed mechanism for the functionality of ankyrin$_B$ and L1 in pre-/unmyelinated axons is the stabilization of axon-axon interactions. As robust inter-axon adhesion via L1 could promote axonal bundling, this would preclude SC investiture and prevent myelination by blocking achievement of the requisite 1:1 SC:axon ratio (reviewed in Bennett and Lambert, 1999). As a result, the axon-associated SC may default to a non-myelinating state and simply ensheathe the bundle. Similarly, it would be of interest to determine the fasciculated nature of axons specifically expressing neurofascin and NrCAM, which are likely to be associated with ankyrin$_G$. Perhaps these molecules generate comparably weaker adhesions than L1 itself and allow for marginal disruption of axon-axon engagement by glial cell process extension. This in turn could promote axonal segregation by pro-myelinating SCs and enable axo-glial interactions leading to myelination.

# Chapter 4

## Local ERM activation and dynamic growth cones at Schwann cell tips implicated in efficient node of Ranvier formation

Localization of microvillar components at SC tips

is an early event in the myelin program

Live cell imaging reveals the existence of a novel, dynamic

"growth cone"-like structure at the tips of myelinating SCs

Local activation of Rho signaling pathway at SC tips gives rise to

caps and influences node formation

Introduction

As previously described, myelination is a vertebrate adaptation which involves a specialized glial cell generating an insulating, multi-lamellar sheath around an associated axon (reviewed in Arroyo and Scherer, 2000; Scherer and Arroyo, 2002). This is coupled with the specific localization of vgscs to gaps in the myelin sheath, known as the nodes of Ranvier. As these channels are enriched in this domain at concentrations of minimally 40-fold excess as compared to internodal regions, the electrical requirements to promote rapid, saltatory conduction of action potentials are met while sparing a concomitant increase in axonal caliber (Ritchie and Rogart, 1977; Shrager, 1989).

The development of the nodes of Ranvier not only involves substantial morphological alterations in the myelinating glial cell but is also hallmarked by the discrete polarization of axonal cell adhesion molecules, cytoskeletal components, and ion channels, as discussed in Chapter 3. Upon myelination, the L1 cell adhesion molecule and the 155 kDa isoform of neurofascin are down-regulated and removed from the axonal plasma membrane. Conversely, the 186 kDa isoform of neurofascin and NrCAM become highly localized to the node in association with ankyrin$_G$ and vgscs (Davis et al., 1996; Kordeli et al., 1995; Lambert et al., 1997; Martini and Schachner, 1986).

The role of axo-glial contacts in promoting vgsc clustering at the node remains controversial. As indicated in Chapter 1, vgsc clusters have been observed in the axons of retinal ganglion cells cultured in the presence of oligodendrocyte conditioned media, but in the absence of cellular contact (Kaplan et al., 1997). Similarly, observations of vgsc clusters in amyelinated regions of axons from the *dystrophic* mouse (Deerinck et al., 1997) support the hypothesis that vgsc clustering is independent of glial cell contacts.

However, *in vitro* myelinating culture studies have shown a requirement for SC contacts in mediating axonal vgsc clustering (Ching et al., 1999). This is supported by *in vivo* observations, which have shown vgscs and other nodal proteins cluster in close proximity to MAG-positive SC processes during myelination of the sciatic nerve (Lambert et al., 1997; Vabnick et al., 1996). Mechanisms underlying these apparently conflicting lines of evidence remain to be determined.

In the mature PNS, axo-glial contacts at the nodes of Ranvier are established by SC microvilli (Ichimura and Ellisman, 1991), which are characterized by expression of F-actin (Trapp et al., 1989), ERMs, and EBP50 (Melendez-Vasquez et al., 2001; Scherer et al., 2001). To investigate a potential role for these microvilli in node formation, we have studied their formation in myelinating DRG explant cultures. We have observed that myelinating SCs polarize microvillar components to novel structures at their distal tips (that we have termed caps) in response to signals that induce myelin formation. These caps are enriched in microvillar components including EBP50, actin, and activated phospho-ERMs. Using EBP50-GFP as a probe in live cell imaging experiments, we observed that SC caps are highly dynamic with behavior reminiscent of an axonal growth cone. We also localized the small GTPase RhoA to the SC cap and found that activation of the Rho pathway was linked to cap formation. Together, these results suggest a localized Rho-mediated activation of ERM proteins at the SC cap. Further, the uncoupling of cap formation and myelination interfered with efficient node formation, implicating the SC as having a direct role in establishment of the nodes of Ranvier.

## Results

### Localization of microvillar components at SC tips is an early event in the myelin program

In this study, myelinating DRG explants were used to examine SC differentiation and formation of the nodes of Ranvier. This system allowed for the controlled induction of myelination upon the addition of serum and ascorbate to the culture media. This enabled the consistent generation of substantially myelinated cultures, as indicated by MBP staining to reveal compacted myelin (Fig. 15B). Occasionally, small numbers of segments were also observed in cultures maintained in standard feed (Fig. 15A). When present, these segments were aberrantly short with irregular morphology and inconsistent nodal association.

To follow the evolution of nodal SC microvilli in our myelinating cultures, we generated an antibody to EBP50. EBP50 was observed to localize to the SC nodal collar of microvilli in mature myelinated (d47/M26), confirming *in vivo* observations in mature sciatic nerve (Melendez-Vasquez et al., 2001). Staining at the nodal regions illustrated EBP50 encompassing ankyrin$_G$, which is known to localize to the electron dense undercoating at the nodal axolemma (Kordeli et al., 1990) (Fig. 15C-G, supplemental material Fig15video2).

EBP50 polarization in less differentiated cultures was then examined. MAG, which is expressed abaxonally by myelinating SCs after approximately 1.5 wraps around its associated axon (Martini and Schachner, 1986; 1988), was used to visualize earlier stages of myelination. After 5-6 days of induction, EBP50 localized to both heminodal and binary intermediates adjacent to MAG-positive SCs (Fig. 15M) and in close proximity to axonal clusters of βIV-spectrin (Fig. 15J), a second marker for the nodal,

# Figure 15 - EBP50/ERM localization to early and mature nodes in myelinating DRG explant cultures

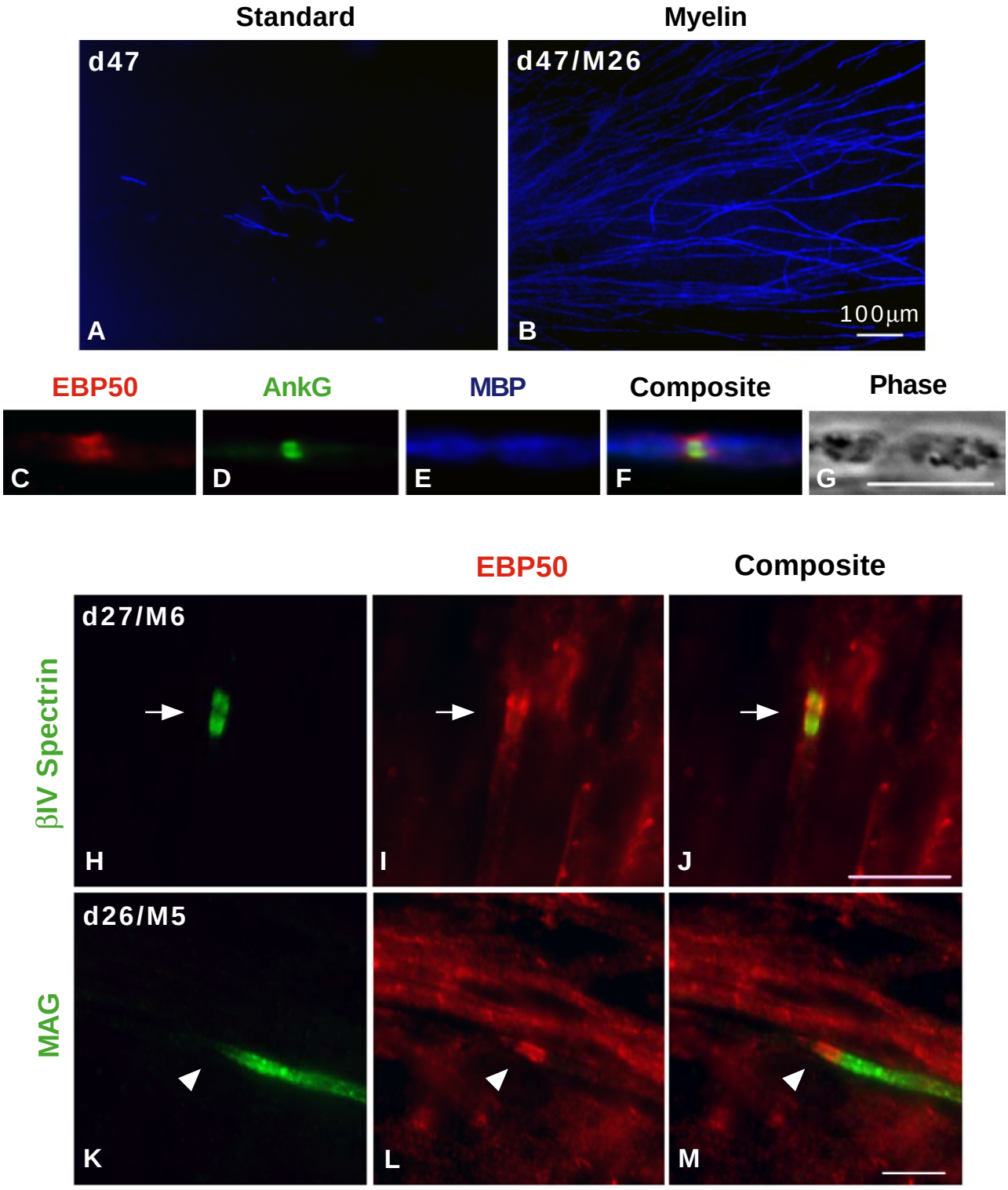

Figure 15 - EBP50/ERM localization to early and mature nodes in myelinating DRG explant cultures

Myelinated and comparable control cultures were stained for MBP to show mature myelin (A-ST:d47, B-MY:d47/M26). EBP50/ankyrin$_G$/MBP triple labeling revealed nodal specializations (C-E). Note SC microvillar EBP50 staining encompassed axonal ankyrin$_G$ (F). See also Fig15video2-node.mov. Less differentiated cultures (M5/6) were stained with EBP50 (I, L) and either βIV-spectrin (axonal marker) (H) or MAG (early myelin marker) (K). EBP50 was clearly present at early hemi- (arrowheads) and binary (arrows) nodes (M, J). Scale bar=10 μm, except where indicated.

axonal, membrane-associated cytoskeleton (Berghs et al., 2000; Komada and Soriano, 2002). These results indicate a distinct localization of microvillar components, if not microvilli proper, at mature and developing nodes.

The three ERM proteins (ezrin, radixin, and moesin) are present in SC microvilli (Melendez-Vasquez et al., 2001; Scherer et al., 2001). Hence, we utilized a pan-ERM antibody in conjunction with our EBP50 antibody to examine microvillar organization in developing SCs. After 6 days *in vitro*, EBP50 and ERM staining revealed numerous microvilli (Fig. 16A-B) covering the surface of migrating glial cells. Mature SCs, characterized by a bipolar phenotype (Jessen et al., 1994), also exhibited numerous microvilli decorating their length (Fig. 16C).

Cultures were then supplemented with serum (15%) and ascorbate (50 μg/mL) to promote myelination (Eldridge et al., 1987), and a dramatic reorganization of the SC microvilli was seen. Upon induction (d27/M6), EBP50 staining became concentrated at the distal tips of the elongated SCs (Fig. 16G), which was not observed in equivalent control cultures (Fig. 16E). Notable variations in tip morphology and EBP50 localization were also observed suggesting a dynamic component involved in cap formation (Fig. 16I-K).

Live cell imaging reveals the existence of a novel, dynamic "growth cone"-like structure at the tips of myelinating SCs

To visualize the dynamics of cap formation in live cells, an EBP50-GFP fusion construct was used. When transfected into myelinating DRG cultures, this construct was observed to localize to cap structures at SC tips (Fig. 17A). Moreover, this localization required the ERM binding site of EBP50 (data not shown, addressed fully in Chapter 5).

# Figure 16 - EBP50/ERM localization in pre-myelinating/induced DRG explant cultures changes from cell surface microvilli to a focal concentration at the SC tip

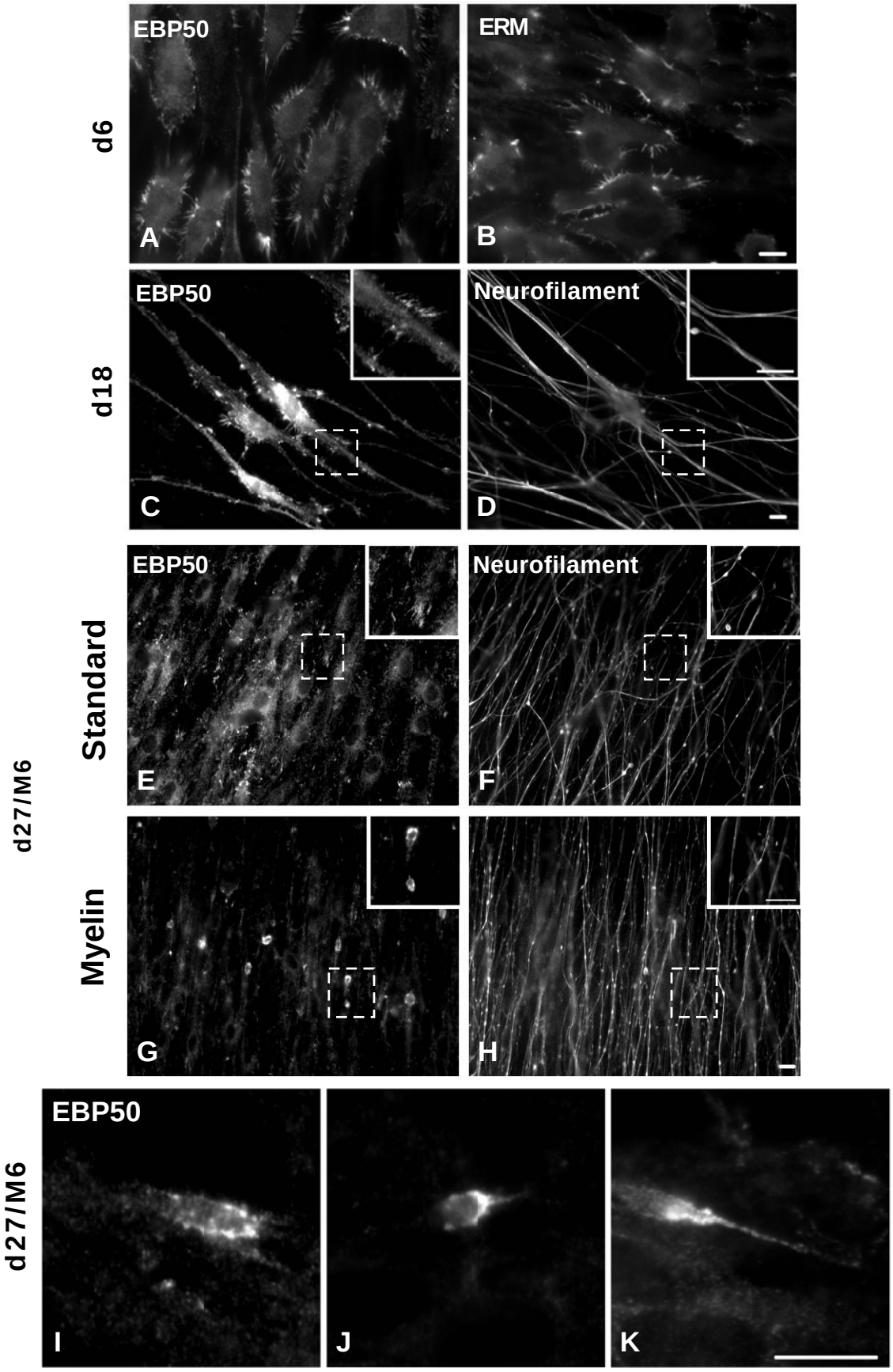

Figure 16 - EBP50/ERM localization in pre-myelinating/induced DRG explant cultures changes from cell surface microvilli to a focal concentration at the SC tip

After 6 days *in vitro*, cultures were stained for EBP50 (A) and ERM (20109W) (B). Note the numerous cell surface microvilli present on migrating SCs. After 18 days, cultures were stained for EBP50 (C) and neurofilament (D). Bipolar SCs displayed microvilli along their length. Matched standard cultures (d27) and cultures induced to myelinate with serum and ascorbate (d27/M6) were stained for EBP50 (E, G) and neurofilament (F, H). There was discrete localization of EBP50 to SC tips in the induced cultures. These EBP50-positive tips were also found with varying morphologies (I-K). Scale bar=10 μm.

# Figure 17 - Dynamic EBP50/ERM-positive SC distal tips

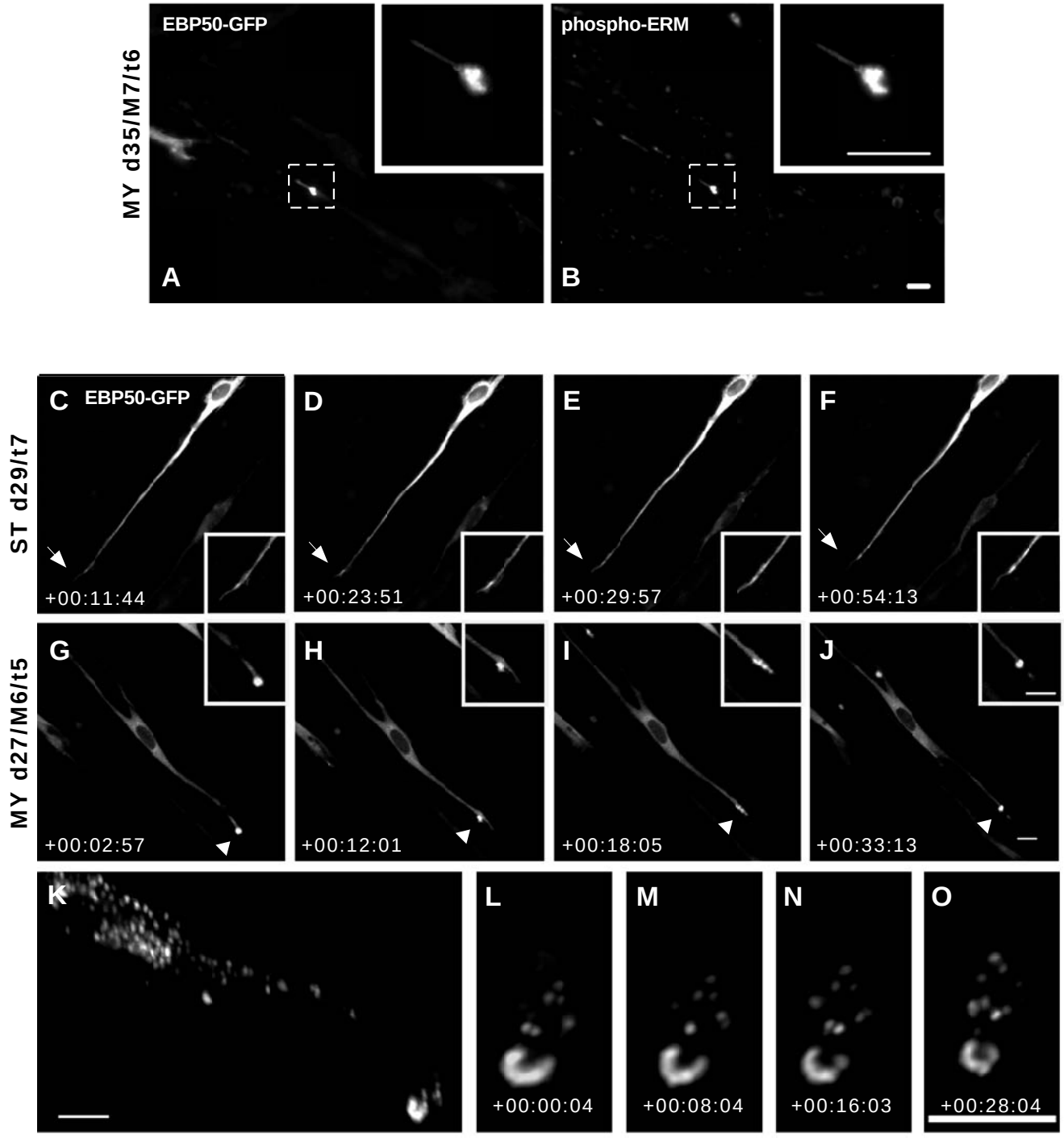

Figure 17 - Dynamic EBP50/ERM-positive SC distal tips

Cultures were transfected after 1 day of induction. After 5 days of transfection, EBP50-GFP (A) was seen to co-localize with endogenous phospho-ERM staining at SC tips (B). These transfected cultures were then examined via time-lapse microscopy. SCs in standard cultures (d29/t7) (C-F) showed no specific localization of EBP50-GFP at their tips (arrows). See also Fig17video3-EB-ST.mov and Fig17video4-EB-tip-ST.mov. SCs in myelinating cultures (d29/M6/t5) (G-J) had dynamic, remodeling EBP50-GFP-positive tips (arrowheads). See also Fig17video5-EB-MY.mov and Fig17video6-EB-tip-MY.mov. Further, deconvolution microscopy revealed EBP50-GFP as having a punctate distribution (K-O). Scale bar=10 μm.

As the binding site for EBP50 is masked on inactive ERM molecules (Gary and Bretscher, 1995; Matsui et al., 1998), these results suggest that localization of EBP50-GFP to SC caps reflects the local activation of ERM molecules at these sites. In support of this idea, EBP50-GFP was found to co-localize with COOH-terminal phospho-ERM staining (Fig. 17B), indicative of active forms of these proteins (Reczek et al., 1997; Reczek and Bretscher, 1998).

Time lapse imaging of explants harboring EBP50-GFP transfected SCs demonstrated the dynamics of the EBP50-positive tips. Cultures sustained in standard feed [29 total days in culture/7 days post-transfection (d29/t7)] maintained EBP50-GFP diffusely throughout the cytoplasm without any distinctive localization (Fig. 17C-F, supplemental material Fig17video3-4). Notably, these EBP50-GFP transfected SCs appear smoother than comparable EBP50-stained SCs under standard conditions (Fig. 16C). Due to the lower magnifications used for time lapse imaging and over-expression of the construct, fluorescence from the cell body overwhelms the signal contributed from the fine microvilli along the SC length. However, in cultures supplemented to promote myelination (d27/M6/t5), EBP50-GFP became highly localized to SC tips and displayed active remodeling (Fig. 17G-J, supplemental material Fig17video5-6). Deconvolution microscopy demonstrated EBP50-GFP in a punctate distribution throughout the cell body as well as concentrating at SC tips (Fig. 17K-O).

To determine whether the GFP-remodeling reflected actual changes in the morphology of the SC tip, we studied acutely dispersed SC preparations. These isolated SCs were derived from P2 sciatic nerve and were cultured in the absence of *in vitro* axonal contact. This allowed for visualization of individual cells that was not possible

without transfection in explants due to the culture complexity. As observed in explant SCs, isolated bipolar cells displayed discrete tips enriched in microvillar components, such as EBP50 and actin (Fig. 18A-H). Further, the tip-localizing ERMs were activated versions of these proteins (Fig. 18I-L), whereas non-phosphorylated ERMs were diffusely present in the SC body and processes (Fig. 18M-P). Concentrations of RhoA were also observed at the SC tips (Fig. 18Q-T). Specifically, 79.1±1.7% (data presented as mean±SEM) of SC tips that were positively immunostained for either EBP50 or phospho-ERM also displayed accumulations of RhoA.

As explant studies demonstrated the specific rearrangement of EBP50 at SC tips, isolated SCs were then imaged to examine the general nature of the cells' distal region. SC tips were reminiscent of actively remodeling axonal growth cones. Isolated cells revealed significant detail including the elaboration of lamellipodia and extension of fillopodia (Fig. 19). We hypothesize that these SC distal tips may then serve as novel glial growth cone-type structures that enable axonal recognition and segregation as well as the establishment of early nodes in the process of myelination.

Local activation of Rho signaling pathway at SC tips gives rise to caps and influences node formation

SC caps were observed to form in response to culture conditions that promoted myelination in DRG explant cultures, namely the addition of serum and ascorbate. To determine which of these components stimulated cap formation, cultures were independently supplemented with either serum or ascorbate. It was observed that the presence of serum was required for cap formation in studies of endogenous EBP50 staining (Fig. 20A-D). Quantitative analysis of this phenomenon using EBP50-GFP

# Figure 18 - EBP50, actin, activated ERMs, and RhoA localize to SC tips

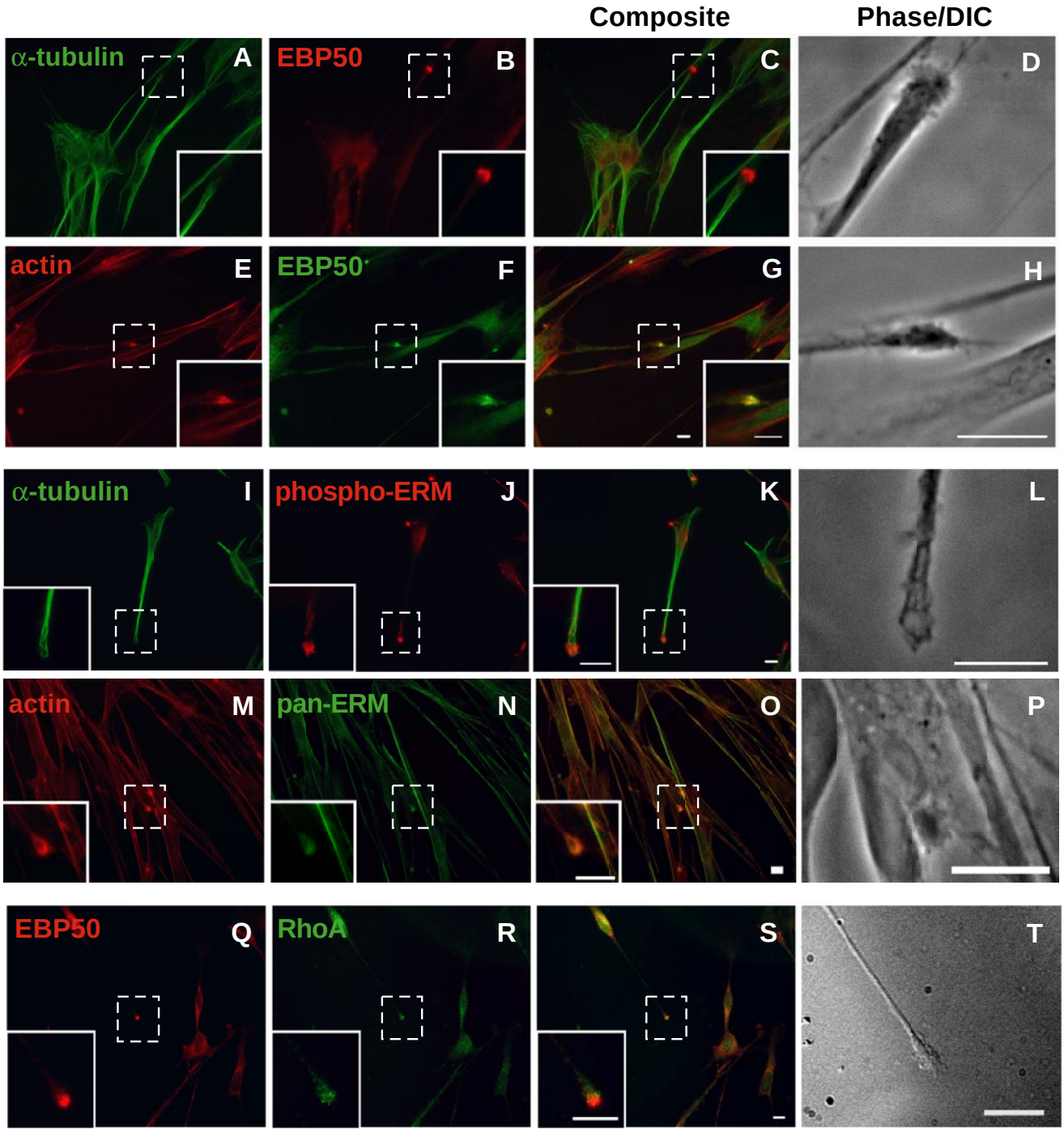

Figure 18 - EBP50, actin, activated ERMs, and RhoA localize to SC tips

Isolated SCs were stained to identify other proteins residing at the tips. EBP50 was found at the tip of α-tubulin containing SC processes (A-C). Actin co-localized with EBP50 at the SC tip (E-G), as did activated, phospho-ERMs (I-K). Pan-ERM antibody (Cell Signaling Technology, Inc.) staining revealed ERMs generally present at the SC tips. However, this staining was less concentrated at these sites than is observed with activated ERMs and more diffusely localized throughout the SC body and processes (M-O). In addition, the small GTPase RhoA localized generally to the SC distal tip in close proximity to EBP50 (Q-S). Quantitatively, 79.1±1.7% of EBP50 or phospho-ERM reactive SC tips displayed distal RhoA accumulations (N=4 independent experiments with an average of 98.5±10.9 cells counted). Scale bar=10 μm.

# Figure 19 - SC tips display novel growth cone-like behavior

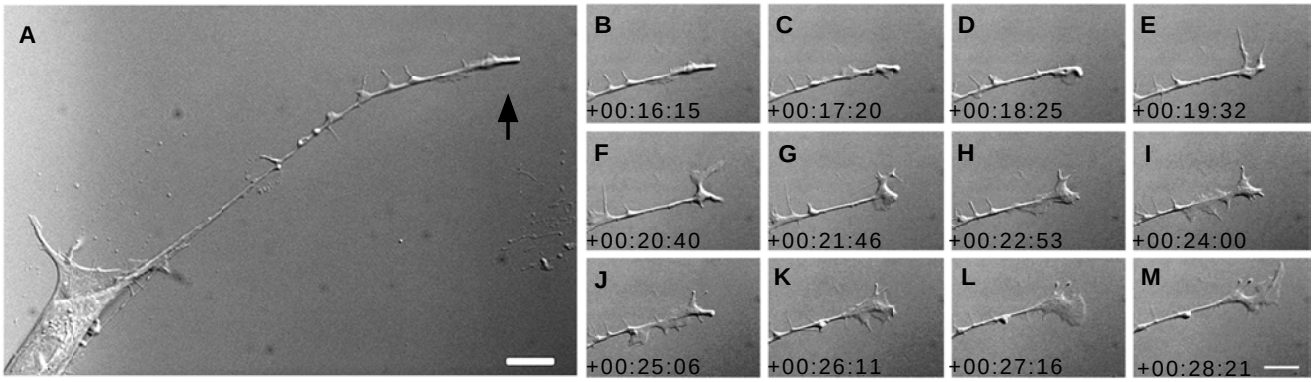

Figure 19 - SC tips display novel growth cone-like behavior

Isolated SCs were studied using time-lapse live cell imaging. SC tips (arrow) displayed dynamic, active remodeling similar to that seen in an axonal growth cone (B-M). Specifically, filopodial extensions (E, F) and lamellipodial elaborations (G-M) were evident. Scale bar=10 μm.

# Figure 20 - Cap formation is dependent upon serum and can be promoted via Rho-stimulation

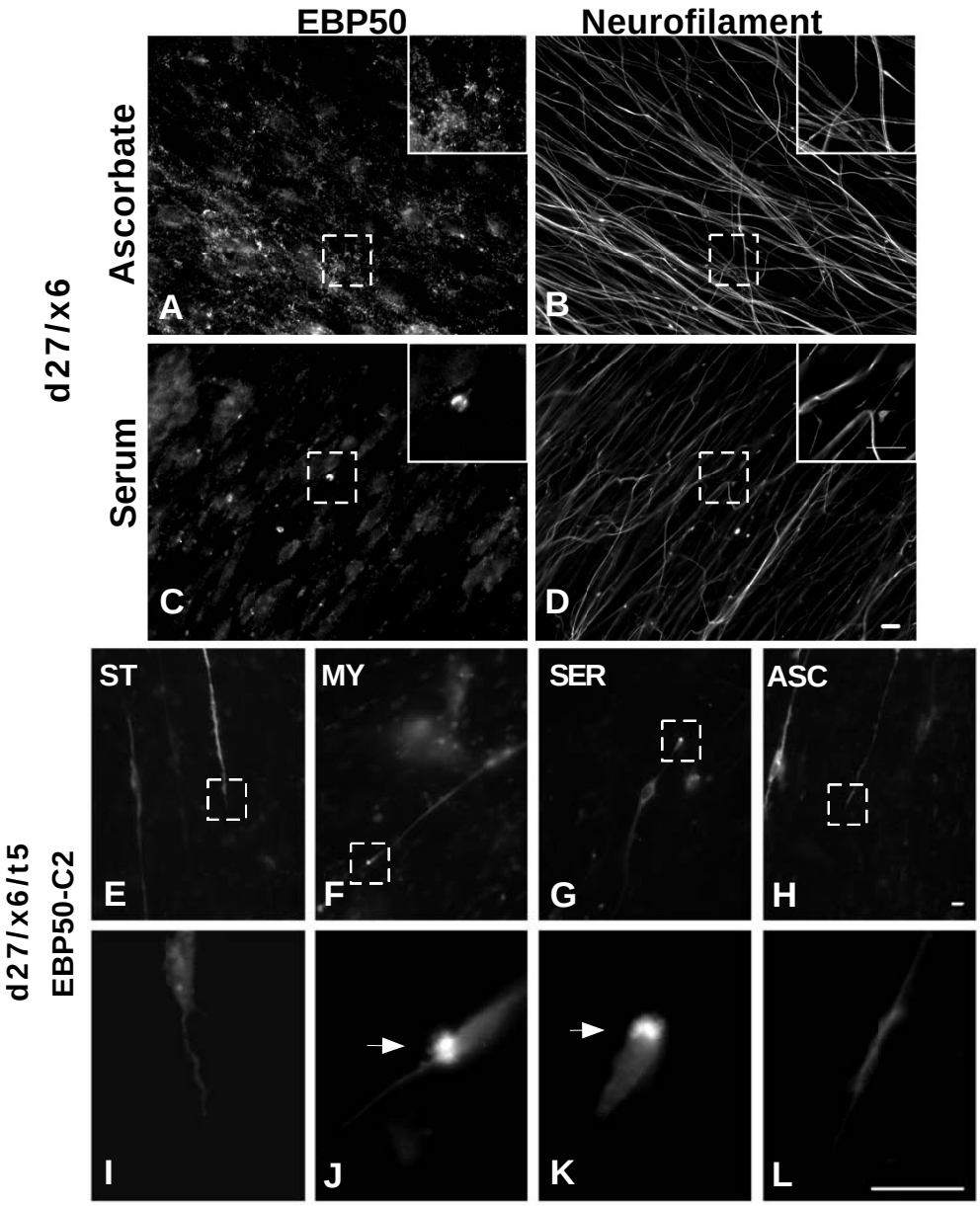


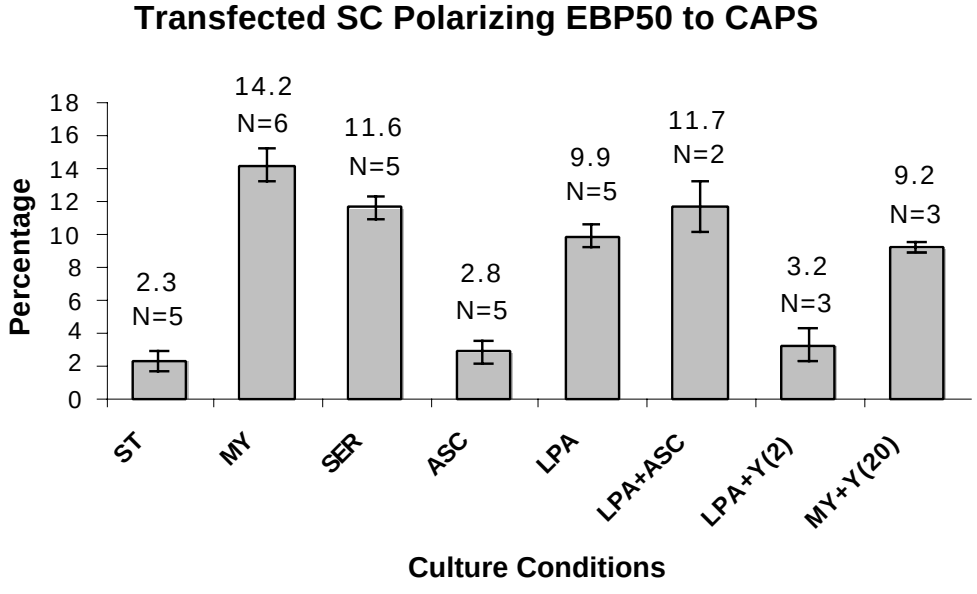

Figure 20 - Cap formation is dependent upon serum and can be promoted via Rho-stimulation

At d21, cultures were supplemented with either serum or ascorbate alone, maintained for 6 days (d27/x6), and then stained for EBP50 (A, C) and neurofilament (B, D). Cap formation was found to be serum-dependent. This was also shown with DRG cultures transfected with EBP50-GFP. At d27/x6/t5, various culture conditions were examined as indicated with panels I-L showing higher magnifications of E-H. EBP50-GFP was found at SC cap structures (arrows) in complete myelin feed (serum+ascorbate) (F, J) and cultures supplemented with serum only (G, K). Cultures were also treated with LPA (1 μM) to simulate serum stimulation of Rho pathways. Quantification revealed the presence of serum induced a 5-6 fold increase in the number of caps as compared to standard feed or ascorbate alone. LPA was able to compensate for serum in both the presence and absence of ascorbate. The Rho-kinase inhibitor Y-27632 (Y 2-20 μM, as indicated) was able to fully block cap formation in the presence of LPA but not complete myelin feed. N=number of coverslips analyzed from at least two independent cultures each having 2 DRGs per coverslip. An average of 423±41 cells per coverslip were counted. Scale bar=10 μm.

transfection experiments (Fig. 20E-L) revealed that the presence of serum induced a 5- to 6-fold increase in the number of EBP50-positve caps as compared to ascorbate alone. Further, ascorbate alone was as ineffective as standard feed in inducing cap formation [2.8±0.8% vs. 2.3±0.6%, respectively, p=0.6305], whereas serum alone produced similar results as compared to complete myelin feed (serum+ascorbate) in promoting cap formation [11.6±0.7% vs. 14.2±1.1%, respectively, p=0.0903] (Fig. 20).

ERM activation has been demonstrated to be downstream of Rho activity (Matsui et al., 1998; Shaw et al., 1998; Yonemura et al., 2002). Our observations, including the effects of serum and Rho localization, implicate a local activation of the Rho pathway in cap formation. We therefore used the serum phospholipid lysophosphatidic acid (LPA) to determine whether or not RhoA pathway activation affected cap formation. LPA has been shown to stimulate Rho-dependent pathways influencing cytoskeletal architecture in various cell types, including SCs (Weiner et al., 2001). Cultures were treated with 1 μM LPA or 1 μM LPA+50 μg/mL ascorbate. It was observed that LPA was able to compensate for an omission of whole serum from the culture medium. LPA alone generated 9.9±0.7% transfected SCs polarizing EBP50-GFP to cap structures, while LPA+ascorbate resulted in 11.7±1.6% (Fig. 20).

Downstream effectors implicated in Rho signaling include the Rho-associated kinases (ROCKs), p140mDia, and the phosphatidyl-inositol 4-phosphate 5-kinase (PI 4,5 kinase) (reviewed in Kaibuchi, 1999). To examine the contribution of the Rho kinases in LPA-induced cap formation, cultures were treated with Y-27632, a pyridine derivative which functions as a specific inhibitor of p160ROCK (ROCKI) and ROCKII (Ishizaki et al., 2000; Uehata et al., 1997). Y-27632 treatment (2 μM) reduced the capacity of LPA

to facilitate cap formation to a level similar to that of control cultures maintained in standard feed (p=0.4379). Surprisingly, cap formation in cultures maintained in complete myelin feed was reduced by only 35% following Y-27632 treatment (20 μM) (Fig. 20). These results demonstrate that LPA can substitute for serum in cap formation and does so via a Rho-kinase stimulated pathway. However, the inability of 2-20 μM Y-27632 to fully inhibit cap formation in the presence of serum suggests that other pathways may also be operating in this process.

Polarization of microvillar components appears to be an early event in myelination. As microvilli are observed to form contacts with developing nodes of Ranvier, we examined whether SC cap formation was linked to the clustering of proteins at the nodal membrane. Cultures were induced to myelinate under various conditions, and myelin segments with associated nodal clusters of ankyrin$_G$ were detected by triple staining with antibodies to MBP, ankyrin$_G$ and phospho-ERM (Fig. 21A-F). 65.6$\pm$3.6% of myelin segments exhibited associated ankyrin$_G$ staining at both ends of the segment in cultures treated with both serum and ascorbate. Cultures treated with ascorbate only exhibited 47.2$\pm$3.6% of myelin segments with associated ankyrin$_G$ staining and a 4-fold increase in the number of myelin segments that showed no associated ankyrin$_G$ staining (17.4$\pm$2.8% of myelin segments vs. 4.1$\pm$0.8% of segments in cultures treated with serum and ascorbate, p=0.0006). In contrast with previous reports (Eldridge et al., 1987), the average number of myelin segments formed in each culture appeared independent of serum. However, the addition of serum did result in segments of greater average length than those observed in ascorbate alone (Fig. 21A, D). No clusters of ankyrin$_G$ staining were observed without accompanying phospho-ERM staining (Fig. 21D-F).

# Figure 21 - Efficient node formation is linked to cap formation

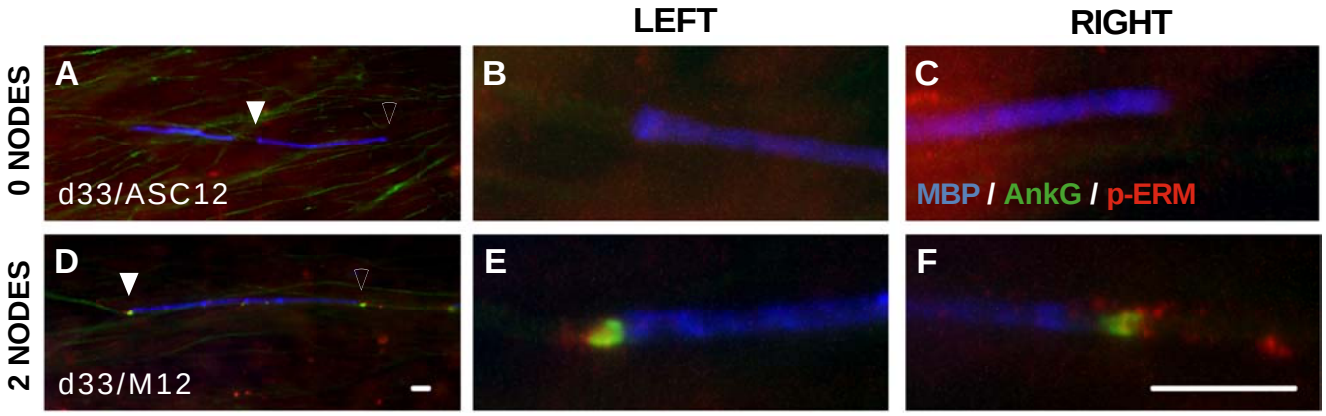


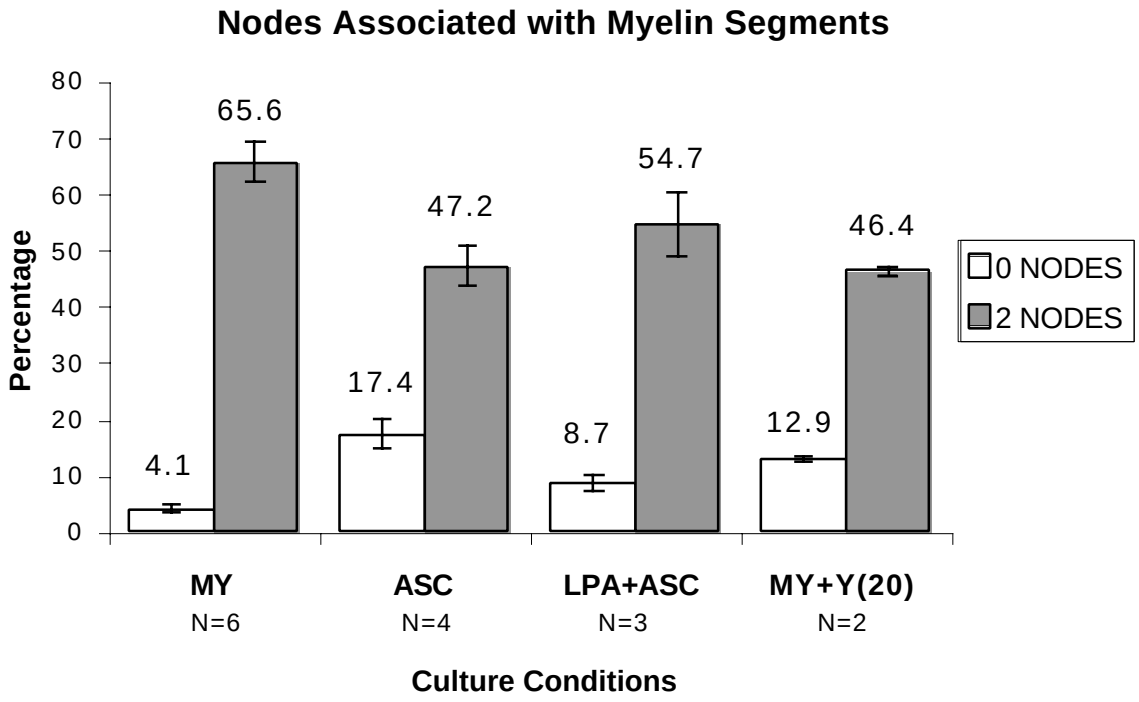

Figure 21 - Efficient node formation is linked to cap formation

Cultures maintained with either ascorbate alone or complete myelin feed were stained for MBP, ankyrin$_G$, and phospho-ERM. Myelin segments were identified and each nodal region associated was examined (A, D) (closed arrowhead – left-most tip of segment, open arrowhead – right-most tip of segment). Each segment was classified based on the presence (E-F) or absence (B-C) of associated nodes. It was observed that serum stimulation in complete myelin feed resulted in a mean of 1.4 times more segments having 2 nodes, whereas ascorbate alone produced a 4-fold increase in the mean number of segments formed in the absence of nodes. In addition, cultures were treated with LPA+ascorbate. While LPA was able to moderately compensate for serum, there was a 2-fold increase in the mean number of segments without nodes. Finally, cultures were treated with complete myelin feed+Y-27632. Here, a 3-fold increase in the mean number of segments without nodes and a 30% decrease in segments with 2 nodes were observed. N=number of coverslips analyzed from at least two independent cultures each having 2 DRGs per coverslip. An average of 297±41 (mean±SEM) segments per coverslip were counted. Scale bar=10 μm.

Cultures were also treated with LPA+ascorbate and complete myelin feed containing Y-27632 to determine their effects on node formation. LPA+ascorbate produced moderately similar results as compared to complete myelin feed (8.7% nodal absence, 54.7% nodal presence). Although, there was a 2-fold increase in the MBP-positive segments formed in the absence of nodes ($p=0.0253$), as compared to complete myelin feed. This indicates that while LPA can substitute for serum in these cultures, it is not quite as efficient in promoting node formation. The addition of Y-27632 to cultures maintained in myelin feed produced considerable effects on the node-segment association (Fig. 21). Here, a 3-fold increase in the mean number of segments without nodes ($p=0.0011$) and a 30% decrease in segments with 2 nodes ($p=0.0266$) were observed, as compared to myelin feed alone. Together these experiments demonstrate that culture conditions promoting formation of SC caps lead to enhanced node formation. In further support of this correlation, quantification of cultures at d32/M11 revealed an 84.1% reduction in the number of caps present in areas enriched in myelin segments (3.9E-05±7.2E-06 caps per $\mu m^2$), as compared to regions devoid of segments (2.5E-04±1.1E-05 caps per $\mu m^2$). This indicates that within a given myelinating culture, a decrease in the mean number of caps in areas of segment formation ensues, suggesting that many cap-forming cells indeed proceed to form myelin segments.

As these results strongly suggest a role for SC microvilli in node formation, a causative relationship has yet to be established. Clarification of this point was addressed by attempted disruption of ERM functionality and, potentially, microvillar structural integrity. This was achieved by employing the available dominant-negative (DN) variants of one microvillar cap-localizing protein, ezrin. SCs were transfected with either

wild type (WT) or DN-ezrin constructs harboring a VSVG-tag for detection (M. Arpin, Instit Curie, Paris, France). After inducing myelination in these cultures, formation of nodes associated with myelin-forming transfected cells was examined (d42/M21/t20). Transfected, myelin-forming SCs were detected, although their occurrence was extremely rare. It appeared that the WT-ezrin construct does not have an effect on node formation as defined by the axonal clustering of ankyrin$_G$. Moreover, the DN-ezrin construct appears to abolish node formation, perhaps via interference with the appropriate formation and functionality of the SC microvilli (Fig. 22). These initial results are encouraging, however, enough of these cells have yet to be identified to present meaningful quantitative data.

Supplemental Material

An animated 3-dimensional rendering of a deconvolved node of Ranvier is available showing the relationship between EBP50 and ankyrin$_G$ staining (Fig15video2). In addition, the original time-lapse videos from which the still images presented in Figure 17 were taken are available for viewing as supplemental material. Fig17video3 contains time-lapse fluorescence microscopy of an EBP50-GFP transfected SC maintained in standard feed. Fig17video4 specifically shows the distal tip of this cell. Fig17video5 shows time-lapse fluorescence microscopy of an EBP50-GFP transfected SC after the induction of myelination using serum and ascorbate. Fig17video6 shows the remodeling EBP50-enriched tip of this cell. Supplemental material is available on the provided CD, and more detailed video descriptions can be found in Appendix II.

# Figure 22 - ERM/microvilli disruption leads to impaired node formation

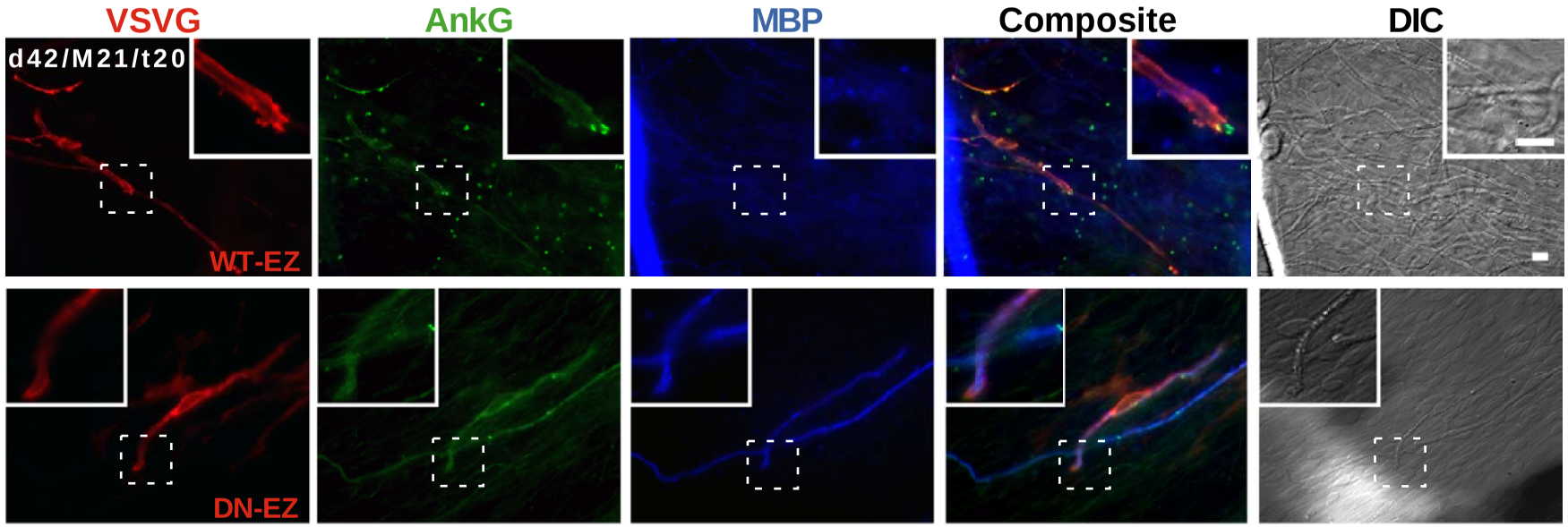

Figure 22 - ERM/microvilli disruption leads to impaired node formation

With efficient node formation correlatively linked to cap formation, direct microvillar disruption was attempted. SCs were transfected with either VSVG-tagged WT- or DN-ezrin (red) constructs and assessed for myelination and node formation (d42/M21/t20). WT-ezrin had no adverse effects on myelination or node formation, as detected by MBP (blue) and ankyrin$_G$ (green) staining, respectively. DN-ezrin transfected SCs were also able to generate compact myelin, but did not appropriately cluster ankyrin$_G$, indicating a failure in node formation. Scale bar=10 μm.

Discussion

In this study, we have examined the development of SC microvilli during myelination in an attempt to understand their potential role in formation of the nodes of Ranvier. We have observed that SCs in DRG explants polarize microvillar components to their distal tips in response to *in vitro* signals involved in myelin formation, particularly serum addition. We have found that these differentiated SC tips (termed caps) are highly dynamic, growth cone-like structures that result from local activation of ERM proteins downstream of Rho signaling. Finally, we have demonstrated that conditions favoring the formation of SC caps are associated with efficient clustering of membrane proteins at developing nodes of Ranvier.

These observations are summarized in the model shown in figure 23. The initial stages of culture establishment include the migration of pre-myelinating SCs along the radially extended axons emanating from the DRG. These cells appear to be aggressively motile with numerous cell surface microvilli. As the cultures develop, SCs assume their characteristic bipolar, myelinating phenotype with microvilli decorating their length. However, treatment of these cultures with serum and ascorbate (particularly serum) results in a reorganization of microvillar components into SC caps. Finally, SCs proceed to form myelin sheaths coupled with the clustering of proteins at the nodes of Ranvier.

These results demonstrate a correlative association between the polarization of microvillar components to SC caps and the clustering of ankyrin$_G$, supporting a role for SC microvilli in node formation. Dynamic remodeling of the SC tip associated with cap formation may be important to the efficient clustering of nodal membrane proteins. Hence, nodes might be formed at much slower rates, if at all, in cultures lacking serum

# Figure 23 – Model - SC progression toward myelination in DRG explant culture system

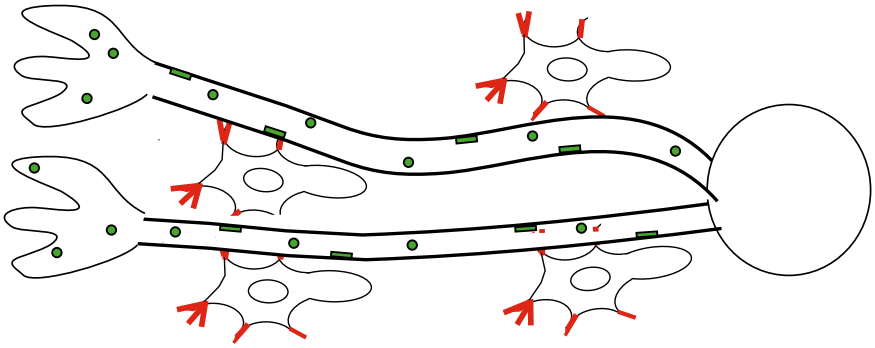

**Migration of pre-myelinating phenotype**

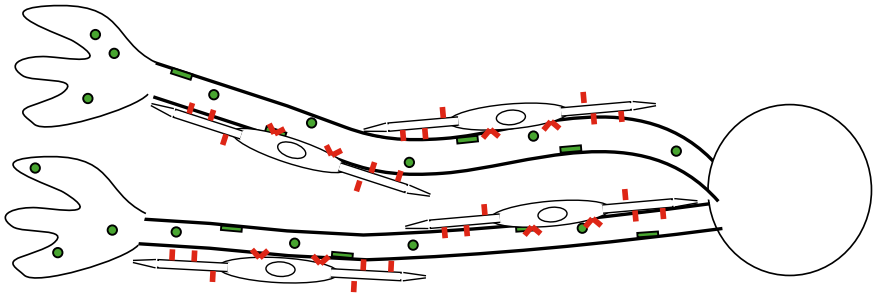

**Morphogenesis of myelinating phenotype**

**Addition of serum and ascorbate**

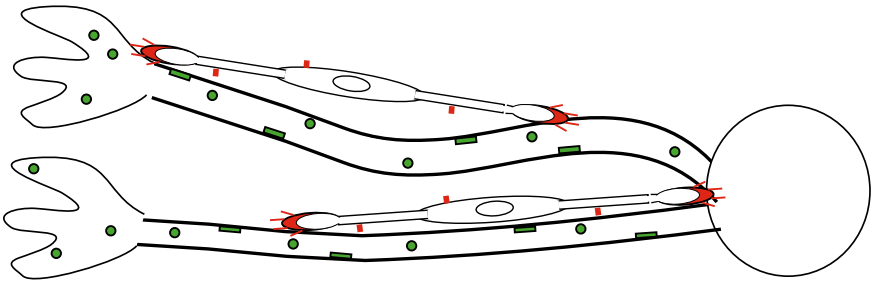

**SC elongation and "cap" formation**

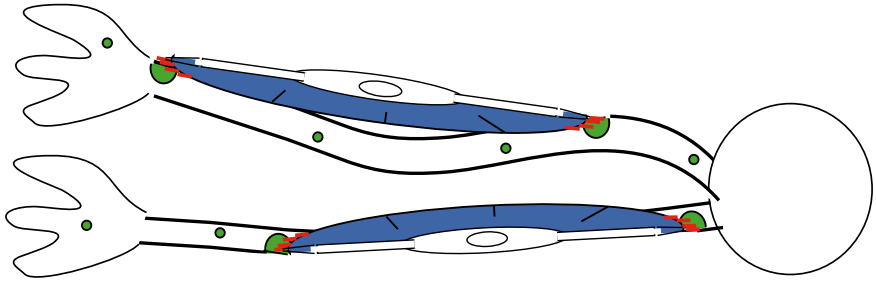

**Myelination and early node formation**

Figure 23 – Model - SC progression toward myelination in DRG explant culture system

Highly motile, pre-myelinating SCs migrate along axons extending from the DRG. These SCs harbor numerous cell surface microvilli (shown in red). Morphogenesis of the SC myelinating phenotype takes place with SCs becoming more longitudinally oriented and axon-aligned while retaining many cell surface microvilli. Upon induction, typically using serum and ascorbate, Rho stimulation then leads to the formation of dynamic SC cap structures specifically enriched in activated ERM proteins and other microvillar components (again shown in red). Elaboration of the myelin membrane (shown in blue) follows with the clustering of axonal components associated with the formation of early nodes (shown in green).

where tip dynamics are greatly reduced. Alternatively, the dynamic formation of SC caps and the clustering of ankyrin$_G$ may not be functionally coupled. In this case, serum would be exerting independent effects on these two processes in myelinating cultures. With promising initial findings, as described herein, we are further testing this idea by directly disrupting ERM function and microvilli formation while observing the effects on nodal protein clustering.

SC caps exhibit morphological and dynamic similarities to axonal growth cones. ERM proteins are also observed in axonal growth cones and their activity appears critical to growth cone function (Paglini et al., 1998). SC caps may also have functional similarities to growth cones, potentially playing a role in axon recognition and segregation during early myelination as well as node formation at later stages. Of importance would be the identification of SC cap proteins that might participate in these processes. These proteins could well be ERM binding proteins such as CD44, which has been implicated in SC-axon adhesion and neuregulin signaling (Sherman et al., 2000). At the node, the cell adhesion molecules neurofascin and NrCAM have been proposed as candidate proteins for the 40-80 nm filaments observed by electron microscopy to link SC microvilli to the nodal membrane (Ichimura and Ellisman, 1991). Perturbing the function of these proteins has been shown to inhibit the clustering of nodal membrane proteins (Lustig et al., 2001). However, potential complementary microvillar receptors for these molecules facilitating SC-axon adhesion remain unknown.

Our data indicate that the addition of serum to DRG explants effects localized changes at SC tips. This might result from concentrations of RhoA that we have observed at the SC tips and/or a potential enrichment of guanine nucleotide exchange

factors (GEFs) or guanosine diphosphate (GDP) dissociation factors at these sites. Given the known effects of Rho on the actin cytoskeleton, it is highly likely that Rho activation at the tip accounts for the dynamic nature of these structures in the presence of serum. As active ERM proteins interact with RhoGDI (GDP dissociation inhibitor) (Takahashi et al., 1997), it is also likely that ERM activation at the tip will further enhance the formation of active Rho molecules.

As well as local activation of molecules at SC tips, serum may also enhance the movement of vesicle-associated proteins to the tip. For example, exogenous EBP50-GFP is localized to a motile population of punctae in transfected SCs. We have observed that serum causes dramatic changes in SC length and produces significantly longer myelin segments than those formed under serum-free conditions. These findings suggest the potential for functional interdependencies between cap formation, SC elongation and segment length, and effective clustering of nodal membrane proteins.

# Chapter 5

## Asymmetric ERM activation and EBP50 recruitment are required in directed motility of mature Schwann cells

### Asymmetric process retraction generates a novel class of functional, motile, unipolar SCs

### Asymmetric ERM activation and EBP50 localization are associated with SC process retraction and migration

### ERM proteins are required for appropriate SC motility and polarity maintenance

Introduction

Schwann cells (SCs) are the myelinating glial cell type in the PNS. The generation of their specialized, multi-lamellar myelin membrane involves axon-glial cell engagement and discrete domain establishment. Distinct morphologic changes and molecular reorganizations in axonal and glial cell membranes are required, and SC motility is crucial to the terminal differentiation of these cells. Mature SCs must infiltrate nerve bundles, segregate individual axons, and attain proper positioning while establishing the correct 1:1 SC:axon relationship prior to the onset of myelination (Chapter 1, Fig. 4) (reviewed in Arroyo and Scherer, 2000; Mirsky and Jessen, 1999; Salzer, 2003).

Several effectors of SC migration have been studied to date. β-neuregulin enhances SC motility via the MAPK pathway by up to 84% in wound healing assays (Meintanis et al., 2001), and another neuregulin family member, GGF2, promotes a 63% increase in early DRG explants (Mahanthappa et al., 1996). Further, IGF-1 induces a 2-fold increase in SC motility via PI3 kinase (Cheng et al., 2000). Other reports indicate heightened gross SC motility in response to nerve damage (Cheng and Zochodne, 2002).

While these studies demonstrate several key pathways involved in generalized SC motility, they do not address the highly specialized motility unique to mature SCs in axonal contact at the onset of myelination. As SCs mature, they attain their hallmark bipolar phenotype and undertake environmentally cued, directed migration along axons. Their bipolarity then presents a challenge in mediating the signal integration necessary to generate a polarized motility response. As we have begun to define the dynamic nature

of the SC tip, we focused on examining the axon-associated modality of migration employed by these cells.

Solving this puzzle may require the identification of differentially localizing and/or activating proteins that could play a role in motility initiation. We have recently demonstrated that SCs specifically polarize microvillar components to their process tips in response to signals that potentially activate the Rho pathway (Gatto et al., 2003). Using fluorescence time-lapse microscopy of transfected SCs within myelinating DRG explants, we now describe asymmetric ERM activation at SC process tips in association with the cycling of these cells between stationary, bipolar and motile, unipolar phenotypes. As ERM proteins have been implicated in mediating fibroblast cell shape (Amieva et al., 1999; Lamb et al., 1997), epithelial cell motility (Crepaldi et al., 1997), and neuronal growth cone morphology, motility, and process stability (Castelo and Jay, 1999; Paglini et al., 1998), these proteins and their specific localizations may be essential to SC plasticity and the resultant motile responses.

Activated ERMs, characterized by COOH-terminal phosphorylation (Matsui et al., 1998), with their upstream activator phosphatidylinositol (4,5)-bisphosphate (PIP2) (Hirao et al., 1996; Yonemura et al., 2002), and their downstream binding partner EBP50 (Reczek et al., 1997), asymmetrically concentrate at the tip of the retracting SC process and become enriched at the rear of the migrating unipolar cell. These unipolar SCs then migrate in a nucleokinetic fashion similar to that described for neurons. Over-expression of EBP50 enhances this unipolar migration suggesting a novel role for the adaptor protein in cell motility. Finally, perturbations of ERM function severely inhibit SC process dynamics and result in an impaired, multipolar phenotype.

The SC neuron-like motility identified in this study suggests a major role for ERMs and associated proteins at the rear of the cell during nucleotaxic migration. This novel study of the motility of bipolar SCs within myelinating DRG explants provides an important step in understanding the dynamic nature of myelination and SC responses to peripheral nerve trauma.

## Results

### Asymmetric process retraction generates a novel class of functional, motile, unipolar SCs

To assess polarity and motility in a highly polarized cell type, we examined mature SCs, which assume distinctive bi- or tripolar morphologies (Jessen et al., 1994; Mirsky and Jessen, 1999). Specifically, we utilized the DRG explant system to examine these SC properties upon the initiation of myelination. DRGs were transfected with GFP to demarcate individual SCs and observed 6 days post-induction/5 days post-transfection (M6/t5). Two discrete morphologic phenotypes were detected (Fig. 24A). Typical bipolar SCs were the most prevalent (69.9±0.9%). However, novel, distinct, unipolar SCs were also common (17.1±0.6%). These unipolar cells persist in the induced cultures over time, albeit at a reduced level (M6 - 17.1±0.6% vs. M14 - 6.8±2.8%). Further, staining for the early myelin marker MAG demonstrated both bi- and unipolar myelinating SCs (Fig. 24B). These results suggest that unipolar SCs may have a functional role in early stages of myelination.

To examine the potential interrelationship of these bi- and unipolar SCs, time-lapse imaging of GFP-transfected cells was performed. This revealed that the atypical, unipolar modality is generated by the specific retraction of one SC process (Fig. 25A, supplemental material Fig25Avideo7). Further, the unipolar morphology was a characteristic migratory phenotype displayed after the induction of myelination with 67.8±5.9% of unipolar SCs actively migrating (Fig. 25B, supplemental material Fig25Bvideo8). This indicates that a substantial portion of unipolar SCs is engaged in directed motility, of which a sub-population may be involved in myelination.

# Figure 24 - Functional bi- and unipolar SCs present in myelinating DRG explants

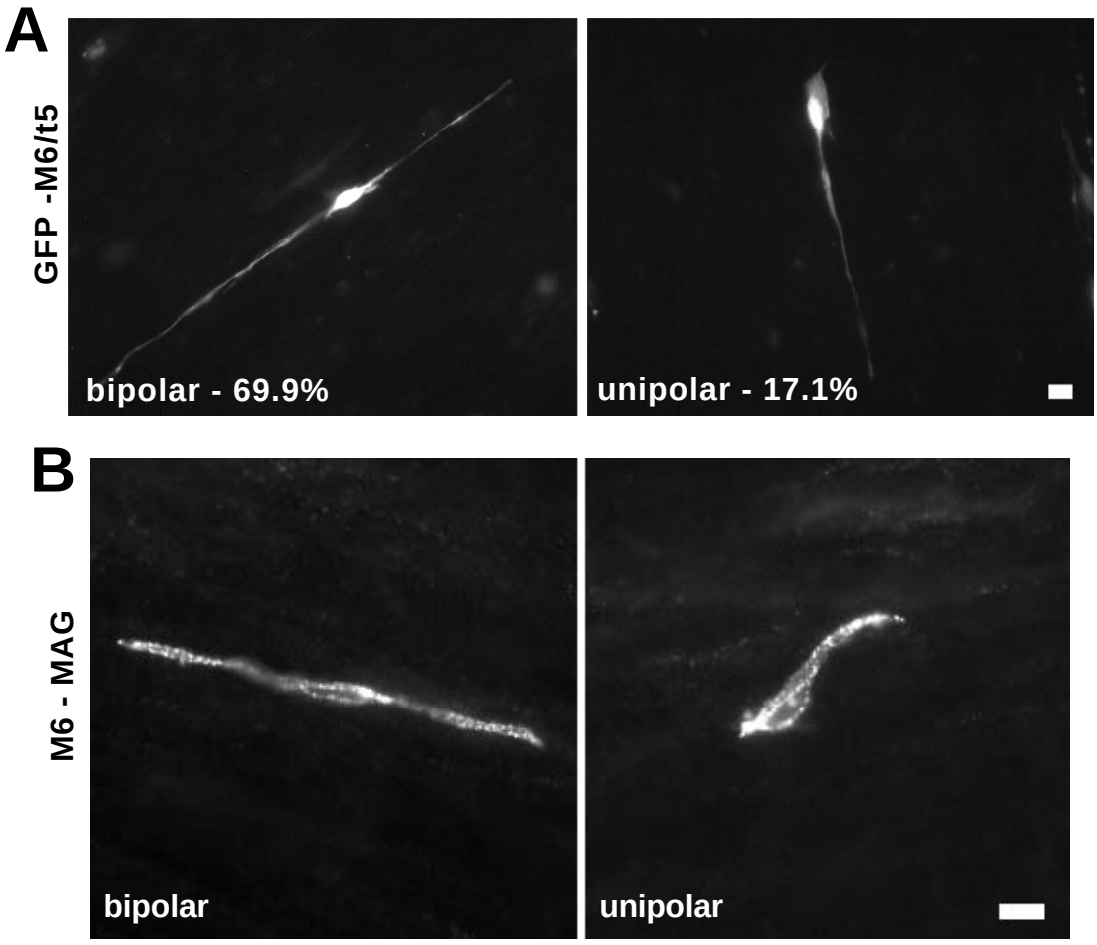

Figure 24 - Functional bi- and unipolar SCs present in myelinating DRG explants

A) After 6 days induction/5 days transfection (M6/t5), GFP-positive SCs display two discrete morphologic phenotypes [bipolar - 69.9±0.9% (left), unipolar - 17.1±0.6% (right)]. These results represent quantification of eight independent experiments wherein an average of 500±65 cells were counted. B) MAG staining, 6 days post-induction, reveals bi- and unipolar myelinating SCs. Scale bar=10 μm.

# Figure 25 - Process retraction generates motile, unipolar SCs

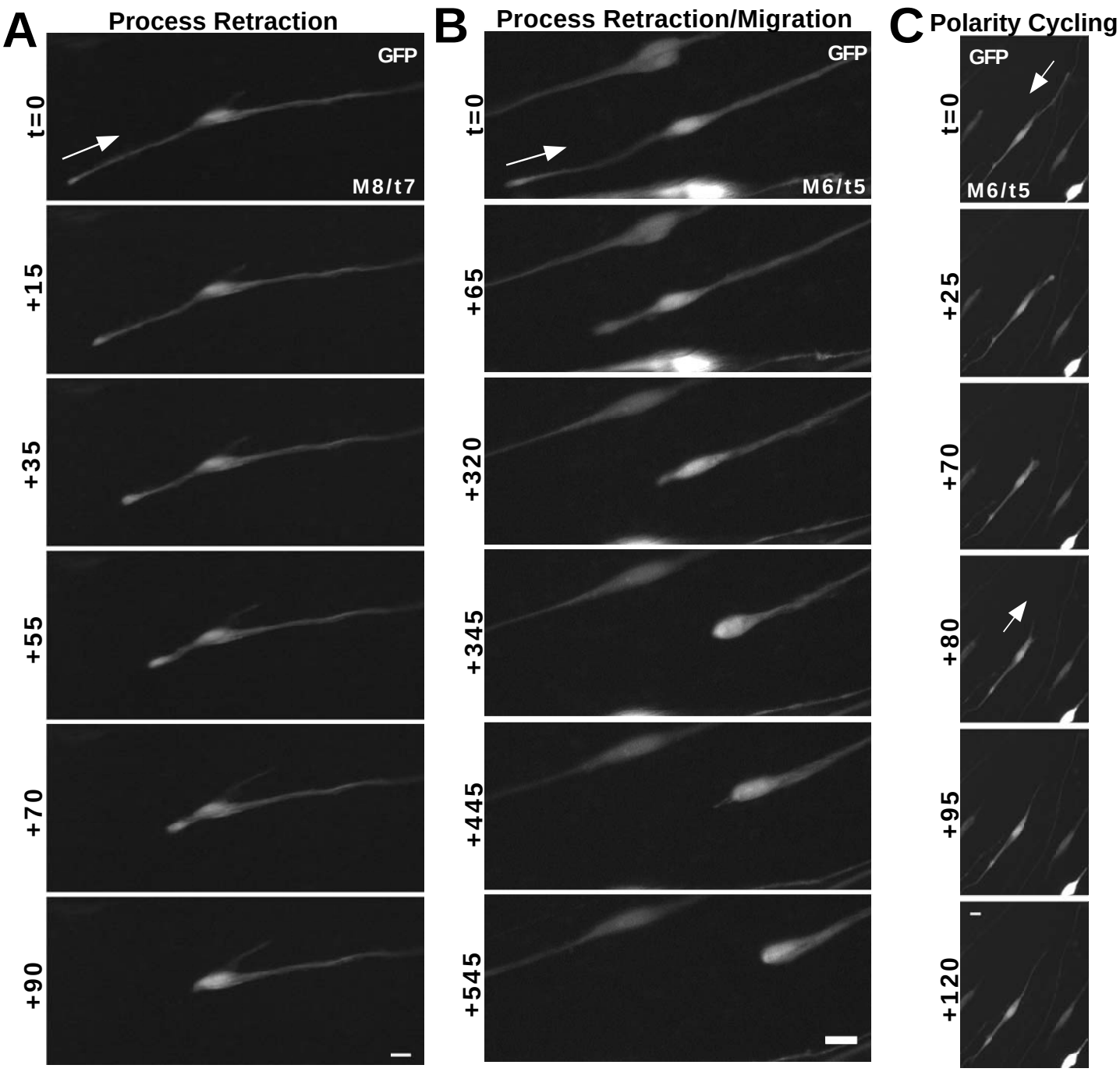

Figure 25 - Process retraction generates motile, unipolar SCs

A) After transfection as described, GFP-transfected SCs were time-lapse imaged with acquisition every 5 minutes over a period of 10 hours. The generation of unipolar SCs results from specific process retraction. These still images illustrate this process over an elapsed 90 minutes. See also Fig25Avideo7-GFP-PR.mov. B) These unipolar SCs then displayed neuron-like, nucleokinetic, migratory activity. Upon completed process retraction toward the SC body, somal translocation occurs. Still images presented span an elapsed 545 minutes. See also Fig25Bvideo8-GFP-MIG.mov. C) SCs are able to cycle through polarity states. This morphologic plasticity is depicted in the still frames presented spanning an elapsed 120 minutes. See also Fig25Cvideo9-GFP-cycle.mov. Arrows indicate the directionality of process retraction or migration. Scale bar=10 μm.

The motility displayed by these unipolar cells is similar to the nucleokinetic, somally translocating migratory patterns seen in neurons (Nadarajah et al., 2003; Nadarajah and Parnavelas, 2002). In addition, this polarity shift is readily reversible via process extension to re-establish bipolarity (Fig. 25C, supplemental material Fig25Cvideo9). Thus, mature SCs have an intrinsic, morphologic plasticity, which enables cycling between uni- and bipolar as dictated by encountered cues.

Asymmetric ERM activation and EBP50 localization are associated with SC process retraction and migration

We have previously localized the microvillar components EBP50 and activated, phospho-ERMs (pERMs) to the distal tips of mature SCs in structures we termed SC caps. It was proposed that these caps represent a region pre-disposed and primed to form axo-glial contacts via SC microvilli (Gatto et al., 2003). To determine if there was a discernable role for these components in earlier stages of SC positioning, we examined the endogenous localization of these proteins in apparently cycling SCs. In GFP transfected SCs, it was frequently observed that both EBP50 and pERM were asymmetrically distributed. In bipolar SCs, the localization was specific to one distal tip that often was associated with an extended, filopodial structure. By contrast, in unipolar SCs, EBP50 and pERM localized to the rear, trailing edge of the cells (Fig. 26A).

The localization of EBP50 and pERM to one SC process tip in bipolar cells and at the rear of the unipolar cell suggests that ERM activation may be asymmetrically associated with the retracting SC process. To address this issue, we used an EBP50-GFP construct, which will bind only to activated ERM proteins (Reczek et al., 1997; Reczek and Bretscher, 1998). We found that EBP50 localization to the SC distal tip was the first

**Figure 26 - Asymmetric pERM and EBP50 localization at SC tip and trailing edge involved in process retraction and migration, respectively**

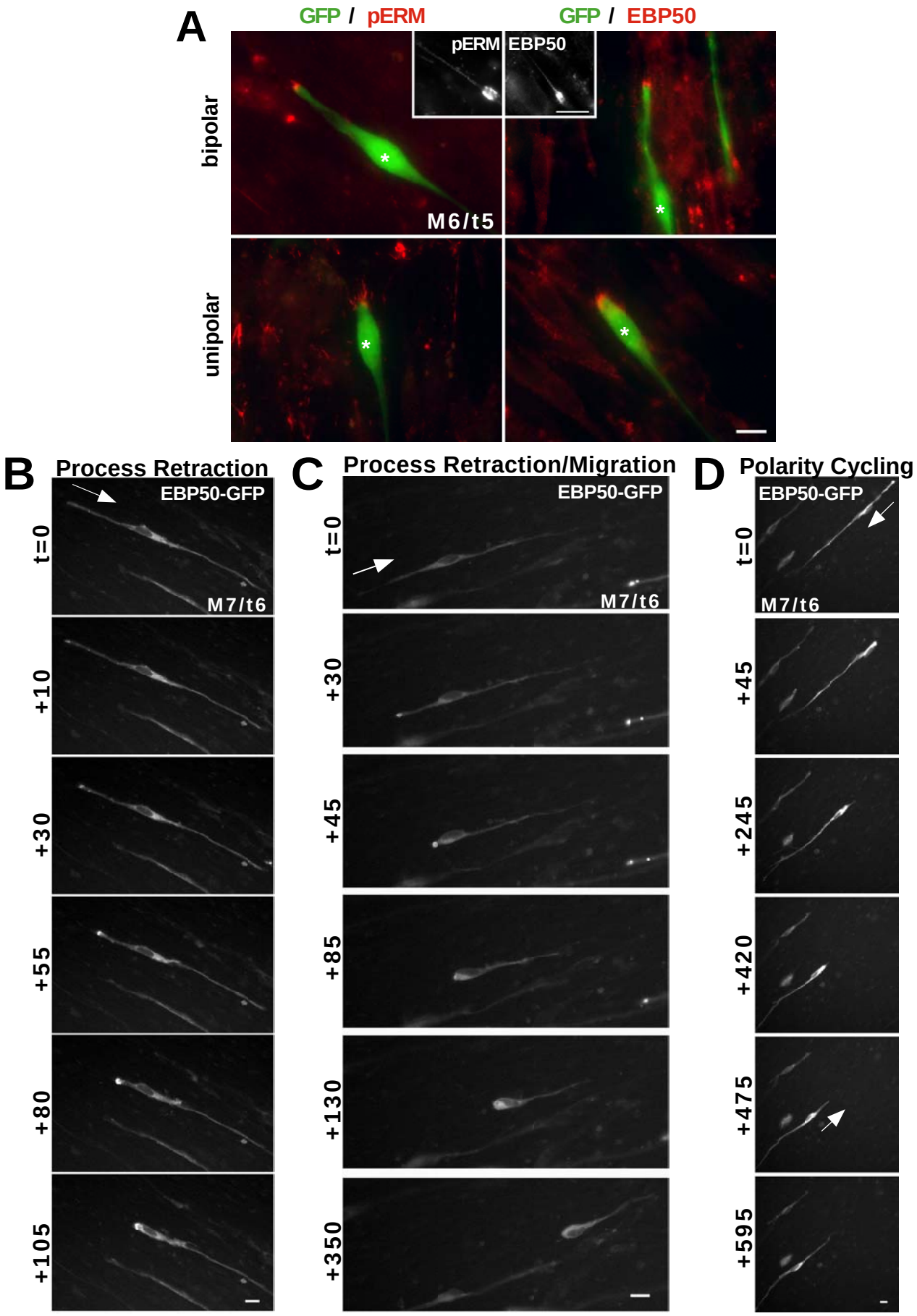

Figure 26 - Asymmetric pERM and EBP50 localization at SC tip and trailing edge involved in process retraction and migration, respectively

A) Both pERM and EBP50 asymmetrically localized to one distal tip of bipolar SCs (top panels) and the rear of unipolar SCs (bottom panels) transfected with GFP (M6/t5). Insets show the localization of pERM and EBP50 to filopodia-like retraction fibers at the SC distal tip. Asterisks denote nuclear positioning for spatial reference. B) EBP50-GFP-transfected SCs (M7/t6) were imaged as described. Process retraction proceeded as described with GFP alone. However, a clear flash of EBP50 could be seen at the tip of the retracting SC process. Still images show an elapsed time of 105 minutes. See also Fig26Bvideo10-EB-PR.mov. C) After achieving unipolarity, the EBP50-GFP-transfected SCs (M7/t6) then migrated as predicted by GFP studies. Still images span an elapsed 350 minutes. See also Fig26Cvideo11-EB-MIG.mov. D) As seen with GFP alone, EBP50-transfected SCs (M7/t6) are capable of cycling though process retraction, migration, and process extension. Still images represent an elapsed 595 minutes. See also Fig26Dvideo12-EB-cycle.mov. Arrows indicate the directionality of process retraction or migration. Scale bar=10 μm.

visually discernable step in SC process retraction (Fig. 26B, supplemental material Fig26Bvideo10) with 92.2±4.6% of cells presenting this EBP50 localization undergoing retraction. The ensuing long, filopodial structures (Fig. 26A, insets) were often left behind during process retraction. Hence, they are likely to represent novel manifestations of retraction fibers. These asymmetric, distal enrichments of EBP50/ERM provide the first molecular markers defining a transient inequality of the SC bipolarity that specifically denotes which SC process will retract generating a mono-oriented, directionally polarized, migratory cell.

Once retraction had commenced, EBP50 was maintained at the tip of the retracting process itself and then at the rear of the migrating unipolar cell. This implies a sustained region of ERM activation in this process (Fig. 26C-D, supplemental material Fig26Cvideo11 and Fig26Dvideo12). Further, discrete EBP50 localization was lost at the rear of the unipolar cell during process re-extension (Fig. 26D). This finding suggests a local signaling switch controlling ERM activation in this morphologic cycling.

We then proceeded to quantify aspects of this unique SC motility. Over-expression of EBP50 was not found to significantly increase the frequency of asymmetric process retraction (Fig. 27A; 45.1±3.8% of either GFP or EBP50-GFP transfected cells exhibited this phenomenon) and marginally increased the speed of process retraction (Fig. 28A; GFP - 0.49±0.06 μm/min vs. EBP50-GFP - 0.71±0.1 μm/min, p=0.0685). However, EBP50 over-expression did significantly enhance the frequency at which unipolar cells were observed to migrate (Fig. 27B; GFP – 67.8±5.9% vs. EBP50-GFP 95.8±4.2%, p=0.0161) and the rate of unipolar SC migration versus control (Fig. 28B; GFP – 0.21±0.03 μm/min, EBP50-GFP – 0.40±0.06 μm/min, p=0.0181).

# Figure 27 - Quantification of SC process retraction and migration frequencies

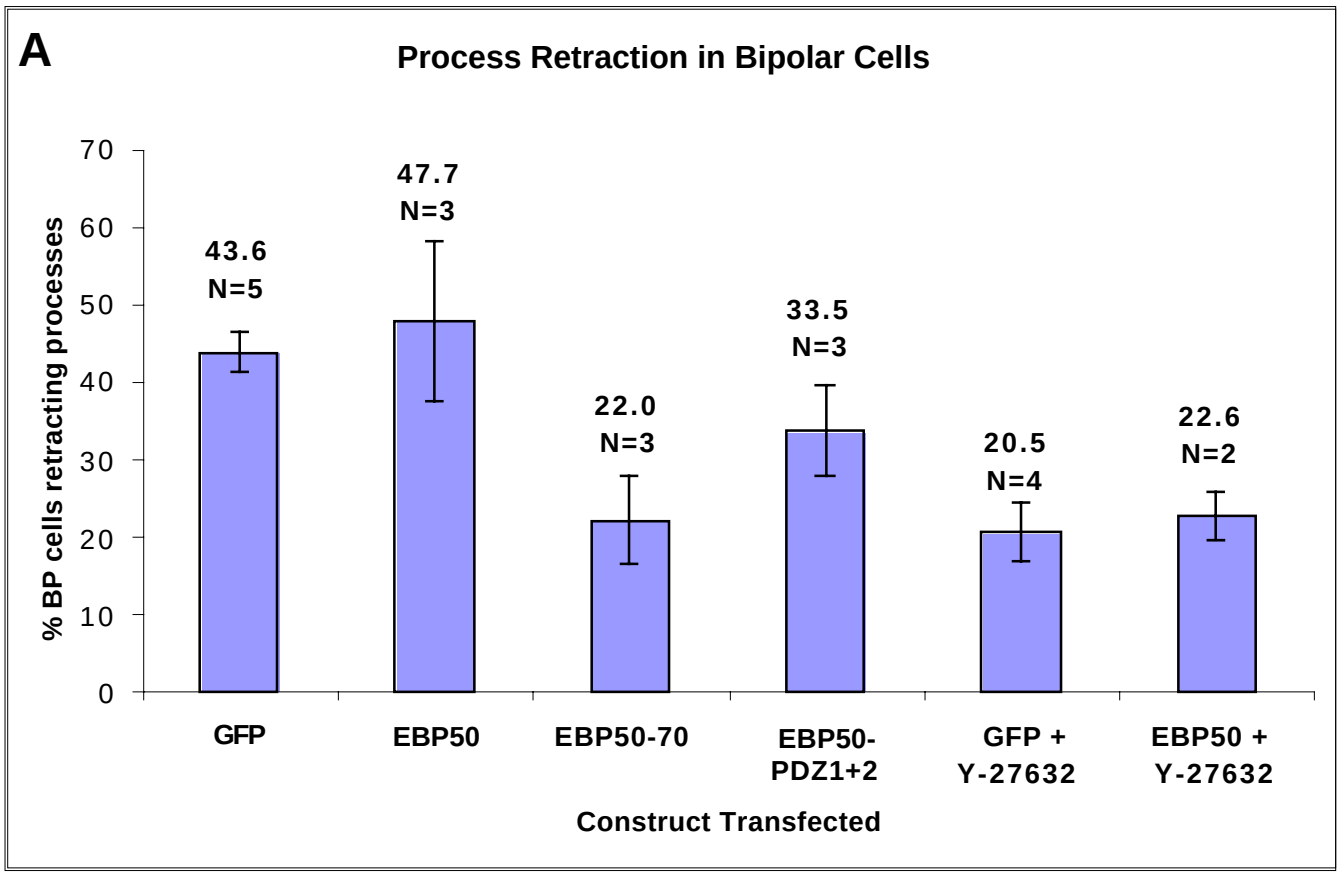


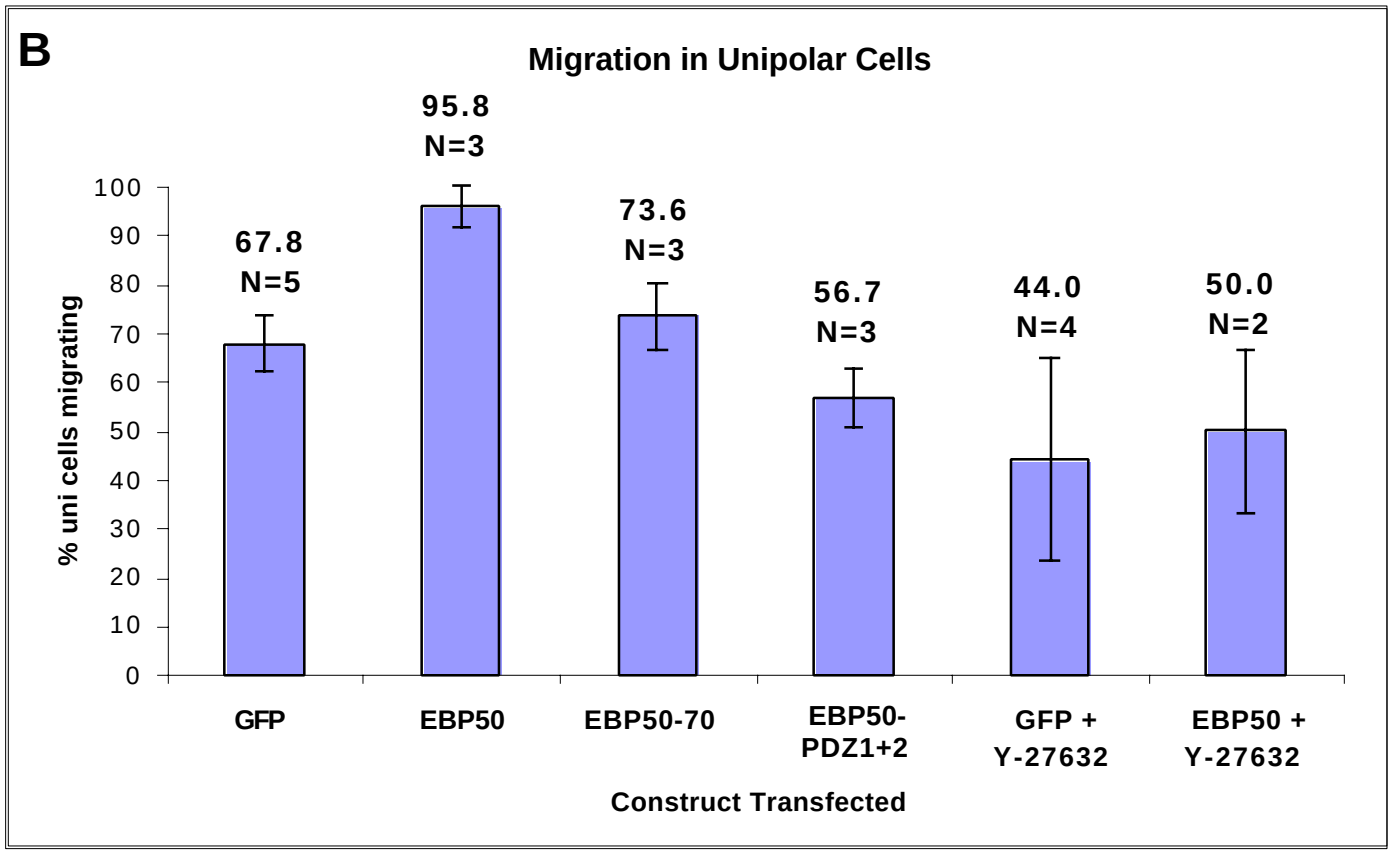

Figure 27 - Quantification of SC process retraction and migration frequencies

A) Presented is a comparison of the effects of various EBP50 constructs on frequencies of process retraction in transfected SCs (M5/t4-M8/t7). Percentages indicate the portion of transfected SCs that displayed process retraction during time-lapse imaging. GFP – 43.6±2.6%, EBP50-GFP – 47.7±10.2%, EBP50-70-GFP – 22.0±5.7%, EBP50-PDZ1+2-GFP – 33.5%, GFP+Y-27632 – 20.5±3.7%, EBP50-GFP+Y-27632 – 22.6±3.2%. N=number of independent experiments in which a minimum of 68±10 cells were observed. B) Presented is a comparison of the effects of various EBP50 constructs on frequencies of unipolar cell migration in transfected SCs (M5/t4-M8/t7). Percentages indicate the portion of transfected SCs that displayed both unipolar morphology and active, directed migration during time-lapse imaging. GFP – 67.8±5.9%, EBP50-GFP – 95.8±4.2%, EBP50-70-GFP – 73.6±6.9%, EBP50-PDZ1+2-GFP – 56.7±5.8%, GFP+Y-27632 – 44.0±20.8%, EBP50-GFP+Y-27632 – 50.0±16.7%. N=number of independent experiments in which a minimum of 68±10 cells were observed.

# Figure 28 - Quantification of SC process retraction and migration rates

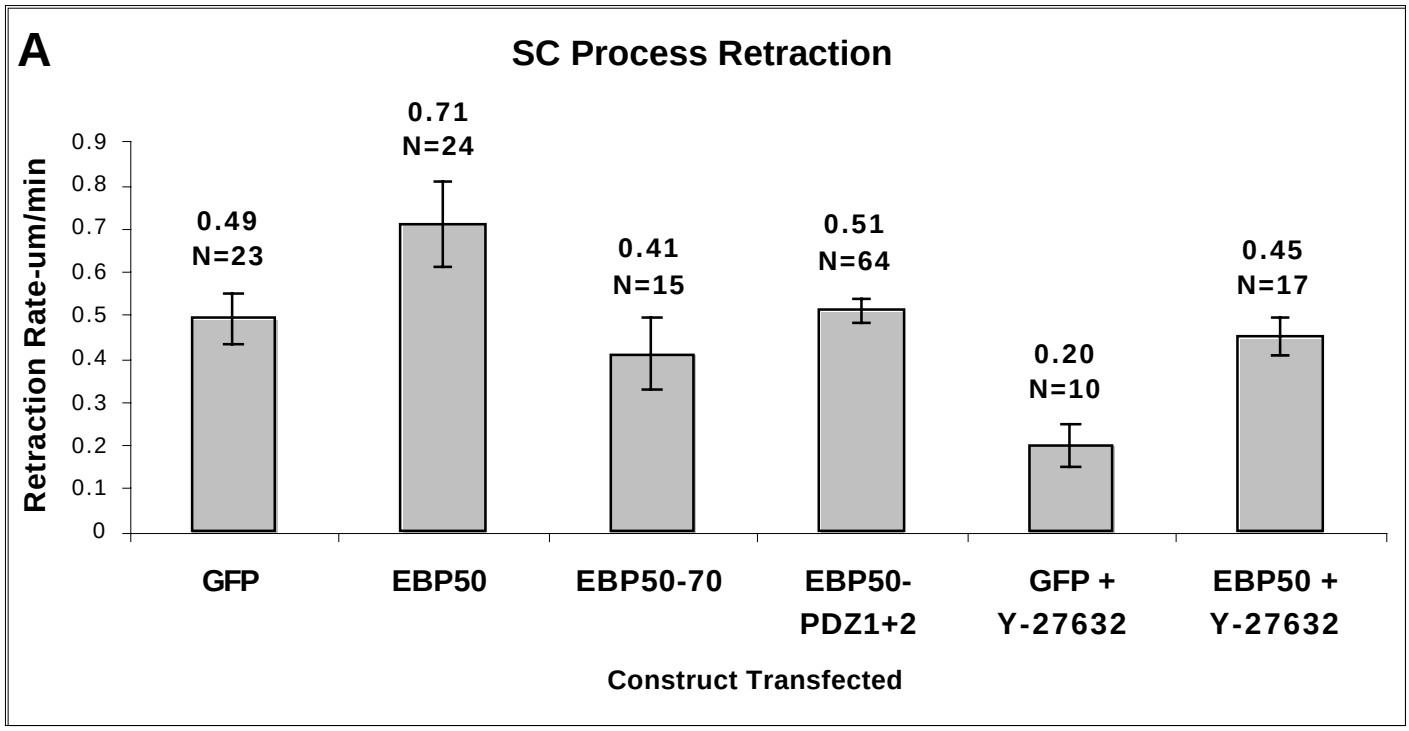


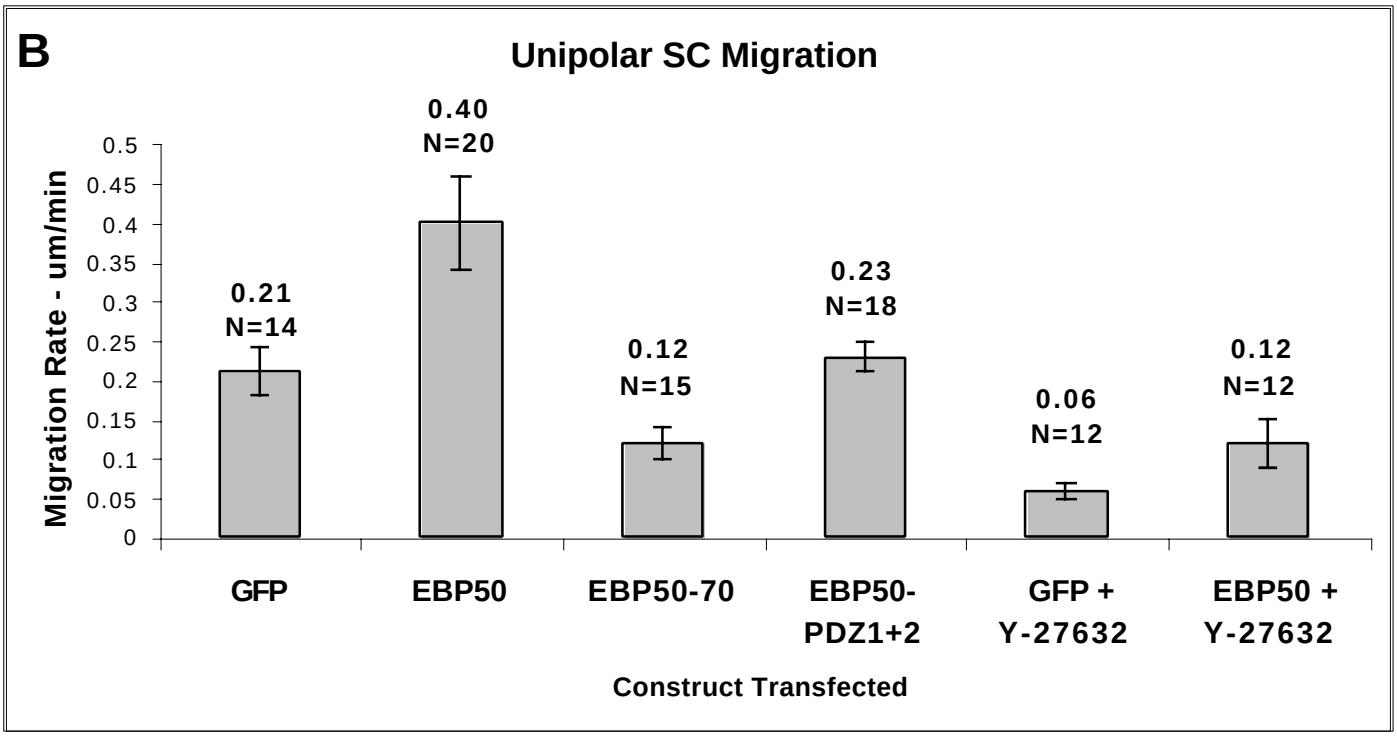

Figure 28 – Quantification of SC process retraction and migration rates

A) Presented is a comparison of the effects of various EBP50 constructs on rates of process retraction in transfected SCs (M5/t4-M8/t7). GFP – 0.49±0.06 μm/min, EBP50-GFP – 0.71±0.10 μm/min, EBP50-70-GFP – 0.41 μm/min, EBP50-PDZ1+2-GFP – 0.51±0.03 μm/min, GFP+Y-27632 – 0.20±0.05 μm/min, EBP50-GFP+Y-27632 – 0.45±0.04 μm/min. N=number of individual SCs monitored in at least 3 independent experiments. B) Presented is a comparison of the effects of various EBP50 constructs on rates of unipolar, transfected SC migration (M5/t4-M8/t7). GFP – 0.21±0.03 μm/min, EBP50-GFP – 0.40±0.06 μm/min, EBP50-70-GFP – 0.12±0.02 μm/min, EBP50-PDZ1+2-GFP – 0.23±0.02 μm/min, GFP+Y-27632 – 0.06±0.01 μm/min, EBP50-GFP+Y-27632 – 0.12±0.03 μm/min. N=number of individual SCs monitored in at least 3 independent experiments.

To map the functional domains of EBP50 involved in motility enhancement, constructs lacking either the ERM binding site (Reczek and Bretscher, 1998) in the COOH-terminal 70 amino acids (EBP50-70-GFP) or both of the PDZ interaction domains (Reczek et al., 1997) (EBP50-PDZ1+2-GFP) were generated. Over-expression of EBP50-70, as compared with GFP and EBP50-GFP transfection, dramatically decreased the frequency of asymmetric process retraction to 22.0±5.7% (p=0.0103) (Fig. 27A). Further, EBP50-70 over-expression substantially impaired unipolar cell migration rates as compared to both EBP50 over-expression (EBP50-70-GFP - 0.12±0.02 μm/min vs. EBP50-GFP - 0.40±0.06 μm/min, p=0.0040) and control values (EBP50-70-GFP - 0.12±0.02 μm/min vs. GFP - 0.21±0.0.03 μm/min, p=0.0176) (Fig. 28B).

As we have shown the localization of EBP50 to the distal tip of SCs appears to be RhoA- dependent (Gatto et al., 2003), we then examined the effect of a ROCK inhibitor, Y-27632, on SC process dynamics. ROCK also has been previously shown to affect neurite retraction and cell motility (Hall, 1998; Kaibuchi et al., 1999a; Nikolic, 2002), suggesting distinct roles for ROCK in both the SC process retraction and unipolar migration phases of this motility cycle. In GFP transfected SCs, Y-27632 reduced both the frequency (Fig. 27A; GFP – 43.6±2.6% vs. GFP+Y-27632 – 20.5±3.7%, p=0.0012) and rates (Fig. 28A; GFP – 0.49±0.06 μm/min vs. 0.20±0.05 μm/min, p=0.0056) of process retraction by more than 50%. Assessing the active migration phase of this motility cycle, the inhibitor did not statistically depress the frequency (Fig. 27B; GFP – 67.8±5.9% vs. GFP+Y-27632 - 44.0±20.8%, p=0.2608) of unipolar SC migration. The inhibitor did, however, diminish the SC migration rate by 71% (Fig. 28B; GFP – 0.21±0.03 μm/min vs. GFP+Y-27632 – 0.06±0.01 μm/min, p=0.0001).

The effectiveness of the ROCK inhibitor on process retraction in the presence of over-expressed EBP50 was not as pronounced. Y-27632 did not statistically reduce the process retraction frequency (Fig. 27A; EBP50-GFP – 47.7±10.2% vs. EBP50-GFP+Y-27632 – 22.6±3.2%, p=0.1574), but did reduce the retraction rate by 37% (Fig. 28A; EBP50-GFP – 0.71±0.10 μm/min vs. EBP50-GFP+Y-27632 – 0.45±0.04, p=0.0423). Unipolar SC migration was as substantially affected by ROCK inhibition in the presence of EBP50-GFP as in the SCs transfected with GFP alone. The migration frequency of EBP50-expressing SCs was reduced by Y-27632 (Fig. 27B; EBP50-GFP – 95.8±4.2% vs. EBP50-GFP+Y-27632 – 50.0±16.7%, p=0.0433), and the unipolar SC migration rate was diminished by 70% (Fig. 28B; EBP50-GFP – 0.40±0.06 μm/min vs. EBP50-GFP+Y-27632 – 0.12±0.03 μm/min, p=0.0017). These results suggest that SC dynamics are affected not only by EBP50-facilitated interactions but also by Rho pathway activation via ROCK.

Clues as to how EBP50 may affect SC motility arise from the localization of active pERMs at the rear of the unipolar cell. Over-expression of EBP50 significantly enhanced the percentage of unipolar cells that displayed pERM staining at their rear by 53% versus GFP transfected controls (Fig. 29D, G; GFP - 52.2±2.9% vs. EBP50-GFP - 79.9±2.6%, p=0.0021). By contrast, over-expression of EBP50-70 severely reduced the number of unipolar cells exhibiting rear pERM staining (Fig. 29E, G; EBP50-70-GFP – 20.4±4.1%), supporting the idea that EBP50 may be involved in the recruitment of molecules that play a role in ERM activation. In contrast to EBP50-70, EBP50-PDZ1+2 was correctly targeted to the tip of the SC process and the rear of the unipolar cell (Fig. 29F). Surprisingly, this construct also appeared to enhance ERM activation at the rear of

# Figure 29 - EBP50 localization and ERM activation – dependence upon ezrin-binding, PDZ-mediated interactions, and ROCK activity

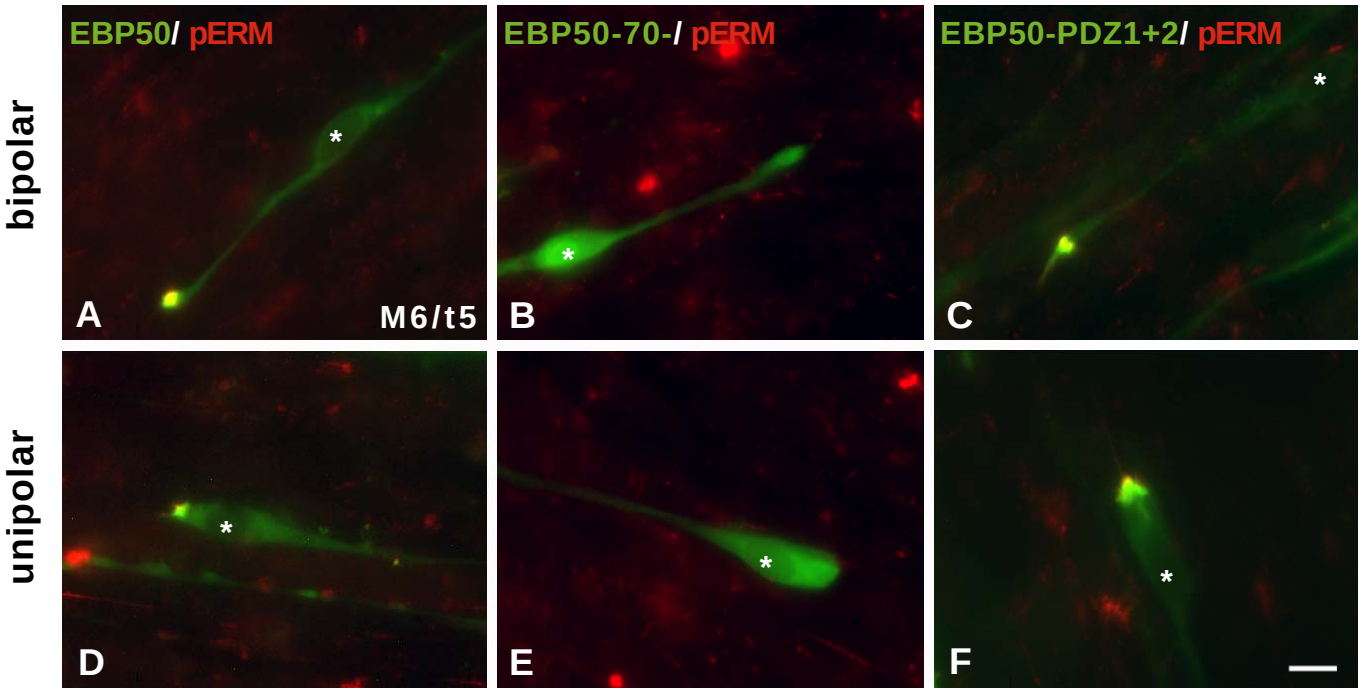


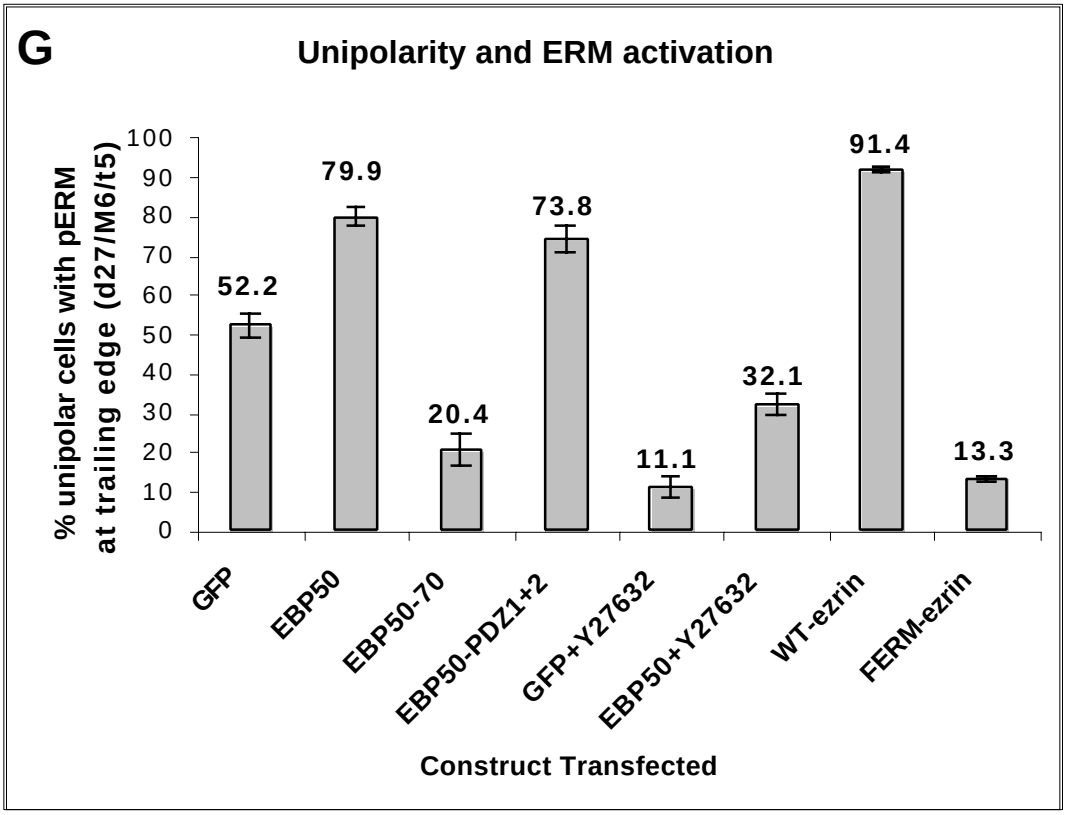

Figure 29 - EBP50 localization and ERM activation – dependence upon ezrin-binding, PDZ-mediated interactions, and ROCK activity

A) Full length WT-EBP50, EBP50-70 (lacking its ERM-binding domain), and EBP50-PDZ1+2 (deleted for the two PDZ binding domains) were transfected into SCs. Composite images (M6/t5) are shown with EBP50-GFP variants in green, activated, pERM in red, and co-localization in yellow. Localizations were assessed at the distal tips of bipolar SCs and at the rear of unipolar SCs. Asterisks denote nuclear positioning for spatial reference. Scale bar=10 μm. B) Presented is a quantification of ERM activation at the cell rear in unipolar SCs after introduction of the specified constructs (M6/t5), expressed as a percentage of the total number of unipolar cells observed. GFP – 52.2±2.9%, EBP50-GFP – 79.9±2.6%, EBP50-70-GFP – 20.4±4.1%, EBP50-PDZ1+2-GFP – 73.8±3.4%, GFP+Y-27632 – 11.1±2.9%, EBP50-GFP+Y-27632 – 32.1±3.0%, WT-ezrin – 91.4±0.1%, FERM-ezrin – 13.3±0.3%. Data are representative of 3 independent experiments wherein an average of 81±5 transfected cells were counted per construct.

the cell (Fig. 29G), while it did not enhance either asymmetric process retraction or the rate of unipolar cell motility (Figs. 27, 28). This result suggests a biphasic regulation involved in unipolar SC motility. The bi-functionality of EBP50 enables interactions involving both the PDZ interaction domains and COOH-terminal region to synergistically mediate enhancement of directed SC migration.

As the frequency and rates associated with SC dynamics appeared to contain a distinct Rho-dependent component, we examined whether this was effected via ROCK-mediated ERM phosphorylation (Matsui et al., 1998). pERM localization at the rear of the unipolar SC in the presence of Y-27632 was depressed by 79% in GFP transfected SC (GFP – 52.2±2.9% vs GFP+Y-27632 – 11.1±2.9%, p=0.0025) and by 60% in EBP50-GFP transfected SCs (EBP50-GFP – 79.9±2.6% vs. EBP50-GFP+Y-27632 - 32.1±3.0%, p=0.0013) (Fig. 29G). Thus, under these conditions, ROCK appears to be a major, but perhaps not the sole, direct contributor to ERM activation via phosphorylation.

While ROCK has been shown to directly phosphorylate ERM proteins, it also affects ERM activation by influencing polyphosphoinositide synthesis. Acting through PI4, 5 kinase, ROCK activation promotes the generation of the membrane phosphatidylinositol, PIP2 (Sechi and Wehland, 2000). PIP2 has been implicated in the initial stages of ERM activation prior to stabilizing COOH-terminal phosphorylation (Hirao et al., 1996; Yonemura et al., 2002). By alleviating the intrinsic conformational regulation displayed by the head-to-tail association of the ERM $NH_2$- and COOH-terminal regions (Hamada et al., 2000), PIP2 encourages ERM activation. However, PIP2 synthesis can also be achieved via a ROCK-independent mechanism, whereby the small GTPase Rac interacts with diacylglycerol kinase (Tolias et al., 1998). This kinase

generates phosphatidic acid, which readily activates PI4, 5 kinase (Jenkins et al., 1994). This alternative pathway may explain the incomplete pERM disruption incurred by Y-27632 in the unipolar SCs.

To determine if PIP2 concentrations are observed at all sites of ERM activation, we used as a PIP2 reporter a GFP-fused pleckstrin homology (PH) domain of phospholipase C-delta (PLCδ), which binds to PIP2 with high affinity and selectivity (Czech, 2000). In transfected SCs (M6/t5), PLCδ-PH-GFP was localized at the SC plasma membrane, concentrating asymmetrically at one distal tip in bipolar SCs and at the trailing edge in unipolar SCs. PLCδ-PH-GFP co-localized with sites of ERM activation, as detected by pERM staining (Fig. 30A). This represents the first demonstration of a spatial and temporal co-localization of PIP2 and active, phosphorylated ERMs, supporting the idea that PIP2 is involved in ERM activation.

ERM proteins are required for appropriate SC motility and polarity maintenance

Our results suggest a major role for ERM activation in the motility of bipolar SCs, which contain all three members of the ERM family (Melendez-Vasquez et al., 2001; Scherer et al., 2001). To more clearly define the precise role of ERM activity in these motility-based processes, functional disruption of the ERMs was undertaken. Over-expression of the ezrin $NH_2$-terminal FERM homology domain perturbs ERM function as a dominant-negative due to extraordinary sequence conservation (~75% identity among family members) (Amieva et al., 1999; Crepaldi et al., 1997). To determine if exogenous ezrin constructs were correctly targeted within SCs, we co-transfected VSVG-tagged full-length, WT-ezrin or the FERM domain itself into myelinating explants along with PLCδ-PH-GFP (M6/t5). Both constructs co-localized with focal concentrations of PLCδ-PH-

# Figure 30 - PIP2 localizes to specific sites of ERM localization and activation

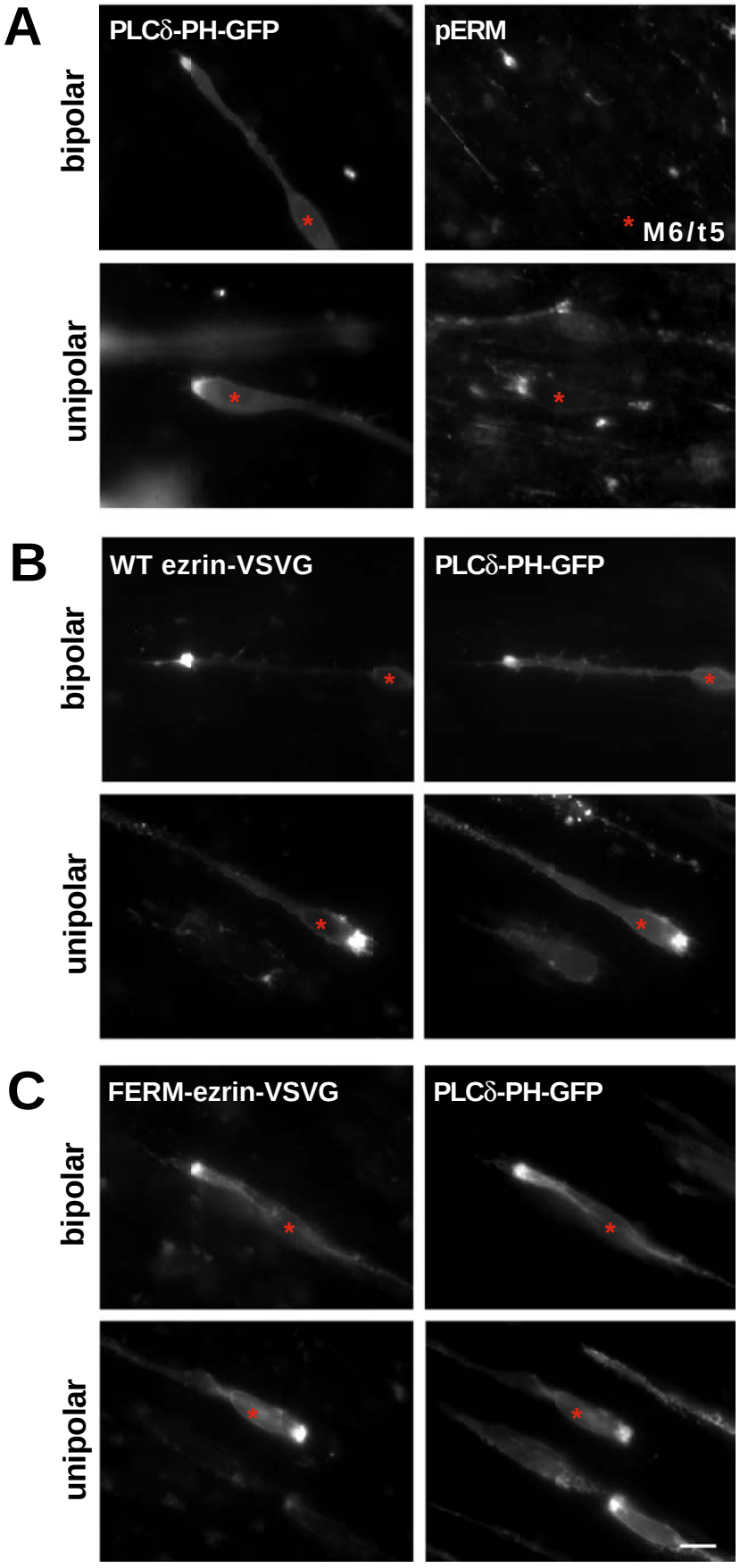

Figure 30 - PIP2 localizes to specific sites of ERM localization and activation

A) SCs were transfected with a GFP-fused PH domain of PLCδ (M6/t5). Cultures were then stained with a phospho-specific ERM antibody, which demonstrates co-localization with PLCδ-PH-GFP in bi- (upper panels) and unipolar (lower panels) SCs. B) PLCδ-PH-GFP was co-transfected with VSVG-tagged WT-ezrin. Localizations of each protein were coordinately assessed at the distal tips (upper panels) and rear (lower panels) of bi- and unipolar SCs (M6/t5), respectively. C) FERM-ezrin and PLCδ-PH-GFP were transfected into SCs (M6/t5). Localizations of both proteins were assessed at the distal tips (upper panels) and rear (lower panels) of bi- and unipolar SCs, respectively. Asterisks denote nuclear positioning for spatial reference. Scale bar=10 μm.

GFP at one tip of the bipolar SCs and at the rear of the unipolar SCs (Fig. 30B-C). When stained for pERM, SCs transfected with WT-ezrin (M6/t5) displayed 91.4±0.1% of unipolar cells with pERM accumulation at the rear, and the FERM variant depressed these levels to 13.3±0.3% ($p<0.0001$) (Fig. 29G). These results support the idea of the FERM domain acting as a dominant-negative repressor of endogenous ERM function potentially competing with endogenous proteins for sites of PIP2 concentration.

While populations of bi- and unipolar SCs were clearly present in SCs transfected with ezrin variants, there were other remarkable findings with regard to SC polarity. The over-expression of WT-ezrin had no overtly adverse effect on SC polarity. The majority of the cells maintained their bipolar, singly axon-aligned morphology. The ezrin FERM domain, however, induced a significant increase in the number of multipolar SCs with numerous process extensions associated with various axons (Fig. 31A, C; WT-ezrin 20.2±1.4% vs. FERM-ezrin - 69.3±1.8%, $p=0.0001$). When co-transfected with EBP50-GFP, 94.1±0.4% of EBP50-GFP-positive cells were also VSVG-positive. Thus, EBP50-GFP fluorescence visualization was employed and considered sufficient to monitor the effects of the ezrin constructs on SC dynamics in time-lapse microscopy.

The ezrin FERM domain clearly and dramatically interfered with appropriate SC motility. Over-expression of this construct yielded an unresolvable, non-motile, multipolar phenotype. Although some cells attempted process retraction, most of these occurrences were incomplete and unable to re-establish bipolarity. Despite the multipolar SCs' inability to substantially migrate, nuclear oscillations within the SC soma were frequently observed. In addition, there were often large, ruffling lamellipodia emanating from the SC body and/or extended processes (Fig. 31B, supplemental material

# Figure 31 - Functional ERM is required for maintenance of SC polarity and appropriate motility

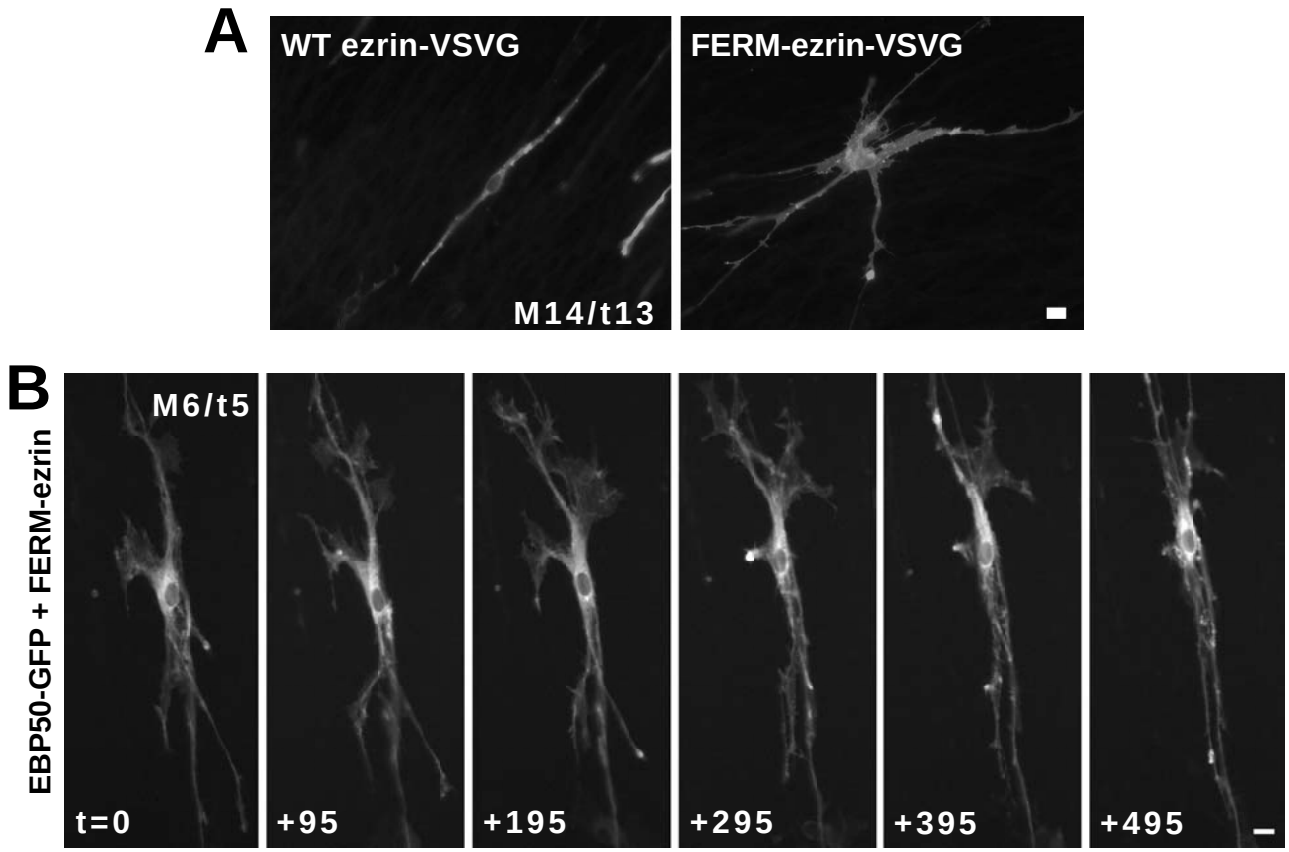


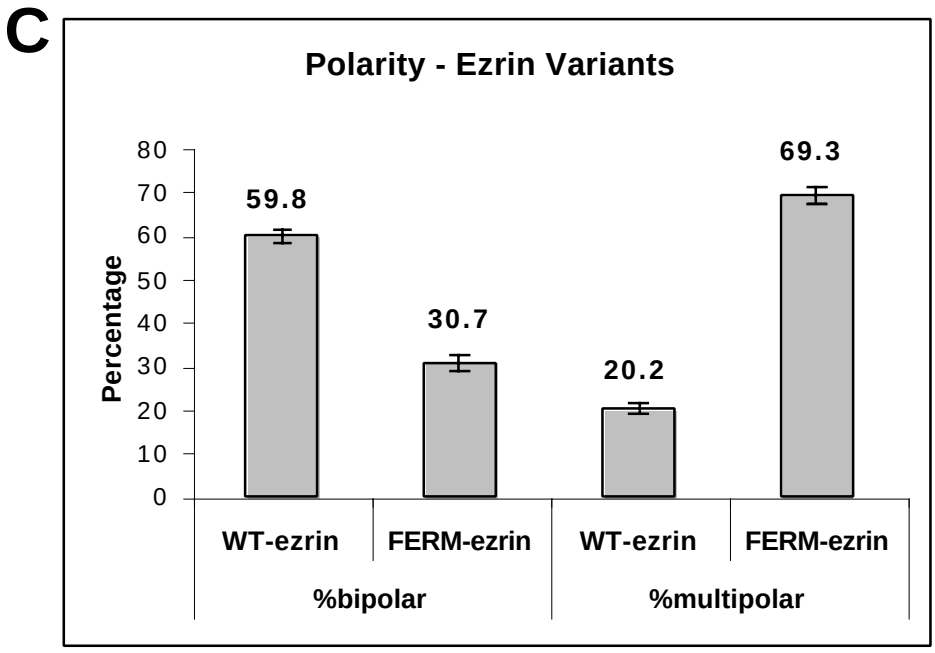

Figure 31 - Functional ERM is required for maintentance of SC polarity and appropriate motility

A) SCs were transfected with either WT (left) or FERM (right) VSVG-tagged ezrin (M14/t13). B) Introducing the FERM-ezrin construct in the presence of EBP50-GFP (M6/t5), the motility of these cells was monitored. Multipolarity and gross motility defects were observed. Frames presented span an elapsed 495 minutes. See also Fig31Bvideo13-DN-ez.mov. Scale bar=10 μm. C) Quantitative presentation of multipolarity induced by transfection of FERM-ezrin as compared to WT-ezrin (M6/t5) (FERM - 69.3±1.8% vs. WT - 20.2±1.4%). Data are representative of 3 individual experiments wherein an average of 696±59 cells were counted per construct.

Fig31Bvideo13). Thus, ERM family members are fundamental in regulating SC process extension and maintaining SC polarity.

Supplemental Material

The time-lapse sequences from which the still images presented in figures 25, 26, and 31 were taken are available for viewing as supplemental material on the provided CD. More detailed video descriptions can be found in Appendix II. Fig25Avideo7 shows process retraction leading to a unipolar morphology in a GFP-transfected SC. Fig25Bvideo8 and Fig25Cvideo9 demonstrate GFP-transfected SCs undergoing unipolar, nucleokinetic migration and bipolarity re-establishment. Fig26Bvideo10 illustrates EBP50-GFP localization coincident with asymmetric process retraction. Fig26Cvideo11 and Fig26Dvideo12 show SC migration and morphologic cycling in EBP50-GFP transfected SCs. Fig31Bvideo13 demonstrates the multipolarity and process dynamics in a SC co-transfected with EBP50-GFP and ezrin-FERM constructs.

Discussion

In this study, we describe a novel form of motility associated with bipolar SCs migrating in association with axons within myelinating DRG explants. As represented in the model shown in figure 32, these cells cycle between static, bipolar and motile, unipolar morphologies associated with asymmetric process retraction and extension. Unipolar cell motility exhibits a nucleotaxic characteristic, reminiscent of neurons migrating on radial glia (Nadarajah et al., 2001; Nadarajah and Parnavelas, 2002). Using GFP fusions of EBP50 as indicators of sites of ERM activation, we observed that these proteins are activated at the tip of the retracting process and concentrated at the rear of the migrating cell. At these sites, ERM proteins co-localized with concentrations of the membrane phospholipid PIP2, considered to be an upstream trigger for ERM activation. Over-expression of EBP50 enhanced unipolar cell movement, suggesting a new role for this adaptor protein in cell motility. Finally, perturbation of ERM function interfered with both process retraction and cell motility, causing SCs to lose their characteristic bipolar shape and assume a multipolar morphology.

Let us first examine process retraction and the relationship between uni- and bipolarity in terms of their necessity in SC migration. Approximately 46% of bipolar SCs retract one distal process and begin directed, unipolar migration. This form of motility appears to obligately require the retraction of one distal process prior to the commencement of gross cell movement. This suggests that the uni- and bipolar SCs observed in the DRG explants simply represent distinct polarity states through which the SCs may cycle. However, the 54% of SCs that do not undergo process retraction maintain their bipolarity and are, primarily, non-motile. This conversely suggests that

# Figure 32 - Model - SC motility cycle

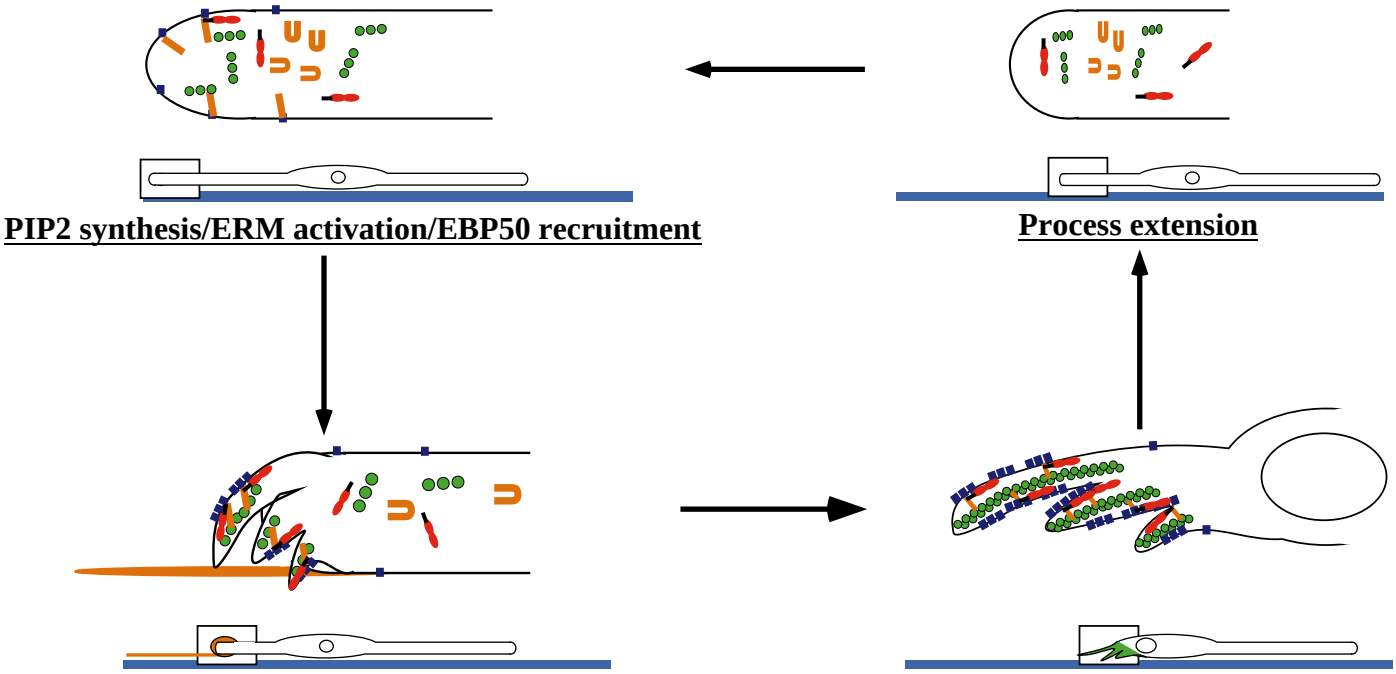

Figure 32 – Model - SC motility cycle

As SCs align themselves along axons and probe their local environment, migration may be required in the absence of stabilizing signals that indicate appropriate positioning. Rho activation and PIP2 synthesis may initiate this process. Upon PIP2 (blue squares) concentration, ERM stabilization and activation (orange), and EBP50 (red) localization to a given actin (green) enriched SC tip, this process of the SC retracts. This is often clearly visualized by the trailing of a distinct retraction fiber. This process retraction generates a motile, unipolar SC that migrates in a neuron-like manner. As these unipolar SCs migrate, PIP2, ERM, EBP50, and actin concentrations are retained. Upon the encounter of an appropriate stimulus, the accumulations of these components at the cell rear dissipate, and process extension re-establishes SC bipolarity.

there may in fact be two classes of SCs at the onset of myelination in the DRG explants, which at least differ in their motility response to global application of serum and ascorbate.

Differentiating between these two hypotheses may be possible by exploiting the asymmetric nature of the apparent signaling that leads to unipolar migration. If all SCs possess the molecular machinery to enable the cycle of process retraction and unipolar migration, perhaps appropriate cue encounter is the limiting factor. Then, directly promoting localized ERM activation and EBP50 recruitment may be sufficient to trigger the predicted motility response. To facilitate discrete, enhanced Rho signaling or PIP2 accumulation, localized application of either LPA or free PIP2, respectively, to one distal tip of a non-motile, bipolar SC, could be employed.

If the otherwise static SCs do not respond to this treatment, it is possible that qualitative differences exist among sub-populations of these cells. Precedents for this type of relationship can be fundamentally derived from the fact there are, indeed, both myelinating and non-myelinating SCs *in vivo*. We have not examined the relative contribution of each class of SCs to the explants' glial composition, nor have we examined the specific developmental phenotype of the migratory SCs. Utilizing the characteristic molecular signatures of myelinating and non-myelinating SCs, we may be able to correlate myelinating status with motility phenotype.

One of the most striking features of the novel SC motility described in this study is its similarity to the migration of neurons on radial glia (Nadarajah et al., 2001; Nadarajah and Parnavelas, 2002). SCs are proposed to acquire their elongated bipolar morphologies from alignment with axons. The similarity in motility mechanisms may

reflect morphological constraints imposed on cells migrating in association with long, extended substrates, such as axons or radial glia. Support for this stems from our studies of early DRG explant development (Gatto et al., 2003). In the first week of culture, SCs migrating from the body of the explant have not yet acquired a bipolar morphology and look fibroblastic in nature. In these cells, active ERM proteins are distributed through the perimeter of the cell, sometimes accumulating at the leading edge, rather than the rear of the migrating cell (Chapter 4, Fig. 16). These observations suggest that the function of active ERMs at the rear of the migrating cell may be peculiar to the developmental staging and morphology of the mature, elongated SC.

The functions of active ERM proteins at the rear of the migrating unipolar cell are unknown. These proteins appear to be associated with active filopodia at the rear of the cell, which might be involved in environmental sensing as the cell advances. Such a "rear-facing" growth cone could be important for process extension, ensuring that the SC is able to maintain its alignment with the axon when bipolarity is re-established. Alternatively, ERM proteins have been extensively implicated in cell adhesion (Bretscher et al., 2002; Louvet-Vallee, 2000; Mangeat et al., 1999), and their localization at the rear of the migrating unipolar cell could reflect a role in the release of rear adhesions necessary for the forward movement of the cell. This concept is evidenced by studies of moesin function in the trailing uropod of migrating neutrophils (Yoshinaga-Ohara et al., 2002). Here, the Rho-mediated retraction of the uropod is achieved via spatiotemporal regulation of moesin phosphorylation. The nature of the adhesions potentially mediated through ERM proteins in SC motility also remains unknown. However, N-cadherin is concentrated at the SC process tip during the early stages of SC-axon alignment (Wanner

and Wood, 2002), and perturbations of N-cadherin mediated SC-axonal contacts in SC/DRG co-cultures result in a multipolar SC phenotype similar to those reported herein upon ERM perturbation.

In this study, we demonstrate, for the first time, a definitive role for the ERM adaptor protein EBP50 in cell motility. Over-expression of EBP50 enhances unipolar cell motility. This enhancement is dependent upon the presence of the molecule's PDZ domains. Similarly, over-expression of the PDZ domains of EBP50 alone in the absence of the ERM binding region inhibits both process retraction and unipolar cell motility, suggesting that EBP50 recruits molecules to sites of active ERMs that facilitate motility. We are intrigued as to why the EBP50-PDZ1+2-GFP construct does not behave as a dominant-negative for EBP50 function, as is observed with the EBP50-70-GFP construct. This may reflect differences in the stoichiometries or affinities of interactions involving the ERM binding site and the PDZ domains. Also, EBP50-70 appears to inhibit the accumulation of pERMs at the rear of the unipolar cell, whereas EBP50-PDZ1+2 enhances this effect similarly as to what is observed with wild type EBP50. Thus, EBP50 functions as a bi-modal adaptor and mediates differential, but equally necessary, interactions leading to appropriate unipolar cell motility.

Understanding these intricacies awaits further identification of the role of EBP50 in cell motility. However, clues as to this function arise from recent observations of an interaction between EBP50 and Rack1 (Liedtke et al., 2003; Liedtke et al., 2002). Rack1 has been extensively implicated in cell motility and binds to both β1 integrin and isoforms of PKC (Besson et al., 2002; Buensuceso et al., 2001; Liliental and Chang, 1998; Schechtman and Mochly-Rosen, 2001). As ezrin has been identified as an effector

for integrin-mediated signaling through PKC (Ng et al., 2001), EBP50 may then provide an important link between integrin-mediated cell signaling and ERM activation.

In addition, with the identification of the SC EBP50/ERM-enriched cap structure as a novel indicator of SC process retraction, and not necessarily a stable precursor to SC microvilli, we must reassess the correlation between cap and node formation previously described (Chapter 4, Fig. 21). Culture conditions that enhance SC cap formation do indeed lead to the more efficient generation of SC microvilli. However, these results, in light of the cap-associated SC dynamics, implicate a novel role for SC motility in achieving proper myelination. Further characterization of SC motility may lead to advances in understanding the elusive mechanics involved in the initiation of myelination.

The functionality of unipolar cell motility in myelination and its initiating signals remain unknown. We have observed that SCs are highly dynamic and exhibit localized concentrations of RhoA (Chapter 4, Fig. 18) (Gatto et al., 2003). Enriched in this signaling molecule, the SC tips themselves may represent the sensors that initiate process retraction. Signals that initiate this event could include axonal contact or contacts with other SCs. The number of unipolar cells observed in myelinating DRG explants falls as the cultures mature and myelination progresses, suggesting a role for this form of motility in the early events of the myelination program. This program requires the defining of precise internodal lengths that, to some extent, must reflect the regular periodic spacing of SCs along the length of the axon. Unipolar cell motility and asymmetric process retraction and extension could play a role in achieving this regular alignment of SCs along the axon prior to the elaboration of myelin sheaths. In support of this, we have

observed unipolar MAG-positive myelinating SCs. This suggests that the general bipolarity of a myelin segment could result from the delayed elongation of a unipolar segment, rather than from SCs achieving obligate bipolarity prior to the onset of myelination. As elongation and compaction of the myelinating SC have been proposed to influence the organization of the axo-glial interface (Pedraza et al., 2001), then process re-extension from the unipolar myelinating cell may be fundamental to factors such as nodal organization.

# Chapter 6

## Discussion and Future Directions

Functionality of EBP50 and Schwann cell caps

Localization of Kv1.5

Cell adhesion/alignment mediated via N-cadherin

Syndecans and membrane-associated complexes

Exploitation of retroviral infection

Myelination is a specialized, intricate process that involves the intimate association of the myelinating glial cell with its target axon. Neural functionality is critically dependent upon the successful generation of myelin segments and associated nodes of Ranvier which coordinate rapid, saltatory action potential conduction. The findings presented herein describe and begin to functionally define the PNS' axo-glial interactions mediated by SC caps upon the induction of myelination. These ERM and EBP50-enriched structures have been linked to appropriate SC process dynamics, SC motility, and efficient node formation. One key question that remains to be answered is what the precise role of EBP50 is in these structures and in SC microvilli proper.

EBP50 is situated to mediate directed targeting and retention of specific membrane proteins to the distal tips of the SC with its two PDZ binding domains and ezrin binding capability (Reczek et al., 1997). EBP50 becomes localized to the nodes of Ranvier in the SC microvilli, which are in close association with the underlying axonal membrane in myelinated tracts. This axonal region undergoes dramatic and repetitive membrane depolarization as action potential propagation continues. To moderate this constant electrical flux, EBP50 could serve to localize appropriate ion channels to the nodal gap that could facilitate ionic buffering.

Our preliminary data suggests that EBP50 may interact with the voltage-dependent, *Shaker*-like, delayed-rectifying potassium channel, Kv1.5, upon the induction of myelination. Co-localization of endogenous EBP50 with a T7-tagged Kv1.5 variant has been demonstrated at the microvillar component-enriched SC distal tips (Fig. 33). Although Kv1.5 has been previously localized to mature SC microvilli (Mi et al., 1995), its interacting partners there were never identified. However, the COOH-terminal amino

# Figure 33 - Kv1.5 co-localizes with EBP50 at SC tips

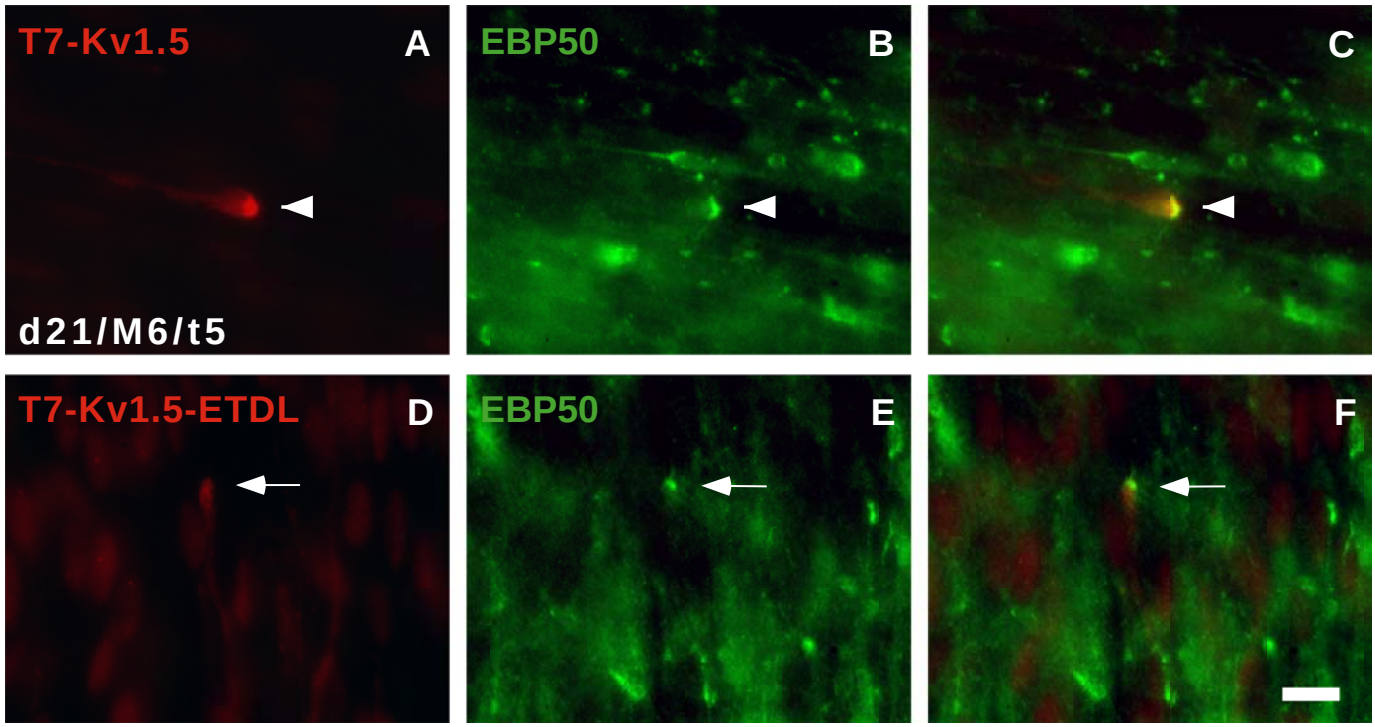

Figure 33 - Kv1.5 co-localizes with EBP50 at SC tips

SCs were transfected with T7-tagged-Kv1.5 (A) and immunostained for endogenous EBP50 (B). At d21/M6/t5, co-localization was evident at the SC distal tip (composite C, arrowheads) and appeared to be, at least partially, dependent upon the PDZ-binding motif (-ETDL) of Kv1.5. Transfected Kv1.5-ETDL (D) resulted in diminished detectable Kv1.5 at the EBP50-reactive (E) SC tip (composite F, arrows). Scale bar=10 μm.

acid sequence of Kv1.5 (–ETDL) closely approximates one derived consensus sequence for binding to EBP50's PDZ domains (-D-S/T-X-L) (Wang et al., 1998). Further, in support of this proposed PDZ-mediated interaction, removal of either the PDZ domains of EBP50 or the –ETDL PDZ-binding sequence of Kv1.5, specifically abrogates their co-localization in SCs (Figs. 34, 35).

These data and our preliminary biochemical examination (unpublished data, B. Walker, Lambert Lab) indicate that EBP50 generally may serve as a scaffold for the linkage of Kv1.5 to cytoskeletal components. This link could be indispensable for the appropriate electrical responsiveness of mature myelinated nerves. Our data implicate Kv1.5 as being resident at the distal tip of a retracting SC process rather than in a static structure, as defined by EBP50 enrichment being linked to process instability. How Kv1.5 functions in the morphologic plasticity exhibited by SCs remains to be determined, but it has been shown that Kv1.1 and 1.5 over-expression in intestinal epithelial cells promotes membrane hyperpolarization and a 4-fold increase in cellular migration rates (Rao et al., 2002). Perhaps then, Kv1.5 is promoting enhanced motility of the SC process with its focal concentration specifically residing at the distal tip of the cell.

Impairing the ionic activity of Kv1.5 by introducing specific inhibitors of this channel would allow us to test this hypothesis. The pharmacologic agent, tyrphostin AG-1478, acts as a potent protein tyrosine kinase inhibitor and rapidly, reversibly inhibits Kv1.5 currents in a concentration-dependent manner (Choi et al., 2002). 4-aminopyridine also inhibits Kv1.5. This inhibition is pulse-frequency-dependent and is associated with a positive shift in activation voltage dependence (Kerr et al., 2001). Treating the explant cultures with these compounds may provide insight as to whether

# Figure 34 - Kv1.5 localization is dependent upon its ETDL motif and the PDZ-binding domains of EBP50

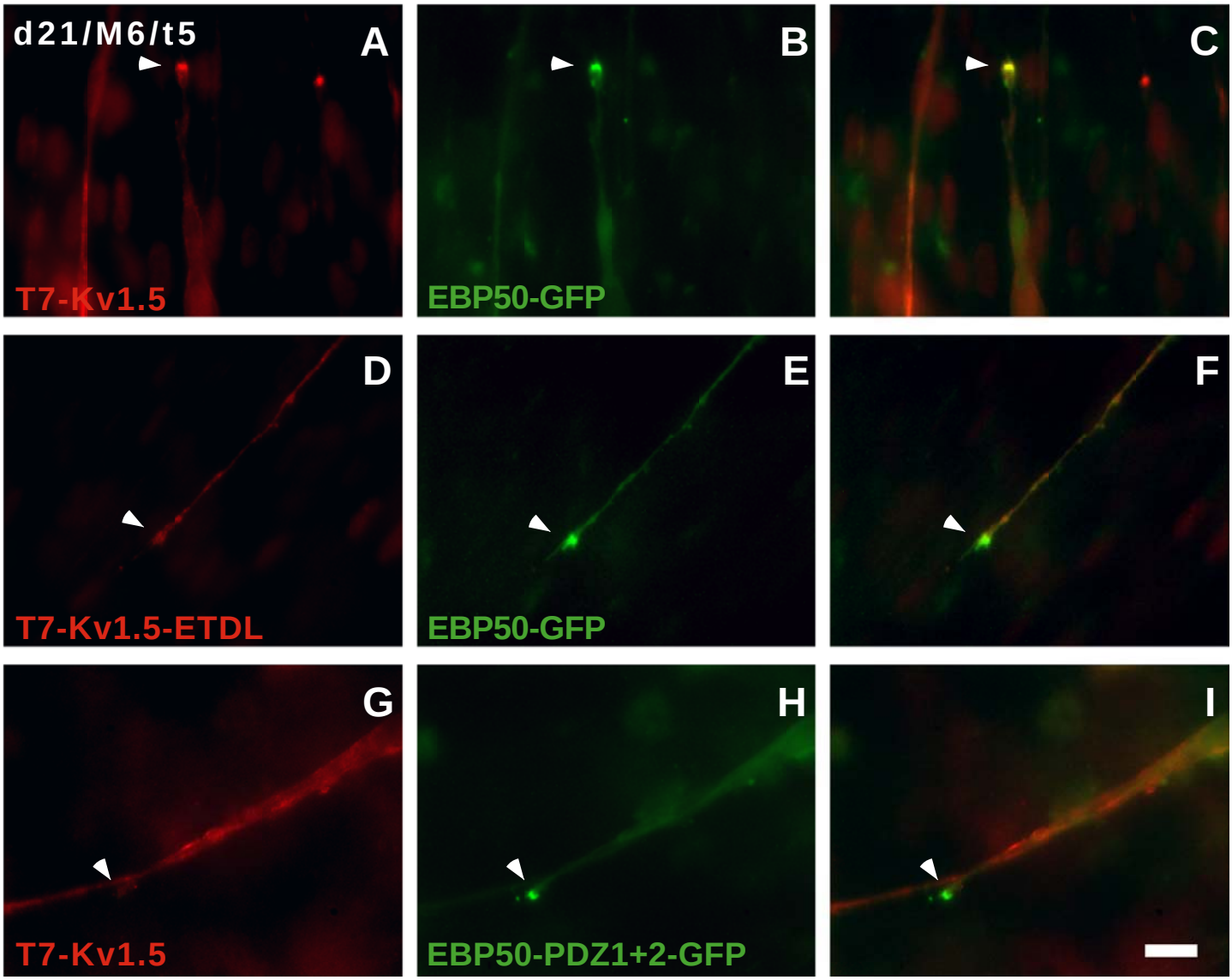

Figure 34 - Kv1.5 localization is dependent upon its –ETDL motif and the PDZ-binding domain of EBP50

SCs were transfected with variants of Kv1.5 and EBP50 to address the domain requirements for their co-localization. Full length T7-Kv1.5 co-localized with full length EBP50-GFP (A-C) at SC distal tips. The co-localization of these two constructs was reciprocally dependent upon the presence of the PDZ binding motif of Kv1.5 (-ETDL) (D-F) and the PDZ domains of EBP50 (G-I). Arrowheads denote SC caps. Scale bar=10μm.

# Figure 35 – Quantification of Kv1.5 cap localization

A

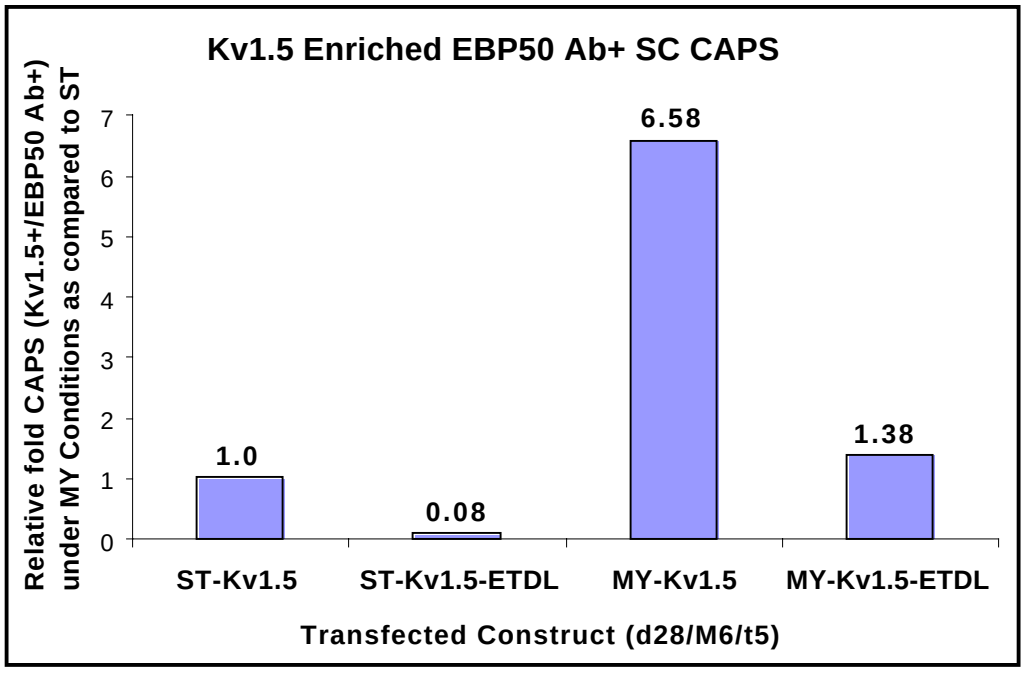


B

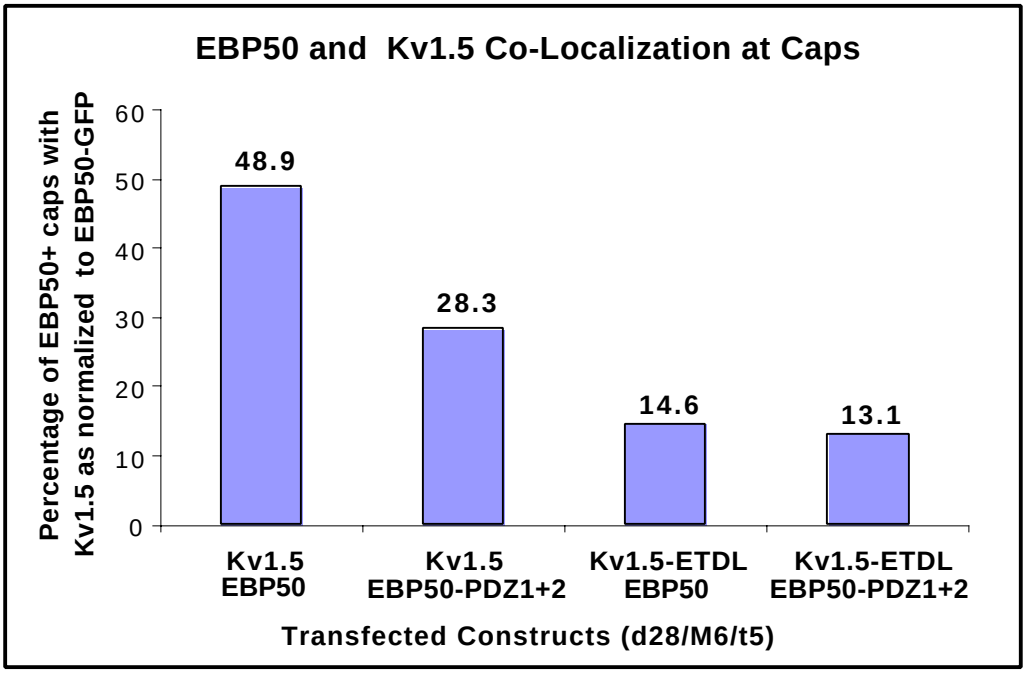

Figure 35 – Quantification of Kv1.5 cap localization

A) Quantitative assessment of Kv1.5-enriched, EBP50-positve SC caps in DRG explant cultures. The basal level of Kv1.5 transfected SCs with EBP50-positive caps (detected by either EBP50-GFP or EBP50 immunoreactivity) was determined examining Kv1.5 transfected cultures under standard conditions and set at 1=0.66%. This minimal percentage was further reduced by the introduction of the Kv1.5 variant lacking its COOH-terminal PDZ binding motif (-ETDL). Upon the induction of myelination, the percentage of Kv1.5/EBP50-reactive caps increased 6.6-fold, which was dependent upon the ability of Kv1.5 to interact with EBP50. B) Presented is a quantitative analysis of the PDZ-mediated dependence of the co-localization of Kv1.5 and EBP50. Using EBP50-GFP enrichment at the SC distal tip as the normalizing indicator of cap formation, the percentage of Kv1.5/EBP50 co-localization was determined. Assuming the maximal number of caps is detectable in EBP50-GFP transfections and taking this value to represent 100%, which itself in these studies occurred in 12.0±0.1% of transfected cells, 48.9% of caps displayed co-localization of T7-Kv1.5 and EBP50-GFP. This was reduced to 28.3% by removing the PDZ binding domain of EBP50 and to 14.6% by removing the PDZ-binding capability of Kv1.5. The lowest percentage of co-localization (13.1%) was seen with the co-transfection of the two mutually PDZ interaction deficient protein variants (EBP50-PDZ1+2-GFP and T7-Kv1.5-ETDL).

Kv1.5 activity is required in promoting SC migration. It also may be helpful to introduce these effectors in the presence of SCs transfected with EBP50-GFP to specifically monitor cap dynamics, as Kv1.5 concentrates at the SC distal tips.

Examining other EBP50/ion channel interactions that may be involved in SC migration, EBP50 is known to bind the $Na^+/H^+$ exchanger isoform 3, NHE3, which enables the electroneutral counter-transport of $H^+$ for $Na^+$ across the plasma membrane (Reczek et al., 1997; Weinman et al., 1993). A link established between pH and cellular morphology indicates that rounding cells are 0.15 pH units more acidic than spreading cells (Schwartz et al., 1989). Thus, cell spreading increases intracellular pH. Considering SC process retraction as the antithesis of spreading, we predict acidification at the SC tip may be required. This could be specifically mediated by down-regulation of NHE3 and/or other local $Na^+/H^+$ antiporters. Thus, the EBP50 concentration at the SC tip may be serving to mediate the turnover and removal of NHE3 from the membrane.

To directly address whether this EBP50 binding partner has a role in SC dynamics, we propose disrupting the functionality of NHE3 in these cells. In fact, treatment of epithelial cells with toxin B of *Clostridium difficile* causes inhibition of NHE3 activity, with decreased NHE3 activity being accompanied by the translocation of exchangers to a subapical endomembrane compartment (Hayashi et al., 2004). In addition, NHE3 is acutely inhibited by the cholinergic agonist carbachol, which prompts elevation of the intracellular concentration of free calcium ions (Lee-Kwon et al., 2003). If these NHE3 inhibitors are applied to myelination-induced DRG explants, we may be able to promote more rapid SC process retraction and/or migration by forcing the cells to

become generally acidotic. However, global shifts in pH may be insufficient in mediating localized effects at the distal tip of bipolar and at the rear of the unipolar SCs.

Lastly, if pH itself is found to be of significance, in terms of mediating process retraction and migration, loading SCs with a pH-sensitive, ratiometric, fluorescent dye may prove useful. 2',7'-Bis(2-carboxyethyl)-5(6)-carboxyfluorescein (BCECF) can be introduced into cells as a nonfluorescent membrane-permeant acetoxymethyl ester, BCECF-AM. Upon hydrolysis, BCECF-AM becomes a membrane impermeable, free-acid derivative (Paradiso et al., 1984; Thomas, 1986). BCECF has a pKa of 6.97, permitting an ideal dynamic range for monitoring pH changes in an intracellular environment with high sensitivity. By monitoring SCs loaded with this dye, we may be able correlate localized changes in intracellular pH and specific motility responses, including process retraction and migration itself.

Considering EBP50 in terms of its influence on SC dynamics, we must further note that cell migration generally requires the extension of a leading process, formation and stabilization of forward adhesions, contraction and advancing of the cell body, and disassembly of rear adhesions (Horwitz and Parsons, 1999). The localization of this membrane adaptor protein to the distal tips of retracting SC processes and to the rear of the migrating unipolar cell implies that EBP50 could aid in localizing components that function in mediating the dissolution of adhesive interactions required to propel the SC forward. Our initial studies have demonstrated the co-localization of EBP50 and/or pERM at SC distal tips in 65.4±3.4% of cap-presenting cells with the cell adhesion molecule N-cadherin (Fig. 36).

# Figure 36 - N-cadherin localizes to the SC distal tip

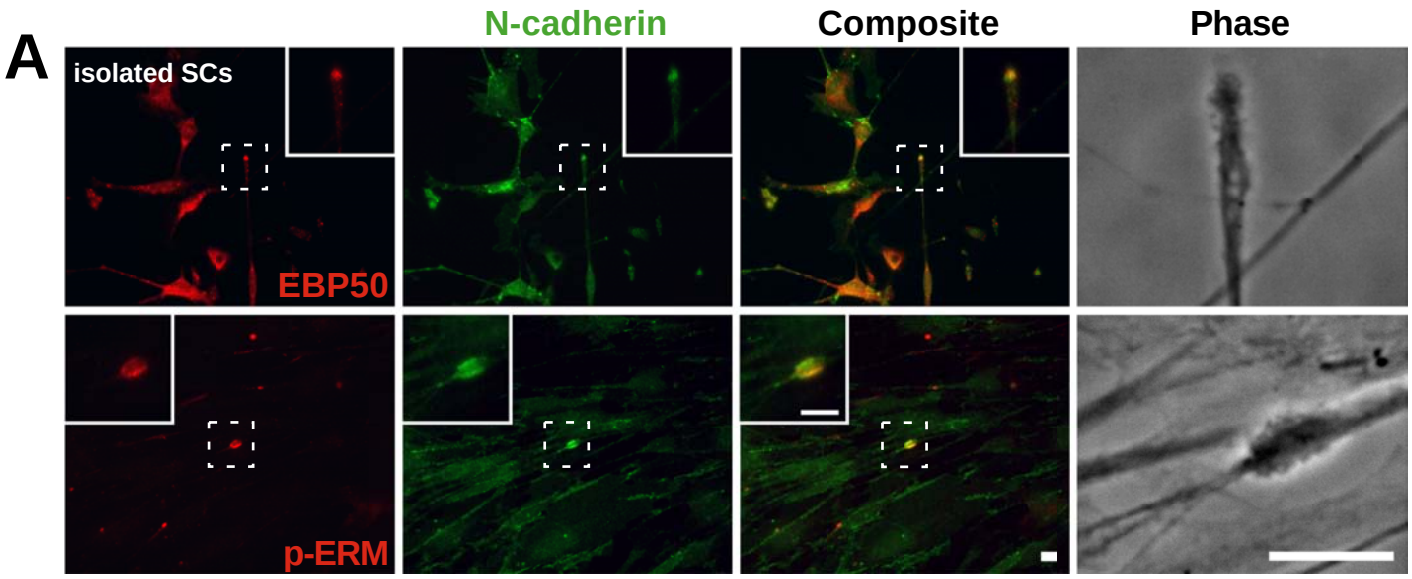


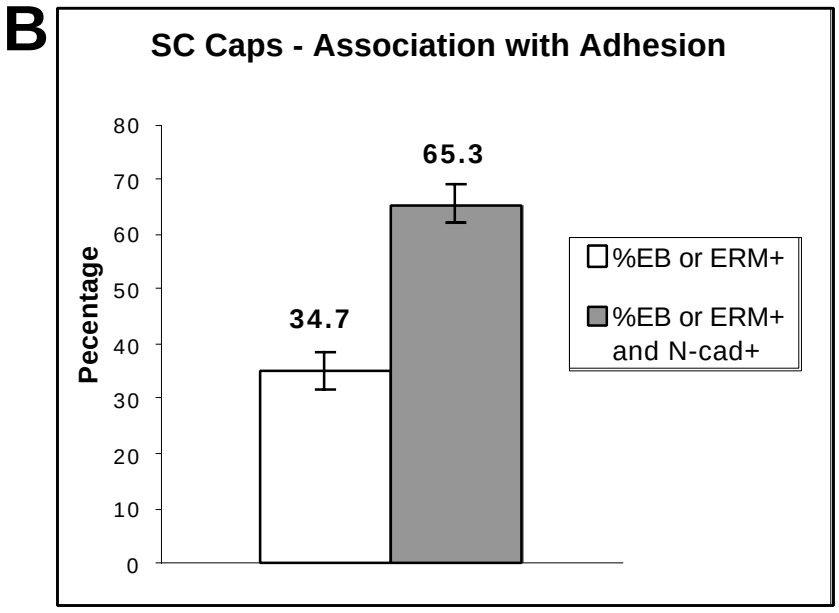

Figure 36 - N-cadherin localizes to the SC distal tip

A) The potential association of adhesive components with the SC distal tip/cap was examined in isolated SCs. Immunostaining with EBP50 or phospho-ERM (red) revealed the frequent co-localization of N-cadherin (green) in areas enriched with these microvillar components. Scale bar=10 μm. B) Quantitatively, 65.3±3.4% of the SC caps were reactive for either EBP50 or phospho-ERM and N-cadherin, while 34.7±3.4% were reactive only for either EBP50 or phospho-ERM. These data represent the average of two independent coverslips examined that were derived from the identical preparation of SCs.

Cadherins mediate cell-cell adhesion via extracellular, calcium-dependent homophilic interactions. Their intracellular regions interact with cytosolic α- and β-catenins. β-catenin serves as a bridge between cadherin and α-catenin, and α-catenin links the complex to the actin filament network (reviewed in Fukata and Kaibuchi, 2001; Kaibuchi et al., 1999b). Together these sets of interactions enable the formation of stable cell-cell adhesions. By protein interaction screening, EBP50 has been identified as a β-catenin-associating molecule (Shibata et al., 2003), with β-catenin harboring a PDZ-binding consensus sequence (-DTDL). Achieving interaction with and sequestration of β-catenin, EBP50 could down regulate N-cadherin mediated cell-cell contacts by disrupting α- and β-catenin interactions.

Both PNS and CNS myelination studies indicate that N-cadherin functions to support contact-mediated, axo-glial alignment of both myelinating SCs and oligodendrocytes, respectively (Schnadelbach et al., 2001; Wanner and Wood, 2002). These studies would suggest that uncoupling N-cadherin signaling could generate a less axon-adhesive, more motile SC. In practice, N-cadherin perturbation leads to 59% of exogenous SCs becoming misaligned with respect to co-cultured DRG axons, with SCs assuming either a multipolar or non-processed, "non-polar" phenotype (Wanner and Wood, 2002). As the multipolarity closely approximates our results following ERM disruption, SCs with perturbed N-cadherin signaling may alternatively exhibit impaired motility. Thus, global N-cadherin disruption studies may not clearly identify the role of N-cadherin in SC process dynamics. However, the effect of this cell adhesion molecule on overall SC motility has not yet been addressed.

Another line of evidence, which focuses on identifying the molecular complexes that define EBP50's functionality in SC processes, involves the syndecans. The

transmembrane, heparan sulfate proteoglycans, syndecan-3 and -4, were shown to localize to the perinodal region of myelinating SCs (Goutebroze et al., 2003). These proteins function as modulators of ligand-dependent activation of primary signaling receptors at the cell surface (reviewed in Carey, 1997). Further, syndecan-3 is most abundant during the late embryonic and early postnatal periods of peripheral nerve development and binds to the non-collagenous $NH_2$-terminal domain of alpha 4 (V) collagen, which mediates heparan sulfate-dependent SC adhesion. Syndecan-3 is susceptible to matrix metalloproteinase-dependent membrane shedding, which modulates its function (Asundi et al., 2003). Syndecan-4 binds fibronectin (Woods and Couchman, 2001) and in conjunction with $\alpha 5\beta 1$ integrin promotes stress fiber and focal adhesion formation (Wilcox-Adelman et al., 2002). However, the interaction of syndecan-4 with an ECM component tenascin-C, which is present in the nodal gap under the SC basal lamina (Martini et al., 1990; Rieger et al., 1986), decreases adhesion (Huang et al., 2001).

As the syndecans modulate adhesion based on local environment, they are well suited to functionally dictate either process retraction or extension in SC cycling. Linking the syndecans to the SC cap, syndecans bind ezrin through a conserved motif originally identified in syndecan-2 (Granes et al., 2003; Granes et al., 2000). As these ezrin-binding proteins are present in the mature, node-associated microvilli, we speculate that they reside at the microvillar component-enriched SC cap that functions in SC process dynamics and motility. Functionally, the COOH-terminal region of syndecan interacts with the PDZ domain-containing protein syntenin (Grootjans et al., 1997), which binds PIP2 (Zimmermann et al., 2002). Syndecan-4, then, is capable of binding and activating PKC in the presence of PIP2 (Bass and Humphries, 2002).

As indicated in Chapter 5, an activated-PKC interactor implicated in cell motility is Rack1. Rack1 binds not only to PKC, but also to EBP50 and β1 integrin (Besson et al., 2002; Buensuceso et al., 2001; Liedtke et al., 2003; Liedtke et al., 2002; Liliental and Chang, 1998; Schechtman and Mochly-Rosen, 2001). Further implicating cap-resident proteins potentially involved, ezrin itself has been identified as an effector of integrin-mediated signaling through PKC (Ng et al., 2001). In addition, syndecan-4 interacts with β1-integrin (Wilcox-Adelman et al., 2002), and β1 integrin is critical in the extension and maintenance of SC processes along axons (Feltri et al., 2002). Therefore, EBP50 may provide an important bridge between integrin-mediated cell signaling and ERM activation and function with the aid of Rack1 and the syndecans generating a key multi-molecular complex at the SC membrane.

In terms of examining the role of the axo-glial interactions themselves in peripheral nerve development, our results indicate a functional coupling of components that mediate the generation of mature SC microvilli (EBP50 and ERMs) and these cells' specific modes of motility at the onset of myelination. This hypothesis suggests a revisiting of genetic mutations known to generate abberant SC microvilli, i.e. the dystroglycan mutant mouse (Saito et al., 2003), and a reassessment of the motile properties of the SCs in these backgrounds.

Dystroglycan is expressed in SCs perinatally just prior to the onset of myelination and binds laminin-2, which is a component of the SCs' specialized ECM, the basal lamina (Previtali et al., 2003). Further, in myelinating SCs, dystroglycan interacts with the dystroglycan-related protein 2 (DRP2), a dystrophin isoform (DP116), and utrophin. Utrophin links the complex to the actin-based cytoskeleton (Sherman et al., 2001).

Disruption of these interactions by selective SC dystroglycan deletion in mice is known to impair microvilli formation and nodal clustering (Saito et al., 2003). It would be of significant interest to determine if dystroglycan-null SCs also posses a resultant disruption in motility. This could provide evidence of a key relationship between SC motility and appropriate node of Ranvier formation mediated via a bi-functionality of microvillar components, perhaps by allowing for correct SC positioning at the onset of myelination and nodal organization at later stages.

The myelinating DRG explant culture system has proven to be extremely powerful. The capability of transfecting axon-associated glial cells has enabled the study of effectors influencing SC development, differentiation, and motility. However, peculiar limitations did present themselves. Most importantly, despite the occasional transfected cell being engaged in active myelination, glial cell transfection appears to impede myelination. We were able to examine the generation and maturation of myelin segments and nodes of Ranvier in general. However, we were unable to effectively address the consequences of molecular perturbations on these processes utilizing exogenous protein introduction.

In pursuit of future experiments to extend these studies, an effective, under-exploited avenue involves the retroviral infection of DRG-originating SCs in the explant cultures (Howe and McCarthy, 1998). Our preliminary usage of GFP-based retroviral constructs allowed for not only the visualization of GFP-positive myelin but also these segments associated with discrete nodal specializations (Fig. 37). By employing a dicistronic retroviral vector enabling a protein of interest to be followed by an internal ribosomal entry site (IRES) and GFP, two open reading frames are generated, each of

# Figure 37 - Retroviral infection produces GFP-positive myelin segments

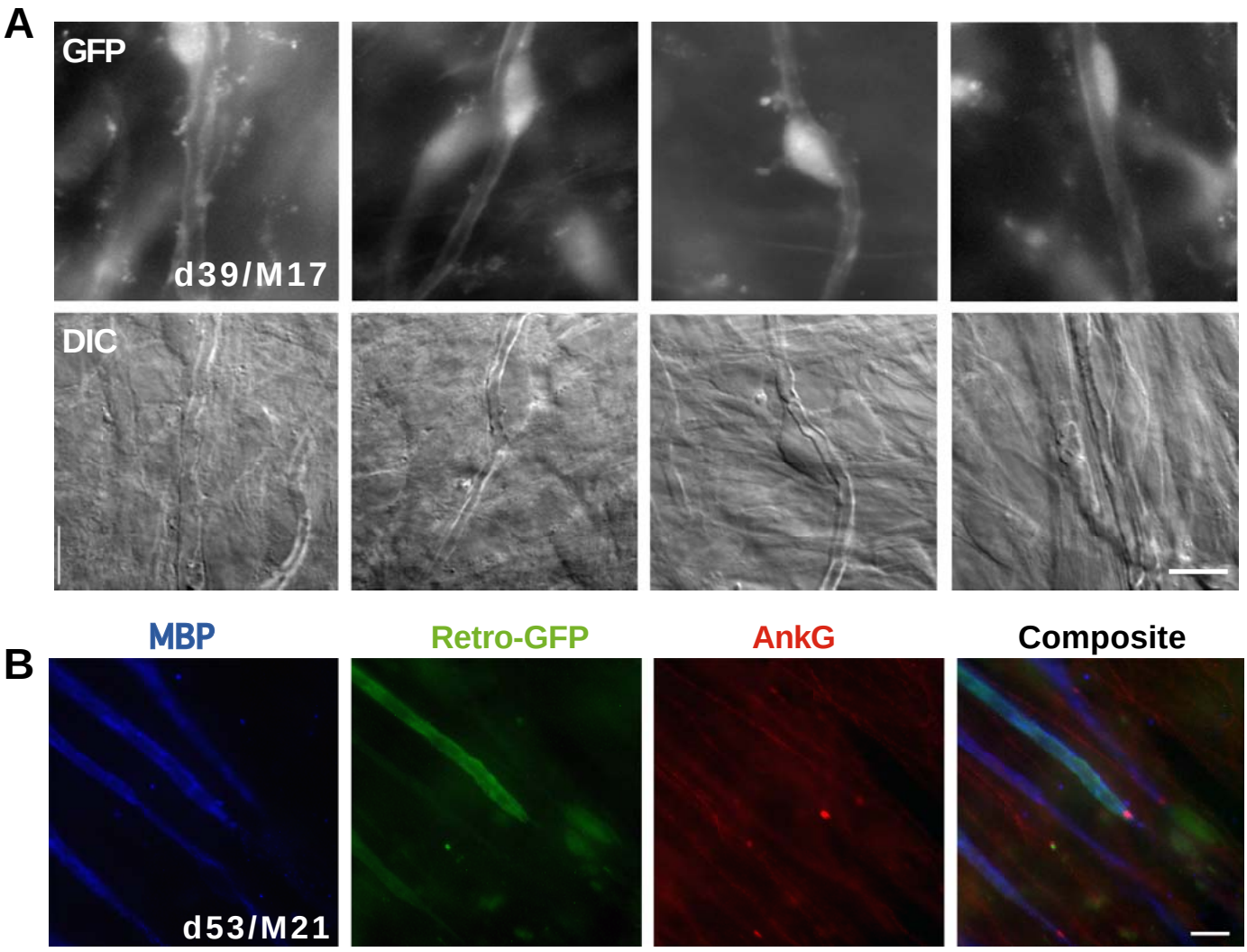

Figure 37 - Retroviral infection produces GFP-positive myelin segments

A) Using IRES-GFP based retroviruses, DRG explants were infected and examined after the induction of myelination. After 17 days induction (d39/M17), GFP-positive SCs were visualized via fluorescence and differential interference contrast (DIC) microscopy, indicating that the infection did not interfere with myelin segment generation. B) To ensure that retroviral infection did not impair node formation, cultures (d53/M21) were immunostained for MBP (blue) and ankyrin$_G$ (red). GFP-expressing SCs involved in segment formation were identified and appropriate nodal clusters of ankyrin$_G$ were present. Scale bar=10 μm.

which can be independently translated. This would specifically allow for the determination of the effect of a particular protein by the identification of GFP-positive cells. Further, the retroviral employment does not itself impair myelination or node formation, allowing for the study of terminal phenotype effects in these processes.

Despite the significant role we have identified for microvillar components in SC development and function, the most significant finding reported thus far in the NHERF-1 (EBP50) knockout mouse appears to be disrupted localization of the sodium-phosphate transporter, Npt2, in the renal proximal tubule cells paired with resultant phosphate wasting. These animals also display muscle weakness and impaired mobility (Shenolikar et al., 2002), suggesting potential neuromuscular deficits. As we have shown significant correlations among SC cap formation, SC motility, and node formation, further study of these animals should provide key insights as to the role of EBP50 and SC microvilli in the functioning of the PNS. These findings could potentially aid in the therapeutic facilitation of SC motility, prompting repair mechanisms in both neural injury and disease states.

## Appendix I – Abbreviations

AnkB – ankyrin$_B$

AnkG - ankyrin$_G$

BCECF - 2',7'-Bis(2-carboxyethyl)-5(6)-carboxyfluorescein

BME – Basal Medium Eagle's

C-ERMAD - COOH-ERM association domain

CFTR – cystic fibrosis transmembrane receptor

$c_m$ – membrane capacitance

CMT – Charcot-Marie-Tooth disease

CNS – central nervous system

COOH - carboxy

DIC – differential interference contrast

DN – dominant negative

DRG – dorsal root ganglion

EBP50 – ezrin binding phosphoprotein 50kDa

ECM – extra-cellular matrix

E"N" – embryonic day N

ERM – ezrin-radixin-moesin family proteins

FERM – four point one, ezrin, radixin, moesin

GalC - galactocerebroside

GPI – glycosyl-phosphatidylinositol

HBSS – Hanks's Balanced Salt Solution

LPA – lysophosphatidic acid

MAG – myelin-associated glycoprotein

MBP – myelin basic protein

N-ERMAD – $NH_2$-ERM association domain

$NH_2$ – amino

NHE3 – $Na^+/H^+$ exchanger isoform 3

NHERF-1 – NHE3 regulatory exchange factor 1

PBS-T – phosphate-buffered saline with 0.2% trition X-100

PDZ - PSD-95/DlgA/ZO-1

pERM – phospho-ERM

PH – plekstrin homology

PI 4, 5 kinase - phosphatidyl inositol 4-phosphate 5 kinase

PIP2 - phosphatidylinositol (4,5)-bisphosphate

PLCδ - phospholipase C delta

PMP22 - peripheral myelin protein 22 kDa

P"N" – post-natal day N

PNS - peripheral nervous system

PKC - protein kinase C

$P_0$ - protein zero

$r_a$ – axial resistance

ROCK – Rho-associated kinase

SC – Schwann cell

SEM – standard error of the mean

vgsc – voltage-gated sodium channel

VSVG – vesicular stomatis viral G protein

WT – wild-type

## Appendix II - Supplemental Video Legends

Video1 – DRG Culture Establishment

Acutely isolated DRGs (d1) were imaged to visualize culture establishment. Using DIC, growth cones originating at the DRG explant can be seen migrating through the field of view. An initial SC followed by a wave of these cells is apparent migrating in close association with the axons. The video clip then advances to approximately 40 hours, and several rounds of SC division are clearly observed. Images were captured every 7 minutes and are shown at 5 frames/sec.

Fig15video2 – Node of Ranvier

This video shows an animated, volumetric rendering of a deconvolved Z-series through a node of Ranvier. The myelinated culture (d36/M15) was stained for MBP (blue), ankyrin$_G$ (green), and EBP50 (red). Note the EBP50-reactive SC microvilli encompassing the axonal ankyrin$_G$ staining at the node. The field rotates and the nodal components alternately fade to better demonstrate their spatial relationship. Special thanks to Brian Schneider (Improvision) for assistance in employing OpenLab and Volocity software to generate these images.

Fig17video3 – EBP50-GFP SC – Standard – Short Term

EBP50-GFP transfected cultures were examined via time-lapse microscopy. Transfected SCs in standard cultures (d29/t7) showed no specific localization of EBP50-GFP at their

tips. Images were captured every 3 minutes over a 60-minute period. The video is shown at 360x real-time (2 frames/sec).

Fig17video4 – EBP50-GFP Standard Tip

Focusing on the SC tip, there is no enrichment of EBP50-GFP in this area under standard conditions (d29/t7). Images were captured every 3 minutes over a 60-minute period. The video is shown at 360x real-time (2 frames/sec).

Fig17video5 – EBP50-GFP Myelin – Short Term

EBP50-GFP transfected cultures were examined via time-lapse microscopy. Transfected SCs in myelinating cultures (d29/M6/t5) had dynamic, remodeling EBP50-GFP positive tips. Images were captured every 3 minutes over a 60-minute period. The video is shown at 360x real-time (2 frames/sec).

Fig17video6 – EBP50-GFP Myelin Tip

Under myelinating conditions (d29/M6/t5), EBP50-GFP becomes highly localized to the actively restructuring cap region. Images were captured every 3 minutes over a 60-minute period. The video is shown at 360x real-time (2 frames/sec).

Fig25Avideo7 – SC process retraction - GFP

After induction of myelination, GFP-filled SCs (d27/M6/t5) demonstrate asymmetric process retraction generating a unipolar morphology. Images were captured every 5

minutes, and this video spans an elapsed 95 minutes, shown at 1500x real time (5 frames/sec).

Fig25Bvideo8 – SC migration – GFP

GFP-filled SCs (d27/M6/t5), upon attaining a unipolar state, undergo nucleokinetic, directed migration. Images were captured every 5 minutes, and this video spans an elapsed 600 minutes, shown at 1500x real time (5 frames/sec).

Fig25Cvideo9 – SC cycling – GFP

GFP-transfected SCs (d27/M6/t5) are able to re-establish bipolarity via process extension. Images were captured every 5 minutes, and this video spans an elapsed 600 minutes, shown at 1500x real time (5 frames/sec).

Fig26Bvideo10 – SC process retraction - EBP50-GFP

EBP50-GFP (d28/M7/t6) becomes highly localized to the SC distal tip in conjunction with process retraction. EBP50-GFP enrichment at a SC distal tip visually marks that process for retraction. Images were captured every 5 minutes, and this video spans an elapsed 150 minutes, shown at 1500x real time (5 frames/sec).

Fig26Cvideo11 –SC migration - EBP50-GFP

EBP50-GFP transfected SC (d28/M7/t6) showing EBP50 localization at one distal tip, associated process retraction, and subsequent unipolar migration. Images were captured

every 5 minutes, and this video shows an elapsed 595 minutes, shown at 1500x real time (5 frames/sec).

Fig26Dvideo12 - SC cycling - EBP50-GFP

EBP50-GFP expressing SC (d28/M7/t6) cycles through polarity states. This clearly illustrates the morphologic plasticity these cells possess, undergoing process retraction, unipolar migration, and process extension re-establishing bipolarity. Images were captured every 5 minutes, and this video spans an elapsed 590 minutes, shown at 1500x real time (5 frames/sec).

Fig31Bvideo13 – Multipolar DN-ezrin (FERM) SC

FERM-ezrin/EBP50-GFP co-transfected SC (d27/M6/t5) displaying severe multipolarity and impaired motility. Images were captured every 5 minutes, and this video spans an elapsed 600 minutes, shown at 1500x real time (5 frames/sec).

## Bibliography


Amieva, M.R., P. Litman, L. Huang, E. Ichimaru, and H. Furthmayr. 1999. Disruption of dynamic cell surface architecture of NIH3T3 fibroblasts by the N-terminal domains of moesin and ezrin: in vivo imaging with GFP fusion proteins. *J Cell Sci*. 112 ( Pt 1):111-25.

Anderson, R.A., and R.E. Lovrien. 1984. Glycophorin is linked by band 4.1 protein to the human erythrocyte membrane skeleton. *Nature*. 307:655-8.

Arroyo, E.J., J.R. Bermingham, Jr., M.G. Rosenfeld, and S.S. Scherer. 1998. Promyelinating Schwann cells express Tst-1/SCIP/Oct-6. *J Neurosci*. 18:7891-902.

Arroyo, E.J., and S.S. Scherer. 2000. On the molecular architecture of myelinated fibers. *Histochem Cell Biol*. 113:1-18.

Arroyo, E.J., T. Xu, S. Poliak, M. Watson, E. Peles, and S.S. Scherer. 2001. Internodal specializations of myelinated axons in the central nervous system. *Cell Tissue Res*. 305:53-66.

Asundi, V.K., R. Erdman, R.C. Stahl, and D.J. Carey. 2003. Matrix metalloproteinase-dependent shedding of syndecan-3, a transmembrane heparan sulfate proteoglycan, in Schwann cells. *J Neurosci Res*. 73:593-602.

Bartsch, U., F. Kirchhoff, and M. Schachner. 1989. Immunohistological localization of the adhesion molecules L1, N-CAM, and MAG in the developing and adult optic nerve of mice. *J Comp Neurol*. 284:451-62.

Bass, M.D., and M.J. Humphries. 2002. Cytoplasmic interactions of syndecan-4 orchestrate adhesion receptor and growth factor receptor signalling. *Biochem J*. 368:1-15.

Bennett, V., and L. Chen. 2001. Ankyrins and cellular targeting of diverse membrane proteins to physiological sites. *Curr Opin Cell Biol*. 13:61-7.

Bennett, V., and S. Lambert. 1999. Physiological roles of axonal ankyrins in survival of premyelinated axons and localization of voltage-gated sodium channels. *J Neurocytol*. 28:303-18.

Berghs, S., D. Aggujaro, R. Dirkx, Jr., E. Maksimova, P. Stabach, J.M. Hermel, J.P. Zhang, W. Philbrick, V. Slepnev, T. Ort, and M. Solimena. 2000. betaIV spectrin, a new spectrin localized at axon initial segments and nodes of ranvier in the central and peripheral nervous system. *J Cell Biol*. 151:985-1002.

Bergoffen, J., S.S. Scherer, S. Wang, M.O. Scott, L.J. Bone, D.L. Paul, K. Chen, M.W. Lensch, P.F. Chance, and K.H. Fischbeck. 1993. Connexin mutations in X-linked Charcot-Marie-Tooth disease. *Science*. 262:2039-42.

Berthold, C.H. 1996. Development of nodes of Ranvier in feline nerves: an ultrastructural presentation. *Microsc Res Tech.* 34:399-421.

Besson, A., T.L. Wilson, and V.W. Yong. 2002. The anchoring protein RACK1 links protein kinase Cepsilon to integrin beta chains. Requirements for adhesion and motility. *J Biol Chem*. 277:22073-84.

Bhat, M.A., J.C. Rios, Y. Lu, G.P. Garcia-Fresco, W. Ching, M. St Martin, J. Li, S. Einheber, M. Chesler, J. Rosenbluth, J.L. Salzer, and H.J. Bellen. 2001. Axon-glia interactions and the domain organization of myelinated axons requires neurexin IV/Caspr/Paranodin. *Neuron*. 30:369-83.

Bhattacharyya, A., E. Frank, N. Ratner, and R. Brackenbury. 1991. P0 is an early marker of the Schwann cell lineage in chickens. *Neuron*. 7:831-44.

Black, J.A., and S.G. Waxman. 1988. The perinodal astrocyte. *Glia*. 1:169-83.

Blanchard, A.D., A. Sinanan, E. Parmantier, R. Zwart, L. Broos, D. Meijer, C. Meier, K.R. Jessen, and R. Mirsky. 1996. Oct-6 (SCIP/Tst-1) is expressed in Schwann cell precursors, embryonic Schwann cells, and postnatal myelinating Schwann cells: comparison with Oct-1, Krox-20, and Pax-3. *J Neurosci Res*. 46:630-40.

Boiko, T., M.N. Rasband, S.R. Levinson, J.H. Caldwell, G. Mandel, J.S. Trimmer, and G. Matthews. 2001. Compact myelin dictates the differential targeting of two sodium channel isoforms in the same axon. *Neuron*. 30:91-104.

Bonnon, C., L. Goutebroze, N. Denisenko-Nehrbass, J.A. Girault, and C. Faivre-Sarrailh. 2003. The paranodal complex of F3/contactin and caspr/paranodin traffics to the cell surface via a non-conventional pathway. *J Biol Chem*. 278:48339-47.

Bourguignon, L.Y., and H. Jin. 1995. Identification of the ankyrin-binding domain of the mouse T-lymphoma cell inositol 1,4,5-trisphosphate (IP3) receptor and its role in the regulation of IP3-mediated internal Ca2+ release. *J Biol Chem*. 270:7257-60.

Bourguignon, L.Y., H. Jin, N. Iida, N.R. Brandt, and S.H. Zhang. 1993. The involvement of ankyrin in the regulation of inositol 1,4,5-trisphosphate receptor-mediated internal Ca2+ release from Ca2+ storage vesicles in mouse T-lymphoma cells. *J Biol Chem*. 268:7290-7.

Bourrguignon, L.Y., N. Iida, C.F. Welsh, D. Zhu, A. Krongrad, and D. Pasquale. 1995. Involvement of CD44 and its variant isoforms in membrane-cytoskeleton interaction, cell adhesion and tumor metastasis. *J Neurooncol*. 26:201-8.

Boyle, M.E., E.O. Berglund, K.K. Murai, L. Weber, E. Peles, and B. Ranscht. 2001. Contactin orchestrates assembly of the septate-like junctions at the paranode in myelinated peripheral nerve. *Neuron*. 30:385-97.

Bretscher, A., D. Chambers, R. Nguyen, and D. Reczek. 2000. ERM-Merlin and EBP50 protein families in plasma membrane organization and function. *Annu Rev Cell Dev Biol*. 16:113-43.

Bretscher, A., K. Edwards, and R.G. Fehon. 2002. ERM proteins and merlin: integrators at the cell cortex. *Nat Rev Mol Cell Biol*. 3:586-99.

Bretscher, A., D. Reczek, and M. Berryman. 1997. Ezrin: a protein requiring conformational activation to link microfilaments to the plasma membrane in the assembly of cell surface structures. *J Cell Sci*. 110 ( Pt 24):3011-8.

Brockes, J.P., K.L. Fields, and M.C. Raff. 1979. Studies on cultured rat Schwann cells. I. Establishment of purified populations from cultures of peripheral nerve. *Brain Res*. 165:105-18.

Bronstein, J.M., K. Chen, S. Tiwari-Woodruff, and H.I. Kornblum. 2000. Developmental expression of OSP/claudin-11. *J Neurosci Res*. 60:284-90.

Buensuceso, C.S., D. Woodside, J.L. Huff, G.E. Plopper, and T.E. O'Toole. 2001. The WD protein Rack1 mediates protein kinase C and integrin-dependent cell migration. *J Cell Sci*. 114:1691-8.

Bunge, M.B., A.K. Williams, P.M. Wood, J. Uitto, and J.J. Jeffrey. 1980. Comparison of nerve cell and nerve cell plus Schwann cell cultures, with particular emphasis on basal lamina and collagen formation. *J Cell Biol*. 84:184-202.

Bunge, R.P., M.B. Bunge, and M. Bates. 1989. Movements of the Schwann cell nucleus implicate progression of the inner (axon-related) Schwann cell process during myelination. *J Cell Biol*. 109:273-84.

Carey, D.J. 1997. Syndecans: multifunctional cell-surface co-receptors. *Biochem J*. 327 ( Pt 1):1-16.

Carey, D.J., C.F. Eldridge, C.J. Cornbrooks, R. Timpl, and R.P. Bunge. 1983. Biosynthesis of type IV collagen by cultured rat Schwann cells. *J Cell Biol*. 97:473-9.

Castelo, L., and D.G. Jay. 1999. Radixin is involved in lamellipodial stability during nerve growth cone motility. *Mol Biol Cell*. 10:1511-20.

Chan, W., E. Kordeli, and V. Bennett. 1993. 440-kD ankyrinB: structure of the major developmentally regulated domain and selective localization in unmyelinated axons. *J Cell Biol*. 123:1463-73.

Charles, P., S. Tait, C. Faivre-Sarrailh, G. Barbin, F. Gunn-Moore, N. Denisenko-Nehrbass, A.M. Guennoc, J.A. Girault, P.J. Brophy, and C. Lubetzki. 2002. Neurofascin is a glial receptor for the paranodin/Caspr-contactin axonal complex at the axoglial junction. *Curr Biol*. 12:217-20.

Cheng, C., and D.W. Zochodne. 2002. In vivo proliferation, migration and phenotypic changes of Schwann cells in the presence of myelinated fibers. *Neuroscience*. 115:321-9.

Cheng, H.L., M.L. Steinway, J.W. Russell, and E.L. Feldman. 2000. GTPases and phosphatidylinositol 3-kinase are critical for insulin-like growth factor-I-mediated Schwann cell motility. *J Biol Chem*. 275:27197-204.

Ching, W., G. Zanazzi, S.R. Levinson, and J.L. Salzer. 1999. Clustering of neuronal sodium channels requires contact with myelinating Schwann cells. *J Neurocytol*. 28:295-301.

Choi, B.H., J.S. Choi, D.J. Rhie, S.H. Yoon, S. Min do, Y.H. Jo, M.S. Kim, and S.J. Hahn. 2002. Direct inhibition of the cloned Kv1.5 channel by AG-1478, a tyrosine kinase inhibitor. *Am J Physiol Cell Physiol*. 282:C1461-8.

Cole, J.S., A. Messing, J.Q. Trojanowski, and V.M. Lee. 1994. Modulation of axon diameter and neurofilaments by hypomyelinating Schwann cells in transgenic mice. *J Neurosci*. 14:6956-66.

Crepaldi, T., A. Gautreau, P.M. Comoglio, D. Louvard, and M. Arpin. 1997. Ezrin is an effector of hepatocyte growth factor-mediated migration and morphogenesis in epithelial cells. *J Cell Biol*. 138:423-34.

Czech, M.P. 2000. PIP2 and PIP3: complex roles at the cell surface. *Cell*. 100:603-6.

D'Urso, D., P.J. Brophy, S.M. Staugaitis, C.S. Gillespie, A.B. Frey, J.G. Stempak, and D.R. Colman. 1990. Protein zero of peripheral nerve myelin: biosynthesis, membrane insertion, and evidence for homotypic interaction. *Neuron*. 4:449-60.

Davis, J.Q., and V. Bennett. 1993. Ankyrin-binding activity of nervous system cell adhesion molecules expressed in adult brain. *J Cell Sci Suppl*. 17:109-17.

Davis, J.Q., S. Lambert, and V. Bennett. 1996. Molecular composition of the node of Ranvier: identification of ankyrin-binding cell adhesion molecules neurofascin (mucin+/third FNIII domain-) and NrCAM at nodal axon segments. *J Cell Biol*. 135:1355-67.

de Waegh, S.M., V.M. Lee, and S.T. Brady. 1992. Local modulation of neurofilament phosphorylation, axonal caliber, and slow axonal transport by myelinating Schwann cells. *Cell*. 68:451-63.

Deerinck, T.J., S.R. Levinson, G.V. Bennett, and M.H. Ellisman. 1997. Clustering of voltage-sensitive sodium channels on axons is independent of direct Schwann cell contact in the dystrophic mouse. *J Neurosci*. 17:5080-8.

Devaux, J., G. Alcaraz, J. Grinspan, V. Bennett, R. Joho, M. Crest, and S.S. Scherer. 2003. Kv3.1b is a novel component of CNS nodes. *J Neurosci*. 23:4509-18.

Devaux, J.J., K.A. Kleopa, E.C. Cooper, and S.S. Scherer. 2004. KCNQ2 is a nodal K+ channel. *J Neurosci*. 24:1236-44.

Einheber, S., G. Zanazzi, W. Ching, S. Scherer, T.A. Milner, E. Peles, and J.L. Salzer. 1997. The axonal membrane protein Caspr, a homologue of neurexin IV, is a component of the septate-like paranodal junctions that assemble during myelination. *J Cell Biol*. 139:1495-506.

Eldridge, C.F., M.B. Bunge, R.P. Bunge, and P.M. Wood. 1987. Differentiation of axon-related Schwann cells in vitro. I. Ascorbic acid regulates basal lamina assembly and myelin formation. *J Cell Biol*. 105:1023-34.

Fannon, A.M., D.L. Sherman, G. Ilyina-Gragerova, P.J. Brophy, V.L. Friedrich, Jr., and D.R. Colman. 1995. Novel E-cadherin-mediated adhesion in peripheral nerve: Schwann cell architecture is stabilized by autotypic adherens junctions. *J Cell Biol*. 129:189-202.

Feltri, M.L., D. Graus Porta, S.C. Previtali, A. Nodari, B. Migliavacca, A. Cassetti, A. Littlewood-Evans, L.F. Reichardt, A. Messing, A. Quattrini, U. Mueller, and L. Wrabetz. 2002. Conditional disruption of beta 1 integrin in Schwann cells impedes interactions with axons. *J Cell Biol*. 156:199-209.

Friede, R.L., and R. Bischhausen. 1980. The precise geometry of large internodes. *J Neurol Sci*. 48:367-81.

Friede, R.L., T. Meier, and M. Diem. 1981. How is the exact length of an internode determined. *J Neurol Sci*. 50:217-28.

Fukata, M., and K. Kaibuchi. 2001. Rho-family GTPases in cadherin-mediated cell-cell adhesion. *Nat Rev Mol Cell Biol*. 2:887-97.

Garbay, B., A.M. Heape, F. Sargueil, and C. Cassagne. 2000. Myelin synthesis in the peripheral nervous system. *Prog Neurobiol*. 61:267-304.

Gary, R., and A. Bretscher. 1995. Ezrin self-association involves binding of an N-terminal domain to a normally masked C-terminal domain that includes the F-actin binding site. *Mol Biol Cell*. 6:1061-75.

Gatto, C.L., B.J. Walker, and S. Lambert. 2003. Local ERM activation and dynamic growth cones at Schwann cell tips implicated in efficient formation of nodes of Ranvier. *J Cell Biol*. 162:489-98.

Gollan, L., D. Salomon, J.L. Salzer, and E. Peles. 2003. Caspr regulates the processing of contactin and inhibits its binding to neurofascin. *J Cell Biol*. 163:1213-8.

Goutebroze, L., M. Carnaud, N. Denisenko, M.C. Boutterin, and J.A. Girault. 2003. Syndecan-3 and syndecan-4 are enriched in Schwann cell perinodal processes. *BMC Neurosci*. 4:29.

Granes, F., C. Berndt, C. Roy, P. Mangeat, M. Reina, and S. Vilaro. 2003. Identification of a novel Ezrin-binding site in syndecan-2 cytoplasmic domain. *FEBS Lett*. 547:212-6.

Granes, F., J.M. Urena, N. Rocamora, and S. Vilaro. 2000. Ezrin links syndecan-2 to the cytoskeleton. *J Cell Sci*. 113 ( Pt 7):1267-76.

Grootjans, J.J., P. Zimmermann, G. Reekmans, A. Smets, G. Degeest, J. Durr, and G. David. 1997. Syntenin, a PDZ protein that binds syndecan cytoplasmic domains. *Proc Natl Acad Sci U S A*. 94:13683-8.

Hagedorn, L., J. Floris, U. Suter, and L. Sommer. 2000a. Autonomic neurogenesis and apoptosis are alternative fates of progenitor cell communities induced by TGFbeta. *Dev Biol*. 228:57-72.

Hagedorn, L., C. Paratore, G. Brugnoli, J.L. Baert, N. Mercader, U. Suter, and L. Sommer. 2000b. The Ets domain transcription factor Erm distinguishes rat satellite glia from Schwann cells and is regulated in satellite cells by neuregulin signaling. *Dev Biol*. 219:44-58.

Hagedorn, L., U. Suter, and L. Sommer. 1999. P0 and PMP22 mark a multipotent neural crest-derived cell type that displays community effects in response to TGF-beta family factors. *Development*. 126:3781-94.

Hall, A. 1998. Rho GTPases and the actin cytoskeleton. *Science*. 279:509-14.

Hall, R.A., L.S. Ostedgaard, R.T. Premont, J.T. Blitzer, N. Rahman, M.J. Welsh, and R.J. Lefkowitz. 1998a. A C-terminal motif found in the beta2-adrenergic receptor, P2Y1 receptor and cystic fibrosis transmembrane conductance regulator determines binding to the Na+/H+ exchanger regulatory factor family of PDZ proteins. *Proc Natl Acad Sci U S A*. 95:8496-501.

Hall, R.A., R.T. Premont, C.W. Chow, J.T. Blitzer, J.A. Pitcher, A. Claing, R.H. Stoffel, L.S. Barak, S. Shenolikar, E.J. Weinman, S. Grinstein, and R.J. Lefkowitz. 1998b. The beta2-adrenergic receptor interacts with the Na+/H+-exchanger regulatory factor to control Na+/H+ exchange. *Nature*. 392:626-30.

Hamada, K., T. Shimizu, T. Matsui, S. Tsukita, and T. Hakoshima. 2000. Structural basis of the membrane-targeting and unmasking mechanisms of the radixin FERM domain. *Embo J*. 19:4449-62.

Hayashi, H., K. Szaszi, N. Coady-Osberg, W. Furuya, A.P. Bretscher, J. Orlowski, and S. Grinstein. 2004. Inhibition and Redistribution of NHE3, the Apical Na+/H+ Exchanger, by Clostridium difficile Toxin B. *J Gen Physiol*.

Heiska, L., K. Alfthan, M. Gronholm, P. Vilja, A. Vaheri, and O. Carpen. 1998. Association of ezrin with intercellular adhesion molecule-1 and -2 (ICAM-1 and ICAM-2). Regulation by phosphatidylinositol 4, 5-bisphosphate. *J Biol Chem*. 273:21893-900.

Henry, E.W., E.M. Eicher, and R.L. Sidman. 1991. The mouse mutation claw paw: forelimb deformity and delayed myelination throughout the peripheral nervous system. *J Hered*. 82:287-94.

Hirao, M., N. Sato, T. Kondo, S. Yonemura, M. Monden, T. Sasaki, Y. Takai, and S. Tsukita. 1996. Regulation mechanism of ERM (ezrin/radixin/moesin) protein/plasma membrane association: possible involvement of phosphatidylinositol turnover and Rho-dependent signaling pathway. *J Cell Biol*. 135:37-51.

Honke, K., Y. Hirahara, J. Dupree, K. Suzuki, B. Popko, K. Fukushima, J. Fukushima, T. Nagasawa, N. Yoshida, Y. Wada, and N. Taniguchi. 2002. Paranodal junction formation and spermatogenesis require sulfoglycolipids. *Proc Natl Acad Sci U S A*. 99:4227-32.

Horwitz, A.R., and J.T. Parsons. 1999. Cell migration--movin' on. *Science*. 286:1102-3.

Howe, D.G., and K.D. McCarthy. 1998. A dicistronic retroviral vector and culture model for analysis of neuron-Schwann cell interactions. *J Neurosci Methods*. 83:133-42.

Huang, W., R. Chiquet-Ehrismann, J.V. Moyano, A. Garcia-Pardo, and G. Orend. 2001. Interference of tenascin-C with syndecan-4 binding to fibronectin blocks cell adhesion and stimulates tumor cell proliferation. *Cancer Res*. 61:8586-94.

Ichimura, T., and M.H. Ellisman. 1991. Three-dimensional fine structure of cytoskeletal-membrane interactions at nodes of Ranvier. *J Neurocytol*. 20:667-81.

Ishizaki, T., M. Uehata, I. Tamechika, J. Keel, K. Nonomura, M. Maekawa, and S. Narumiya. 2000. Pharmacological properties of Y-27632, a specific inhibitor of rho-associated kinases. *Mol Pharmacol*. 57:976-83.

Jenkins, G.H., P.L. Fisette, and R.A. Anderson. 1994. Type I phosphatidylinositol 4-phosphate 5-kinase isoforms are specifically stimulated by phosphatidic acid. *J Biol Chem*. 269:11547-54.

Jessen, K.R., A. Brennan, L. Morgan, R. Mirsky, A. Kent, Y. Hashimoto, and J. Gavrilovic. 1994. The Schwann cell precursor and its fate: a study of cell death and differentiation during gliogenesis in rat embryonic nerves. *Neuron*. 12:509-27.

Jessen, K.R., and R. Mirsky. 1991. Schwann cell precursors and their development. *Glia*. 4:185-94.

Jessen, K.R., and R. Mirsky. 1997. Embryonic Schwann cell development: the biology of Schwann cell precursors and early Schwann cells. *J Anat*. 191 ( Pt 4):501-5.

Jessen, K.R., and R. Mirsky. 1998. Origin and early development of Schwann cells. *Microsc Res Tech*. 41:393-402.

Jessen, K.R., and R. Mirsky. 1999. Why do Schwann cells survive in the absence of axons? *Ann N Y Acad Sci*. 883:109-15.

Jessen, K.R., L. Morgan, H.J. Stewart, and R. Mirsky. 1990. Three markers of adult non-myelin-forming Schwann cells, 217c(Ran-1), A5E3 and GFAP: development and regulation by neuron-Schwann cell interactions. *Development*. 109:91-103.

Kaibuchi, K. 1999. Regulation of cytoskeleton and cell adhesion by Rho targets. *Prog Mol Subcell Biol*. 22:23-38.

Kaibuchi, K., S. Kuroda, and M. Amano. 1999a. Regulation of the cytoskeleton and cell adhesion by the Rho family GTPases in mammalian cells. *Annu Rev Biochem*. 68:459-86.

Kaibuchi, K., S. Kuroda, M. Fukata, and M. Nakagawa. 1999b. Regulation of cadherin-mediated cell-cell adhesion by the Rho family GTPases. *Curr Opin Cell Biol*. 11:591-6.

Kalomiris, E.L., and L.Y. Bourguignon. 1988. Mouse T lymphoma cells contain a transmembrane glycoprotein (GP85) that binds ankyrin. *J Cell Biol*. 106:319-27.

Kandel, E.R., J.H. Schwartz, and T.M. Jessell. 1991. Principles of neural science. Appleton & Lange, Norwalk, Conn. xliv, 1135 pp.

Kaplan, M.R., M.H. Cho, E.M. Ullian, L.L. Isom, S.R. Levinson, and B.A. Barres. 2001. Differential control of clustering of the sodium channels Na(v)1.2 and Na(v)1.6 at developing CNS nodes of Ranvier. *Neuron*. 30:105-19.

Kaplan, M.R., A. Meyer-Franke, S. Lambert, V. Bennett, I.D. Duncan, S.R. Levinson, and B.A. Barres. 1997. Induction of sodium channel clustering by oligodendrocytes. *Nature*. 386:724-8.

Kerr, P.M., O. Clement-Chomienne, K.S. Thorneloe, T.T. Chen, K. Ishii, D.P. Sontag, M.P. Walsh, and W.C. Cole. 2001. Heteromultimeric Kv1.2-Kv1.5 channels underlie 4-aminopyridine-sensitive delayed rectifier K(+) current of rabbit vascular myocytes. *Circ Res*. 89:1038-44.

Kirkpatrick, L.L., and S.T. Brady. 1994. Modulation of the axonal microtubule cytoskeleton by myelinating Schwann cells. *J Neurosci*. 14:7440-50.

Kirkpatrick, L.L., A.S. Witt, H.R. Payne, H.D. Shine, and S.T. Brady. 2001. Changes in microtubule stability and density in myelin-deficient shiverer mouse CNS axons. *J Neurosci*. 21:2288-97.

Komada, M., and P. Soriano. 2002. [Beta]IV-spectrin regulates sodium channel clustering through ankyrin-G at axon initial segments and nodes of Ranvier. *J Cell Biol*. 156:337-48.

Kordeli, E., J. Davis, B. Trapp, and V. Bennett. 1990. An isoform of ankyrin is localized at nodes of Ranvier in myelinated axons of central and peripheral nerves. *J Cell Biol*. 110:1341-52.

Kordeli, E., S. Lambert, and V. Bennett. 1995. AnkyrinG. A new ankyrin gene with neural-specific isoforms localized at the axonal initial segment and node of Ranvier. *J Biol Chem*. 270:2352-9.

Koszowski, A.G., G.C. Owens, and S.R. Levinson. 1998. The effect of the mouse mutation claw paw on myelination and nodal frequency in sciatic nerves. *J Neurosci*. 18:5859-68.

Kunimoto, M. 1995. A neuron-specific isoform of brain ankyrin, 440-kD ankyrinB, is targeted to the axons of rat cerebellar neurons. *J Cell Biol*. 131:1821-9.

Kunimoto, M., E. Otto, and V. Bennett. 1991. A new 440-kD isoform is the major ankyrin in neonatal rat brain. *J Cell Biol*. 115:1319-31.

Lamb, R.F., B.W. Ozanne, C. Roy, L. McGarry, C. Stipp, P. Mangeat, and D.G. Jay. 1997. Essential functions of ezrin in maintenance of cell shape and lamellipodial extension in normal and transformed fibroblasts. *Curr Biol*. 7:682-8.

Lambert, S., J.Q. Davis, and V. Bennett. 1997. Morphogenesis of the node of Ranvier: co-clusters of ankyrin and ankyrin-binding integral proteins define early developmental intermediates. *J Neurosci*. 17:7025-36.

Lambert, S., H. Yu, J.T. Prchal, J. Lawler, P. Ruff, D. Speicher, M.C. Cheung, Y.W. Kan, and J. Palek. 1990. cDNA sequence for human erythrocyte ankyrin. *Proc Natl Acad Sci U S A*. 87:1730-4.

Lee-Kwon, W., J.H. Kim, J.W. Choi, K. Kawano, B. Cha, D.A. Dartt, D. Zoukhri, and M. Donowitz. 2003. Ca2+-dependent inhibition of NHE3 requires PKC alpha which binds to E3KARP to decrease surface NHE3 containing plasma membrane complexes. *Am J Physiol Cell Physiol*. 285:C1527-36.

Lemaillet, G., B. Walker, and S. Lambert. 2003. Identification of a conserved ankyrin-binding motif in the family of sodium channel alpha subunits. *J Biol Chem*. 278:27333-9.

Li, Z.P., E.P. Burke, J.S. Frank, V. Bennett, and K.D. Philipson. 1993. The cardiac Na+-Ca2+ exchanger binds to the cytoskeletal protein ankyrin. *J Biol Chem*. 268:11489-91.

Liedtke, C.M., V. Raghuram, C. Yun, and X. Wang. 2003. Role of a PDZ1 domain of NHERF1 in the binding of airway epithelial RACK1 to NHERF1. *Am J Physiol Cell Physiol*.

Liedtke, C.M., C.H. Yun, N. Kyle, and D. Wang. 2002. Protein kinase C epsilon-dependent regulation of cystic fibrosis transmembrane regulator involves binding to a receptor for activated C kinase (RACK1) and RACK1 binding to Na+/H+ exchange regulatory factor. *J Biol Chem*. 277:22925-33.

Liliental, J., and D.D. Chang. 1998. Rack1, a receptor for activated protein kinase C, interacts with integrin beta subunit. *J Biol Chem*. 273:2379-83.

Lobsiger, C.S., P.M. Smith, J. Buchstaller, B. Schweitzer, R.J. Franklin, U. Suter, and V. Taylor. 2001. SpL201: a conditionally immortalized Schwann cell precursor line that generates myelin. *Glia*. 36:31-47.

Lobsiger, C.S., V. Taylor, and U. Suter. 2002. The early life of a Schwann cell. *Biol Chem*. 383:245-53.

Louvet-Vallee, S. 2000. ERM proteins: from cellular architecture to cell signaling. *Biol Cell*. 92:305-16.

Lustig, M., G. Zanazzi, T. Sakurai, C. Blanco, S.R. Levinson, S. Lambert, M. Grumet, and J.L. Salzer. 2001. Nr-CAM and neurofascin interactions regulate ankyrin G and sodium channel clustering at the node of Ranvier. *Curr Biol*. 11:1864-9.

Lux, S.E., K.M. John, and V. Bennett. 1990. Analysis of cDNA for human erythrocyte ankyrin indicates a repeated structure with homology to tissue-differentiation and cell-cycle control proteins. *Nature*. 344:36-42.

Mahanthappa, N.K., E.S. Anton, and W.D. Matthew. 1996. Glial growth factor 2, a soluble neuregulin, directly increases Schwann cell motility and indirectly promotes neurite outgrowth. *J Neurosci*. 16:4673-83.

Mangeat, P., C. Roy, and M. Martin. 1999. ERM proteins in cell adhesion and membrane dynamics. *Trends Cell Biol*. 9:187-92.

Marfatia, S.M., R.A. Leu, D. Branton, and A.H. Chishti. 1995. Identification of the protein 4.1 binding interface on glycophorin C and p55, a homologue of the Drosophila discs-large tumor suppressor protein. *J Biol Chem*. 270:715-9.

Marfatia, S.M., R.A. Lue, D. Branton, and A.H. Chishti. 1994. In vitro binding studies suggest a membrane-associated complex between erythroid p55, protein 4.1, and glycophorin C. *J Biol Chem*. 269:8631-4.

Martini, R. 2001. The effect of myelinating Schwann cells on axons. *Muscle Nerve*. 24:456-66.

Martini, R., and M. Schachner. 1986. Immunoelectron microscopic localization of neural cell adhesion molecules (L1, N-CAM, and MAG) and their shared carbohydrate epitope and myelin basic protein in developing sciatic nerve. *J Cell Biol*. 103:2439-48.

Martini, R., and M. Schachner. 1988. Immunoelectron microscopic localization of neural cell adhesion molecules (L1, N-CAM, and myelin-associated glycoprotein) in regenerating adult mouse sciatic nerve. *J Cell Biol*. 106:1735-46.

Martini, R., M. Schachner, and A. Faissner. 1990. Enhanced expression of the extracellular matrix molecule J1/tenascin in the regenerating adult mouse sciatic nerve. *J Neurocytol*. 19:601-16.

Mathis, C., N. Denisenko-Nehrbass, J.A. Girault, and E. Borrelli. 2001. Essential role of oligodendrocytes in the formation and maintenance of central nervous system nodal regions. *Development*. 128:4881-90.

Matsui, T., M. Maeda, Y. Doi, S. Yonemura, M. Amano, K. Kaibuchi, and S. Tsukita. 1998. Rho-kinase phosphorylates COOH-terminal threonines of ezrin/radixin/moesin (ERM) proteins and regulates their head-to-tail association. *J Cell Biol*. 140:647-57.

Maudsley, S., A.M. Zamah, N. Rahman, J.T. Blitzer, L.M. Luttrell, R.J. Lefkowitz, and R.A. Hall. 2000. Platelet-derived growth factor receptor association with Na(+)/H(+) exchanger regulatory factor potentiates receptor activity. *Mol Cell Biol*. 20:8352-63.

Mehta, H., C. Orphe, M.S. Todd, C.J. Cornbrooks, and D.J. Carey. 1985. Synthesis by Schwann cells of basal lamina and membrane-associated heparan sulfate proteoglycans. *J Cell Biol*. 101:660-6.

Meintanis, S., D. Thomaidou, K.R. Jessen, R. Mirsky, and R. Matsas. 2001. The neuron-glia signal beta-neuregulin promotes Schwann cell motility via the MAPK pathway. *Glia*. 34:39-51.

Melendez-Vasquez, C.V., J.C. Rios, G. Zanazzi, S. Lambert, A. Bretscher, and J.L. Salzer. 2001. Nodes of Ranvier form in association with ezrin-radixin-moesin (ERM)-positive Schwann cell processes. *Proc Natl Acad Sci U S A*. 98:1235-40.

Menichella, D.M., E.J. Arroyo, R. Awatramani, T. Xu, P. Baron, J.M. Vallat, J. Balsamo, J. Lilien, G. Scarlato, J. Kamholz, S.S. Scherer, and M.E. Shy. 2001. Protein zero is necessary for E-cadherin-mediated adherens junction formation in Schwann cells. *Mol Cell Neurosci*. 18:606-18.

Menichella, D.M., D.A. Goodenough, E. Sirkowski, S.S. Scherer, and D.L. Paul. 2003. Connexins are critical for normal myelination in the CNS. *J Neurosci*. 23:5963-73.

Mi, H., T.J. Deerinck, M.H. Ellisman, and T.L. Schwarz. 1995. Differential distribution of closely related potassium channels in rat Schwann cells. *J Neurosci*. 15:3761-74.

Michaely, P., and V. Bennett. 1993. The membrane-binding domain of ankyrin contains four independently folded subdomains, each comprised of six ankyrin repeats. *J Biol Chem*. 268:22703-9.

Michaely, P., and V. Bennett. 1995. Mechanism for binding site diversity on ankyrin. Comparison of binding sites on ankyrin for neurofascin and the Cl-/HCO3- anion exchanger. *J Biol Chem*. 270:31298-302.

Mirsky, R., C. Dubois, L. Morgan, and K.R. Jessen. 1990. 04 and A007-sulfatide antibodies bind to embryonic Schwann cells prior to the appearance of galactocerebroside; regulation of the antigen by axon-Schwann cell signals and cyclic AMP. *Development*. 109:105-16.

Mirsky, R., and K.R. Jessen. 1996. Schwann cell development, differentiation and myelination. *Curr Opin Neurobiol*. 6:89-96.
Mirsky, R., and K.R. Jessen. 1999. The neurobiology of Schwann cells. *Brain Pathol*. 9:293-311.
Miyazaki, T., Y. Takeda, Y. Murakami, H. Kawano, T. Shimazu, S. Toya, and K. Uyemura. 1995. Distribution of PASII/PMP22 and connexin 32 proteins in the peripheral nervous system. *Neurochem Int*. 27:377-83.
Monuki, E.S., G. Weinmaster, R. Kuhn, and G. Lemke. 1989. SCIP: a glial POU domain gene regulated by cyclic AMP. *Neuron*. 3:783-93.
Morita, K., H. Sasaki, K. Fujimoto, M. Furuse, and S. Tsukita. 1999. Claudin-11/OSP-based tight junctions of myelin sheaths in brain and Sertoli cells in testis. *J Cell Biol*. 145:579-88.
Murphy, P., P. Topilko, S. Schneider-Maunoury, T. Seitanidou, A. Baron-Van Evercooren, and P. Charnay. 1996. The regulation of Krox-20 expression reveals important steps in the control of peripheral glial cell development. *Development*. 122:2847-57.
Nadarajah, B., P. Alifragis, R.O. Wong, and J.G. Parnavelas. 2003. Neuronal migration in the developing cerebral cortex: observations based on real-time imaging. *Cereb Cortex*. 13:607-11.
Nadarajah, B., J.E. Brunstrom, J. Grutzendler, R.O. Wong, and A.L. Pearlman. 2001. Two modes of radial migration in early development of the cerebral cortex. *Nat Neurosci*. 4:143-50.
Nadarajah, B., and J.G. Parnavelas. 2002. Modes of neuronal migration in the developing cerebral cortex. *Nat Rev Neurosci*. 3:423-32.
Nakamura, F., M.R. Amieva, and H. Furthmayr. 1995. Phosphorylation of threonine 558 in the carboxyl-terminal actin-binding domain of moesin by thrombin activation of human platelets. *J Biol Chem*. 270:31377-85.
Ng, T., M. Parsons, W.E. Hughes, J. Monypenny, D. Zicha, A. Gautreau, M. Arpin, S. Gschmeissner, P.J. Verveer, P.I. Bastiaens, and P.J. Parker. 2001. Ezrin is a downstream effector of trafficking PKC-integrin complexes involved in the control of cell motility. *Embo J*. 20:2723-41.
Niggli, V., C. Andreoli, C. Roy, and P. Mangeat. 1995. Identification of a phosphatidylinositol-4,5-bisphosphate-binding domain in the N-terminal region of ezrin. *FEBS Lett*. 376:172-6.
Nikolic, M. 2002. The role of Rho GTPases and associated kinases in regulating neurite outgrowth. *Int J Biochem Cell Biol*. 34:731-45.
Novakovic, S.D., S.R. Levinson, M. Schachner, and P. Shrager. 1998. Disruption and reorganization of sodium channels in experimental allergic neuritis. *Muscle Nerve*. 21:1019-32.
Odermatt, B., K. Wellershaus, A. Wallraff, G. Seifert, J. Degen, C. Euwens, B. Fuss, H. Bussow, K. Schilling, C. Steinhauser, and K. Willecke. 2003. Connexin 47 (Cx47)-deficient mice with enhanced green fluorescent protein reporter gene reveal predominant oligodendrocytic expression of Cx47 and display vacuolized myelin in the CNS. *J Neurosci*. 23:4549-59.

Otto, E., M. Kunimoto, T. McLaughlin, and V. Bennett. 1991. Isolation and characterization of cDNAs encoding human brain ankyrins reveal a family of alternatively spliced genes. *J Cell Biol*. 114:241-53.

Paglini, G., P. Kunda, S. Quiroga, K. Kosik, and A. Caceres. 1998. Suppression of radixin and moesin alters growth cone morphology, motility, and process formation in primary cultured neurons. *J Cell Biol*. 143:443-55.

Paradiso, A.M., R.Y. Tsien, and T.E. Machen. 1984. Na+-H+ exchange in gastric glands as measured with a cytoplasmic-trapped, fluorescent pH indicator. *Proc Natl Acad Sci U S A*. 81:7436-40.

Pareek, S., U. Suter, G.J. Snipes, A.A. Welcher, E.M. Shooter, and R.A. Murphy. 1993. Detection and processing of peripheral myelin protein PMP22 in cultured Schwann cells. *J Biol Chem*. 268:10372-9.

Pearson, M.A., D. Reczek, A. Bretscher, and P.A. Karplus. 2000. Structure of the ERM protein moesin reveals the FERM domain fold masked by an extended actin binding tail domain. *Cell*. 101:259-70.

Pedraza, L., and D.R. Colman. 2000. Fluorescent myelin proteins provide new tools to study the myelination process. *J Neurosci Res*. 60:697-703.

Pedraza, L., J.K. Huang, and D.R. Colman. 2001. Organizing principles of the axoglial apparatus. *Neuron*. 30:335-44.

Peles, E., M. Nativ, M. Lustig, M. Grumet, J. Schilling, R. Martinez, G.D. Plowman, and J. Schlessinger. 1997. Identification of a novel contactin-associated transmembrane receptor with multiple domains implicated in protein-protein interactions. *Embo J*. 16:978-88.

Pestonjamasp, K., M.R. Amieva, C.P. Strassel, W.M. Nauseef, H. Furthmayr, and E.J. Luna. 1995. Moesin, ezrin, and p205 are actin-binding proteins associated with neutrophil plasma membranes. *Mol Biol Cell*. 6:247-59.

Poliak, S., L. Gollan, R. Martinez, A. Custer, S. Einheber, J.L. Salzer, J.S. Trimmer, P. Shrager, and E. Peles. 1999. Caspr2, a new member of the neurexin superfamily, is localized at the juxtaparanodes of myelinated axons and associates with K+ channels. *Neuron*. 24:1037-47.

Poliak, S., L. Gollan, D. Salomon, E.O. Berglund, R. Ohara, B. Ranscht, and E. Peles. 2001. Localization of Caspr2 in myelinated nerves depends on axon-glia interactions and the generation of barriers along the axon. *J Neurosci*. 21:7568-75.

Poliak, S., and E. Peles. 2003. The local differentiation of myelinated axons at nodes of Ranvier. *Nat Rev Neurosci*. 4:968-80.

Previtali, S.C., A. Nodari, C. Taveggia, C. Pardini, G. Dina, A. Villa, L. Wrabetz, A. Quattrini, and M.L. Feltri. 2003. Expression of laminin receptors in schwann cell differentiation: evidence for distinct roles. *J Neurosci*. 23:5520-30.

Raine, C.S. 1982. Differences between the nodes of Ranvier of large and small diameter fibres in the P.N.S. *J Neurocytol*. 11:935-47.

Raine, C.S. 1984. On the association between perinodal astrocytic processes and the node of Ranvier in the C.N.S. *J Neurocytol*. 13:21-7.

Rao, J.N., O. Platoshyn, L. Li, X. Guo, V.A. Golovina, J.X. Yuan, and J.Y. Wang. 2002. Activation of K(+) channels and increased migration of differentiated intestinal epithelial cells after wounding. *Am J Physiol Cell Physiol*. 282:C885-98.

Reczek, D., M. Berryman, and A. Bretscher. 1997. Identification of EBP50: A PDZ-containing phosphoprotein that associates with members of the ezrin-radixin-moesin family. *J Cell Biol*. 139:169-79.

Reczek, D., and A. Bretscher. 1998. The carboxyl-terminal region of EBP50 binds to a site in the amino-terminal domain of ezrin that is masked in the dormant molecule. *J Biol Chem*. 273:18452-8.

Rieger, F., J.K. Daniloff, M. Pincon-Raymond, K.L. Crossin, M. Grumet, and G.M. Edelman. 1986. Neuronal cell adhesion molecules and cytotactin are colocalized at the node of Ranvier. *J Cell Biol*. 103:379-91.

Ritchie, J.M., and R.B. Rogart. 1977. Density of sodium channels in mammalian myelinated nerve fibers and nature of the axonal membrane under the myelin sheath. *Proc Natl Acad Sci U S A*. 74:211-5.

Saito, F., S.A. Moore, R. Barresi, M.D. Henry, A. Messing, S.E. Ross-Barta, R.D. Cohn, R.A. Williamson, K.A. Sluka, D.L. Sherman, P.J. Brophy, J.D. Schmelzer, P.A. Low, L. Wrabetz, M.L. Feltri, and K.P. Campbell. 2003. Unique role of dystroglycan in peripheral nerve myelination, nodal structure, and sodium channel stabilization. *Neuron*. 38:747-58.

Salzer, J.L. 2003. Polarized domains of myelinated axons. *Neuron*. 40:297-318.

Schechtman, D., and D. Mochly-Rosen. 2001. Adaptor proteins in protein kinase C-mediated signal transduction. *Oncogene*. 20:6339-47.

Scherer, S.S. 1996. Molecular specializations at nodes and paranodes in peripheral nerve. *Microsc Res Tech*. 34:452-61.

Scherer, S.S., and E.J. Arroyo. 2002. Recent progress on the molecular organization of myelinated axons. *J Peripher Nerv Syst*. 7:1-12.

Scherer, S.S., S.M. Deschenes, Y.T. Xu, J.B. Grinspan, K.H. Fischbeck, and D.L. Paul. 1995. Connexin32 is a myelin-related protein in the PNS and CNS. *J Neurosci*. 15:8281-94.

Scherer, S.S., T. Xu, P. Crino, E.J. Arroyo, and D.H. Gutmann. 2001. Ezrin, radixin, and moesin are components of Schwann cell microvilli. *J Neurosci Res*. 65:150-64.

Schnadelbach, O., I. Ozen, O.W. Blaschuk, R.L. Meyer, and J.W. Fawcett. 2001. N-cadherin is involved in axon-oligodendrocyte contact and myelination. *Mol Cell Neurosci*. 17:1084-93.

Schwartz, M.A., G. Both, and C. Lechene. 1989. Effect of cell spreading on cytoplasmic pH in normal and transformed fibroblasts. *Proc Natl Acad Sci U S A*. 86:4525-9.

Scotland, P., D. Zhou, H. Benveniste, and V. Bennett. 1998. Nervous system defects of AnkyrinB (-/-) mice suggest functional overlap between the cell adhesion molecule L1 and 440-kD AnkyrinB in premyelinated axons. *J Cell Biol*. 143:1305-15.

Sechi, A.S., and J. Wehland. 2000. The actin cytoskeleton and plasma membrane connection: PtdIns(4,5)P(2) influences cytoskeletal protein activity at the plasma membrane. *J Cell Sci*. 113 Pt 21:3685-95.

Shaw, R.J., M. Henry, F. Solomon, and T. Jacks. 1998. RhoA-dependent phosphorylation and relocalization of ERM proteins into apical membrane/actin protrusions in fibroblasts. *Mol Biol Cell*. 9:403-19.

Shenolikar, S., J.W. Voltz, C.M. Minkoff, J.B. Wade, and E.J. Weinman. 2002. Targeted disruption of the mouse NHERF-1 gene promotes internalization of proximal

tubule sodium-phosphate cotransporter type IIa and renal phosphate wasting. *Proc Natl Acad Sci U S A*. 99:11470-5.

Sherman, D.L., C. Fabrizi, C.S. Gillespie, and P.J. Brophy. 2001. Specific disruption of a schwann cell dystrophin-related protein complex in a demyelinating neuropathy. *Neuron*. 30:677-87.

Sherman, L.S., T.A. Rizvi, S. Karyala, and N. Ratner. 2000. CD44 enhances neuregulin signaling by Schwann cells. *J Cell Biol*. 150:1071-84.

Shibata, T., M. Chuma, A. Kokubu, M. Sakamoto, and S. Hirohashi. 2003. EBP50, a beta-catenin-associating protein, enhances Wnt signaling and is over-expressed in hepatocellular carcinoma. *Hepatology*. 38:178-86.

Short, D.B., K.W. Trotter, D. Reczek, S.M. Kreda, A. Bretscher, R.C. Boucher, M.J. Stutts, and S.L. Milgram. 1998. An apical PDZ protein anchors the cystic fibrosis transmembrane conductance regulator to the cytoskeleton. *J Biol Chem*. 273:19797-801.

Shrager, P. 1989. Sodium channels in single demyelinated mammalian axons. *Brain Res*. 483:149-54.

Simons, P.C., S.F. Pietromonaco, D. Reczek, A. Bretscher, and L. Elias. 1998. C-terminal threonine phosphorylation activates ERM proteins to link the cell's cortical lipid bilayer to the cytoskeleton. *Biochem Biophys Res Commun*. 253:561-5.

Smith, K.J., W.F. Blakemore, J.A. Murray, and R.C. Patterson. 1982a. Internodal myelin volume and axon surface area. A relationship determining myelin thickness? *J Neurol Sci*. 55:231-46.

Smith, K.J., H. Bostock, and S.M. Hall. 1982b. Saltatory conduction precedes remyelination in axons demyelinated with lysophosphatidyl choline. *J Neurol Sci*. 54:13-31.

Srinivasan, Y., L. Elmer, J. Davis, V. Bennett, and K. Angelides. 1988. Ankyrin and spectrin associate with voltage-dependent sodium channels in brain. *Nature*. 333:177-80.

Starr, R., B. Attema, G.H. DeVries, and M.J. Monteiro. 1996. Neurofilament phosphorylation is modulated by myelination. *J Neurosci Res*. 44:328-37.

Sternberger, N.H., Y. Itoyama, M.W. Kies, and H.D. Webster. 1978. Myelin basic protein demonstrated immunocytochemically in oligodendroglia prior to myelin sheath formation. *Proc Natl Acad Sci U S A*. 75:2521-4.

Stewart, H.J., K.R. Jessen, R. Curtis, and R. Mirsky. 1992. Schwann cells, neurons and GAP-43. *Perspect Dev Neurobiol*. 1:45-52.

Stewart, H.J., L. Morgan, K.R. Jessen, and R. Mirsky. 1993. Changes in DNA synthesis rate in the Schwann cell lineage in vivo are correlated with the precursor--Schwann cell transition and myelination. *Eur J Neurosci*. 5:1136-44.

Sward, C., C.H. Berthold, I. Nilsson-Remahl, and M. Rydmark. 1995. Axonal constriction at Ranvier's node increases during development. *Neurosci Lett*. 190:159-62.

Tait, S., F. Gunn-Moore, J.M. Collinson, J. Huang, C. Lubetzki, L. Pedraza, D.L. Sherman, D.R. Colman, and P.J. Brophy. 2000. An oligodendrocyte cell adhesion molecule at the site of assembly of the paranodal axo-glial junction. *J Cell Biol*. 150:657-66.

Takahashi, K., T. Sasaki, A. Mammoto, K. Takaishi, T. Kameyama, S. Tsukita, and Y. Takai. 1997. Direct interaction of the Rho GDP dissociation inhibitor with ezrin/radixin/moesin initiates the activation of the Rho small G protein. *J Biol Chem*. 272:23371-5.

Thomas, J.A. 1986. Intracellularly trapped pH indicators. *Soc Gen Physiol Ser*. 40:311-25.

Tolias, K.F., A.D. Couvillon, L.C. Cantley, and C.L. Carpenter. 1998. Characterization of a Rac1- and RhoGDI-associated lipid kinase signaling complex. *Mol Cell Biol*. 18:762-70.

Tran Quang, C., A. Gautreau, M. Arpin, and R. Treisman. 2000. Ezrin function is required for ROCK-mediated fibroblast transformation by the Net and Dbl oncogenes. *Embo J*. 19:4565-76.

Trapp, B.D., S.B. Andrews, A. Wong, M. O'Connell, and J.W. Griffin. 1989. Co-localization of the myelin-associated glycoprotein and the microfilament components, F-actin and spectrin, in Schwann cells of myelinated nerve fibres. *J Neurocytol*. 18:47-60.

Trapp, B.D., and G.J. Kidd. 2000. Axo-glial septate junctions. The maestro of nodal formation and myelination? *J Cell Biol*. 150:F97-F100.

Tsukita, S., K. Oishi, N. Sato, J. Sagara, and A. Kawai. 1994. ERM family members as molecular linkers between the cell surface glycoprotein CD44 and actin-based cytoskeletons. *J Cell Biol*. 126:391-401.

Turunen, O., T. Wahlstrom, and A. Vaheri. 1994. Ezrin has a COOH-terminal actin-binding site that is conserved in the ezrin protein family. *J Cell Biol*. 126:1445-53.

Uehata, M., T. Ishizaki, H. Satoh, T. Ono, T. Kawahara, T. Morishita, H. Tamakawa, K. Yamagami, J. Inui, M. Maekawa, and S. Narumiya. 1997. Calcium sensitization of smooth muscle mediated by a Rho-associated protein kinase in hypertension. *Nature*. 389:990-4.

Vabnick, I., A. Messing, S.Y. Chiu, S.R. Levinson, M. Schachner, J. Roder, C. Li, S. Novakovic, and P. Shrager. 1997. Sodium channel distribution in axons of hypomyelinated and MAG null mutant mice. *J Neurosci Res*. 50:321-36.

Vabnick, I., S.D. Novakovic, S.R. Levinson, M. Schachner, and P. Shrager. 1996. The clustering of axonal sodium channels during development of the peripheral nervous system. *J Neurosci*. 16:4914-22.

Wang, S., R.W. Raab, P.J. Schatz, W.B. Guggino, and M. Li. 1998. Peptide binding consensus of the NHE-RF-PDZ1 domain matches the C-terminal sequence of cystic fibrosis transmembrane conductance regulator (CFTR). *FEBS Lett*. 427:103-8.

Wanner, I.B., and P.M. Wood. 2002. N-cadherin mediates axon-aligned process growth and cell-cell interaction in rat Schwann cells. *J Neurosci*. 22:4066-79.

Waxman, S.G. 1980. Determinants of conduction velocity in myelinated nerve fibers. *Muscle Nerve*. 3:141-50.

Waxman, S.G., and J.A. Black. 1987. Macromolecular structure of the Schwann cell membrane. Perinodal microvilli. *J Neurol Sci*. 77:23-34.

Weiner, J.A., N. Fukushima, J.J. Contos, S.S. Scherer, and J. Chun. 2001. Regulation of Schwann cell morphology and adhesion by receptor-mediated lysophosphatidic acid signaling. *J Neurosci*. 21:7069-78.

Weinman, E.J., D. Steplock, and S. Shenolikar. 1993. CAMP-mediated inhibition of the renal brush border membrane Na+-H+ exchanger requires a dissociable phosphoprotein cofactor. *J Clin Invest*. 92:1781-6.

Wilcox-Adelman, S.A., F. Denhez, and P.F. Goetinck. 2002. Syndecan-4 modulates focal adhesion kinase phosphorylation. *J Biol Chem*. 277:32970-7.

Wood, P.M. 1976. Separation of functional Schwann cells and neurons from normal peripheral nerve tissue. *Brain Res*. 115:361-75.

Woods, A., and J.R. Couchman. 2001. Syndecan-4 and focal adhesion function. *Curr Opin Cell Biol*. 13:578-83.

Yonemura, S., T. Matsui, and S. Tsukita. 2002. Rho-dependent and -independent activation mechanisms of ezrin/radixin/moesin proteins: an essential role for polyphosphoinositides in vivo. *J Cell Sci*. 115:2569-80.

Yonemura, S., and S. Tsukita. 1999. Direct involvement of ezrin/radixin/moesin (ERM)-binding membrane proteins in the organization of microvilli in collaboration with activated ERM proteins. *J Cell Biol*. 145:1497-509.

Yoshinaga-Ohara, N., A. Takahashi, T. Uchiyama, and M. Sasada. 2002. Spatiotemporal regulation of moesin phosphorylation and rear release by Rho and serine/threonine phosphatase during neutrophil migration. *Exp Cell Res*. 278:112-22.

Young, P., O. Boussadia, P. Berger, D.P. Leone, P. Charnay, R. Kemler, and U. Suter. 2002. E-cadherin is required for the correct formation of autotypic adherens junctions of the outer mesaxon but not for the integrity of myelinated fibers of peripheral nerves. *Mol Cell Neurosci*. 21:341-51.

Zhang, X., and V. Bennett. 1996. Identification of O-linked N-acetylglucosamine modification of ankyrinG isoforms targeted to nodes of Ranvier. *J Biol Chem*. 271:31391-8.

Zhang, X., and V. Bennett. 1998. Restriction of 480/270-kD ankyrin G to axon proximal segments requires multiple ankyrin G-specific domains. *J Cell Biol*. 142:1571-81.

Zhang, X., J.Q. Davis, S. Carpenter, and V. Bennett. 1998. Structural requirements for association of neurofascin with ankyrin. *J Biol Chem*. 273:30785-94.

Zhou, D., S. Lambert, P.L. Malen, S. Carpenter, L.M. Boland, and V. Bennett. 1998. AnkyrinG is required for clustering of voltage-gated Na channels at axon initial segments and for normal action potential firing. *J Cell Biol*. 143:1295-304.

Zimmermann, P., K. Meerschaert, G. Reekmans, I. Leenaerts, J.V. Small, J. Vandekerckhove, G. David, and J. Gettemans. 2002. PIP(2)-PDZ domain binding controls the association of syntenin with the plasma membrane. *Mol Cell*. 9:1215-25.